THE UNIVERSITY OF CHICAGO

CELL MIGRATION, A MULTISCALE INTEGRATION PROCESS: UNDERSTANDING THE SUB-CELLULAR MECHANISMS OF DIRECTED CELL MIGRATION DURING CONTACT GUIDANCE AND ELUCIDATING THE ROLE OF TISSUE SCALE MIGRATION IN *DROSOPHILA* EGG CHAMBERS

A DISSERTATION SUBMITTED TO
THE FACULTY OF THE DIVISION OF THE THE PHYSICAL SCIENCES
AND
THE FACULTY OF THE DIVISION OF THE BIOLOGICAL SCIENCES
AND THE PRITZKER SCHOOL OF MEDICINE
IN CANDIDACY FOR THE DEGREE OF
DOCTOR OF PHILOSOPHY

GRADUATE PROGRAM IN BIOPHYSICAL SCIENCES

BY
GUILLERMINA ROCHELLE RAMÍREZ SAN JUAN

CHICAGO, ILLINOIS
MARCH 2017

Para mi familia: Guillermo, Elizabeth, Isaac y David.

Habrá que creer ...

TABLE OF CONTENTS

LIST OF FIGURES

ACKNOWLEDGMENTS

This work wouldn't have been possible with the contribution of a lot of people. I thank my advisor, Margaret Gardel, for sharing her extreme enthusiasm about science with me, and providing critical advice both for my research and training as a scientist. I would also like to thank her for her unconditional support and cheers. I thank my thesis committee members: Sally Horne-Badovinac, Karl Matlin and Edwin Munro. I thank Sally for giving me the opportunity to work in her lab and for being extremely generous with her time and advice during my first years of graduate school. I thank Karl and Ed for giving me an open door policy, where I could discuss science with them at any time, and for their helpful comments and advice.

During my PhD I had the opportunity to collaborate with incredible people, thanks to them this work was possible. I thank Maureen Cetera and Patrick Oakes for being infinitely patient with me while training me as a grad student. I thank them for their enthusiasm and all the exciting scientific discussions we had. And also for their friendship and support through all the hard times. I would also like to acknowledge my labmates, who always provided insightful comments on my work and created a stimulating working atmosphere. Particularly my fellow grad students: Tim Fessenden, Patrick McCall and Sam Stam. I thank Tim for being the source of all my literature knowledge and always open to help with experiments, for editing all my drafts and ideas, for answering all my annoying questions. I thank Patrick and Sam for being extremely supportive, providing me feedback with analysis and editing anything I'd send their way.

The work of my PhD was mostly a work of faith. I thank God for giving me the hope and strength to move past difficult moments, as well as the enthusiasm to carry out my work with love. I thank him for all the coincidences and blessings, for all his unconditional love.

I thank my parents for their unconditional love and support, for always cheering me on. For their example of strength, hard work and perseverance. I thank my brothers Isaac and David, for being so loving and caring with me, for always being there for anything and everything I needed, for all the laughs we share. I also want to thank my extended family, who has always been there to cheer me on, to share and celebrate and also to support me through hard times. I want to thank specially my cousin Guillermo Ortiz for listening to my incessant rambling and anxieties about the future. I am still marveled at the coincidences that led us to the unexpected paths we're in today.

I'd also like to thank my friends, without them grad school would have been so much more boring. I want to thank specially my fellow classmates: Pete and Bo. I thank Pete for all his advice, all the cups of coffee we shared and for his help and support. I thank Bo for always encouraging me to forget about negative things and for all the fun adventures we shared. I thank the "biophysics frat": Eugene, Herman, Kevin and Vaughn. For all the laughs, for all the unconditional support, for being silly when I needed them to be silly and serious at times. I thank Eugene for being a terrible running partner and a great friend, Herman for being the best sous-chef I could've asked for, Kevin for always looking pretty in pictures and Vaughn for always being whiling to help. I'd also like to thank Stew and Miquela, for not allowing me to be homeless and being so welcoming.

I thank Reto, for happening to me at the least expected of times. For making me remember what really matters, taking care of me and making me feel needy. For all his unconditional love and support through the hard times, for toning down my craziness during the crazy times, for all the laughs and cheers. For all the new landscapes, for all the new roads, and all the new paths that appear in our horizon.

ABSTRACT

Directed cell migration is essential for wound healing, development and tissue morphogenesis. *In vivo*, geometrical cues from the extra-cellular matrix (ECM) are critical for the regulation of directed migration. During contact guidance, the fibrillar architecture of the ECM helps control cell shape and migration direction. Micropatterning has been a powerful tool to demonstrate that cells respond to the geometrical presentation of ligands, however mechanistic understanding of how cells sense changes in ECM geometry has been lacking. Here, we use micropatterning to systematically vary a single spatial dimension in ECM geometry and show that micron scale changes are sufficient to induce contact guidance. By manipulating the regulation of protrusive activity using different cellular mechanisms we show that contact guidance relies on spatial control of protrusive activity to direct migration. Specifically, we prove that area and orientation are the two physical parameters of protrusion that determine the ability of cells to undergo contact guidance. Contact guidance requires cells to translate subcellular changes in ECM geometry into cellular scale behaviors. To sculpt tissues, cell migration can be used to integrate changes at the cellular level and translate them into tissue scale behaviors. An example of such a process is the tissue level patterning in *Drosophila* egg chambers. During egg chamber elongation, the follicular epithelium undergoes collective migration causing the egg chamber to rotate within its surrounding ECM. Rotation coincides with the formation of a parallel array of actin bundles in the epithelium and fibrils in the ECM. By studying the cellular mechanisms of migration in egg chambers, we show that rotation plays a critical role in building the actin tissue-scale pattern. Rotation begins shortly after egg chamber formation and requires lamellipodial protrusions at each follicle cells leading edge. During early stages, rotation is necessary for tissue-level actin bundle alignment, but it becomes dispensable after the ECM is polarized. This work highlights how cell migration can be used to build a polarized tissue scale organization.

CHAPTER 1

INTRODUCTION

Cell migration plays a central role in several developmental, physiological and pathological processes. During development cell migration is required for diverse morphogenetic processes conserved among organisms, ranging from branching morphogenesis of kidney and breast tissue, to migration of neural crest cells out of the neural tube [50, 103, 9, 94]. In adults, leukocytes are required to translocate to areas of insult to mediate phagocytic and immune function [61]. Migration of fibroblasts and vascular endothelial cells is essential for wound healing [37]. In cancer metastasis, multicellular masses invade their ECM and migrate into the bloodstream [31].

Migration of single cells is a process that has been studied extensively over the past years and is relatively well understood. Despite its complexity, single cell migration can be thought as consisting of four discrete steps: protrusion of the cell's leading cell edge, adhesion to the extra-cellular-matrix (ECM), generation of traction stresses against adhesions and release of rear adhesions and cell body contraction [35]. For efficient movement, these processes must be tightly coordinated in space and time. The ability of cells to coordinate these processes is controlled by numerous internal and external cues. Internally, localized Rac activity and membrane tension can determine the sites of growth of the leading edge [44], and regions of high Rho activity can inhibit local cell protrusion [111] and favor adhesion disassembly and retraction of the trailing edge. Externally, the way in which a cell migrates is influenced by the chemical, physical and topographical cues from the cellular microenvironment. The ECM *in vivo* is a major component of this microenvironment, therefore a critical regulator of cell migration. It is composed of a fibrous mesh of glycoproteins and proteoglycans, including both the collagens and a diverse array of non-collagenous proteins such as laminins, tenascins, and fibronectin [46, 89].

Physical characteristics of the ECM such as rigidity, density and geometry can direct cell migration [13, 80]. For instance, changes in geometry or spatial arrangement of adhesive cues provided by the ECM can guide cell motility [80]. During this process, termed contact guidance, aligned ECM fibrils promote changes to cell morphology and migration direction. Classical studies *in vivo* have shown that cells interacting with fibrillar ECM networks alter their shape and migration direction in response to ECM orientation [27, 113]. For instance, during amphibian gastrulation, aligned ECM fibrils facilitate mesodermal cell migration towards the animal pole [70]. More recently, orientation of ECM fibrils has been linked to morphogenesis during *Drosophila* egg chamber elongation [41]. The development of new techniques such as micropatterning of the ECM, has enabled the characterization *in vitro* of cellular responses to changes in shape and size of ECM adhesive regions [99], however the subcellular mechanisms by which cells are able to sense ECM geometry and translate it into changes in shape and migration direction, are not understood.

Contact guidance requires cells to translate subcellular changes in ECM geometry into cellular scale behaviors. By contrast *in vivo*, to sculpt tissues, cells need to integrate changes at the cellular level and translate them into tissue scale behaviors. During migration of multicellular assemblies, cells establish a multicellular polarity, reflected in supracellular organization of the actin cytoskeleton, generate a protrusive force that drives migration and maintain cell-cell junctions during motion [31]. Of particular interest to this work is the collective migration that occurs in *Drosophila* egg chambers. *Drosophila* egg chambers are multicellular structures in the fly ovary that each give rise to a single egg after a series of developmental steps. Although initially spherical, egg chambers lengthen across the anterior-posterior axis as they mature [8, 36]. This change in egg chamber shape depends on a tissue-scale circumferential array of ECM and actin, that is thought to act as a 'molecular corset' restricting growth perpendicular to the anterior-posterior (A-P) axis [41, 42]. At the same time elongation correlates with the ability of cells to undergo collective migration perpendicular to

the A-P axis [41]. While there is evidence that collective migration is required to build the ECM pattern, the relationship between migration and the tissue-level actin pattern as well as the cellular mechanisms of migration in this context, remain unknown.

In its initial chapters, this thesis will describe work done to understand the phenomenon of contact guidance, first by characterizing the influence of fibril-like ECM geometries on cell motility and then elucidating the subcellular mechanisms that allow cells to sense ECM geometry. Later chapters will explore the role of collective cell migration in the storage of polarity information across a tissue, using *Drosophila* egg chambers as a model system. Together this work sheds light into how ECM geometry is sensed by subcellular organelles and translated into cellular scale behaviors. At the same time it provides a foundation to understand the relationship between collective cell migration and tissue-scale patterning of the actin cytoskeleton.

1.1 Cellular mechanisms for migration

To migrate directionally, cells must first establish front-back polarity. The acquisition of cell polarity is fundamental to initiate migration and can be enforced by physical cues such as tension in the plasma membrane [44], and intracellular signaling primarily mediated by the differential activity of the small GTPases Cdc42, Rac1 and RhoA [111, 106, 78]. Once cells become polarized, they can move in a preferred direction. While complex, the process of cell migration can be broken down into four discrete steps: protrusion of the cell's leading edge, adhesion to the ECM, generation of traction stresses and release of rear adhesions and cell body contraction. These morphological changes and physical forces necessary for migration are largely generated by the actin cytoskeleton [35].

Actin polymerization at the cell's leading edge, mediated primarily by the Arp2/3 complex, drives protrusion formation. This protrusive actin network is known as the lamellipodia.

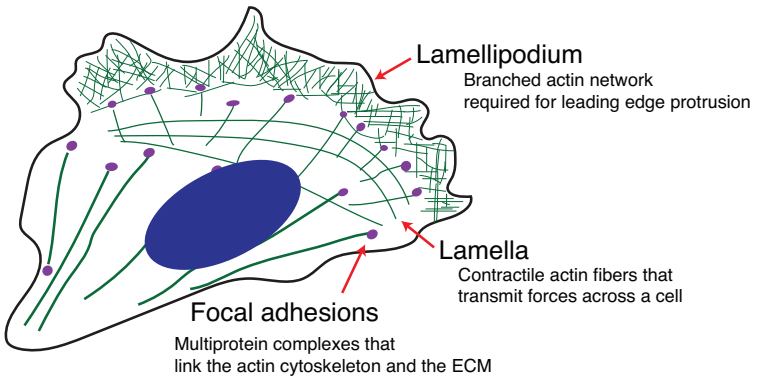

Figure 1.1: Schematic of the cellular actin cytoskeleton. The lamellipodium (green cross-hatches) is a branched actin network responsible for leading edge protrusion. The lamella (thin gridded lines) is composed of contractile fibers that transmit force across the cell. Focal adhesions (purple circles) are multiprotein complexed that provide attachment to the ECM.

A few microns back from the lamellipodia is the lamella, a contractile network of bundled actin, that contains myosin. In the contractile lamella, myosin II mediates actin retrograde flow, creating force that is transmitted to the ECM, moving the cell body forward (Figure 1.1) [81]. For productive leading edge advancement, cells need to couple protrusion formation with stabilization. Conversely, for productive advancement of the cell body, contraction must be coupled to deadhesion. Integrins are the major family of receptors that promote attachment to the ECM during migration. Integrin-based adhesions are highly complex structures with over 150 different associated molecules. At the leading edge activated integrins associate with the ECM and recruit vinculin, talin, paxilin, and several other adaptor proteins to assemble macromolecular complexes, termed focal adhesions [45]. Nascent adhesions assemble in the lamellipodia [75] and, in the absence of myosin activity, turn over rapidly [14]. Contractile stresses generated by myosin II in lamellar actin networks drive a retrograde frictional slip of nascent adhesions until a tension stabilizes the plaques to the ECM [3]. As the leading edge advances, signal transduction largely governs the decision of focal adhesions to mature further or turnover [38, 112].

Upstream of actin polymerization are Rho GTPases. Their primary function is to act as a

molecular switch to control signal transduction pathways by cycling GDP-bound, inactive forms and a GTP-bound active state. In their GTP-bound state they interact with downstream effectors to regulate actin dynamics [85]. Rho activity in migrating cells is associated with focal adhesion maturation and cell contractility, and it is responsible for cell body contraction and rear end retraction. While Rac regulates the polymerization of actin to form leading edge lamellipodia protrusions and nascent adhesion formation [78, 22].

1.2 Contact guidance

During migration, cells encounter a wide variety of extracellular environments. Since the ECM is a major component of the cellular microenvironment, it is not surprising that its physical properties such as rigidity, density and geometry regulate migration [13]. The ECM, composed of a fibrous mesh of glycoproteins and proteoglycans [46]. Most notable are the proteins that make up the core of basement membranes: type IV collagens, laminin, nidogen, and perlecan [118], and fibrillar collagens that surround a wide variety of cell types such as the mammary epithelium, glial and mesodermal cells [67, 84, 101, 69] (Figure 1.2). Classical studies have shown that cells interacting with a fibrillar ECM alter their morphology and migration [34, 113]. In this process known as contact guidance, the physical structure of the surrounding ECM helps control cell shape and migration [80].

The complexity of the *in vivo* microenvironment makes difficult to isolate the influence of different ECM properties on cell migration. Therefore, *in vitro* approaches have been very powerful to elucidate the influence of individual ECM physical properties on migration. In particular, micropatterned and microengineered cell adhesion substrates have enabled the study of cell phenotypes in response to selective cell attachment to the ECM [25, 95, 99]. These approaches allow the engineering of aligned ECMs with structure at the nano- and micro- scale. At both of these scales, cells respond by preferentially elongating and aligning parallel to the patterned features [116, 20, 117, 26, 23, 96]. In addition to controlling

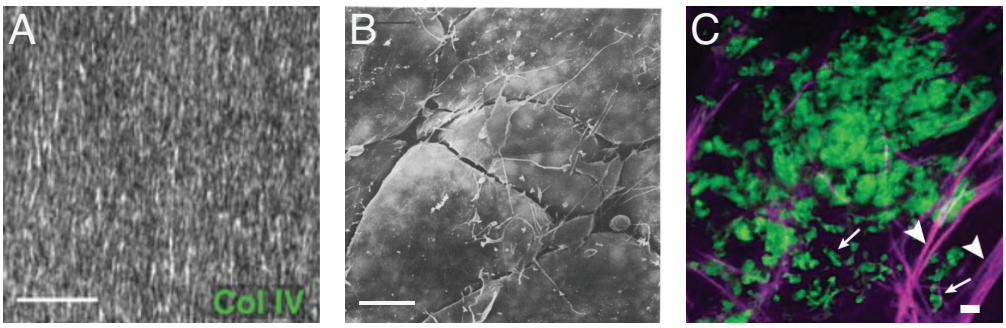

Figure 1.2: Fibril-like structure of the ECM *in vivo*. A) Immunofluorescence image showing the Collagen IV structure surrounding epithelial cell layer in *Drosophila* egg chambers (Scale bar=10μm). Image adapted from [12]. B) Scanning electron micrograph of the inner surface of the dorsal ectodermal layer of an *Ambystoma maculatum* embryo showing ECM fibrils (Scale bar=10 μm). Image adapted from [69]. C) Multiphoton microscopy image of carcinoma cells (green) moving on an aligned ECM fibrils (purple)(Scale bar=25μm). Image adapted from [16].

cell shape, nano and micro architecture in the ECM can influence alignment of the actin cytoskeleton. Filipodia and lamellipodia generally extend parallel to the underlying features with aligned stress fibers and focal adhesions that scale with the width of the underlying substrate [92, 96, 97]. In conjunction with its effects in cell polarity, structured ECMs can also influence migration. For instance, the migration speed of fibroblasts depends on the width of the ECM features [25], while the separation between features can dictate the direction of migration [51, 96, 116].

As described in the previous section, many of the fundamental processes that regulate cell migration at the micro and nano scale have been identified and described in detail. Surprisingly, mechanistic understanding of how cells sense changes in ECM geometry at these scales has been lacking. While significant research has been made to characterize cellular phenotypes in response to structured ECMs the molecular mechanisms underlying contact guidance remain elusive. A few distinct possibilities have arisen in the literature, previous studies in structured ECM showed that Rac was activated at sites of adhesion formation, consequently stimulating protrusion formation at those sites [116]. While myosin II activity

was shown to be important for the cell shape changes that occur in response to structured ECM [30, 90], illustrating the importance of the core migration machinery during contact guidance.

1.3 Overview of *Drosophila* egg chamber development

During development tissues undergo dramatic changes in architecture linked to collective cell migration [50, 94]. While there are several examples of well understood migration mediated morphogenetic processes [87], understanding the cellular basis of migration and morphogenesis in developmental systems is challenging. *Drosophila* egg chambers are egg precursors within the fly ovary that provide a tractable model for morphogenesis and migration. Each egg chamber is encased in its own ECM and its development can be considered isolated. Individual egg chambers are composed of only two different cell types, the germline surrounded by a somatic epithelium of follicle cells (FC). FCs are in contact with germline cells at the apical side, while their basal surface lies on an ECM. When an egg chamber is first formed, it is ≈ 20 μm in diameter and roughly spherical. Egg chambers are formed in a structure known as the germarium, to form a mature egg they must progress through 14 developmental stages (Figure 1.3) [36, 43, 8]. Each developmental stage can be distinguished by changes in morphology, since although initially spherical, egg chambers undergo preferential growth along the A-P axis, a process that results in an egg chamber that is 2.5 times longer than it is wide. (Figure 1.4).

During egg chamber growth there are well defined restricted periods of growth. The germline grows through periods of endoreplication, followed by growth via vitillogenesis, which drive a >5000-fold expansion of the follicle volume. Meanwhile, the FC epithelium proliferates to $\approx$ 650-1000 cells from stages 1 to the end of stage 6, when cell divisions cease. After stage 6, FCs grow only through endoreplication, therefore changes in egg chamber morphology after stage 6 correspond to pure morphogenesis [21]. The most obvious morphogenetic change in

Figure 1.3: A Developmental array of *Drosophila* egg chambers. Developmental stages shown are 4, 5, 7, 9, 10 and 13. Each stage can be distinguished by morphological changes. Egg chambers are expressing Collagen-IV GFP and are stained with phalloidin for F-actin. Figure adapted from [8].

egg chamber morphology occurs at stage 5, where egg chambers begin to elongate to acquire an elliptical shape. Elongation of the egg chamber occurs parallel to the anterior-posterior (A-P) axis. At stage 7 egg chambers are already elliptical (Figure 1.4). Egg chambers achieve 75% of their final elongation during stages 5 and 9, therefore this period corresponds to the major phase in elongation. By stage 10, egg chambers reach their final shape since at the end of stage 10, the contents of the nurse cells are transferred into the occyte in a process called dumping [62].

1.4 Planar polarity and migration in the *Drosophila* egg chamber

In addition to apico-basal polarity, many epithelia also display polarity within the plane of the tissue. Planar polarity refers to the organization of morphological and/or molecular structures within and/or across a tissue in a plane orthogonal to its apico/basal axis [39].

In the case of *Drosophila* egg chambers, planar polarity is manifested in the appearance of aligned actin filaments at the basal side of the epithelium along with spatial segregation of proteins such as Misshapen, Fat2 and Lar (Figure 1.5) [57, 107, 32, 40]. Actin filaments within each FC show a common orientation. At certain stages during development, this

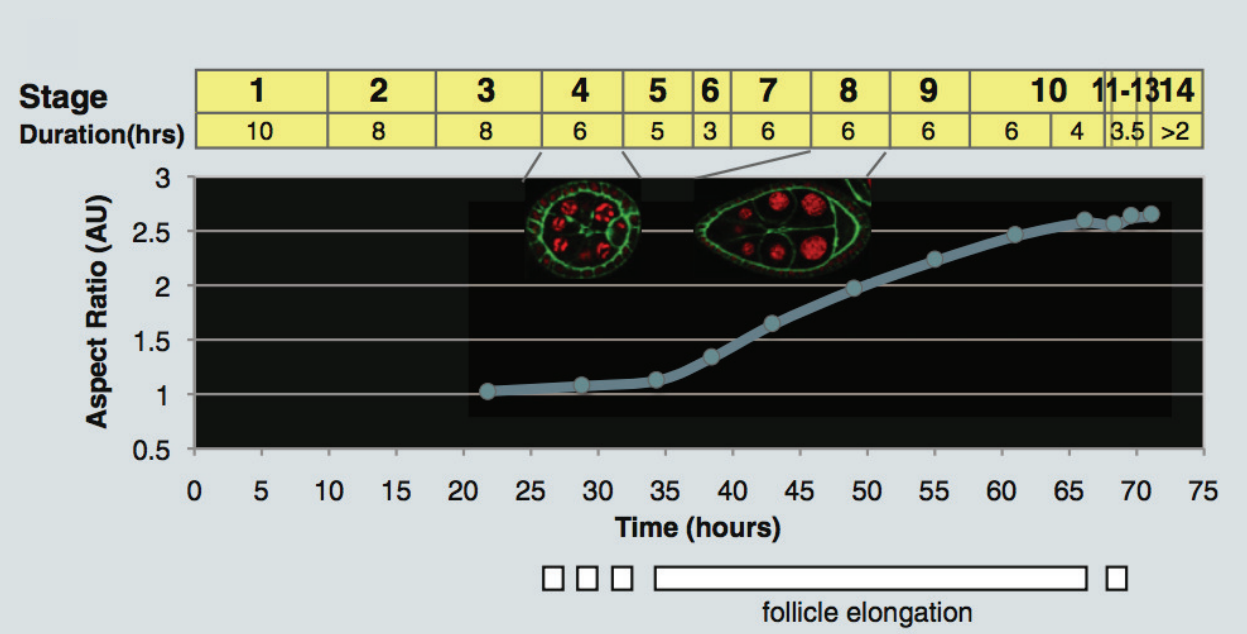

Figure 1.4: *Drosophila* egg chamber elongation depicted as the aspect ratio at different developmental times. Yellow table on top of the graph indicates the stage and its duration in hours. Figure adapted from [8].

orientation is coordinated throughout the epithelium, creating a tissue-scale level array of parallel actin filaments perpendicular to the A-P axis [40]. This planar polarized actin organization is evident in the germarium, however previous literature showed that from exiting the germarium through stage 4, egg chambers lost tissue-scale actin organization [32]. Actin filaments were thought to regain orientation across several cells during stage 5, afterwards this organization became increasingly robust until late stage 8, after which they become disorganized as FCs undergo further morphogenetic events (Figure 1.5) [7, 19, 32, 40, 42].

Appearance of tissue-scale polarity of the actin cytoskeleton occurs concurrently with egg chamber elongation, at stage 5 [32, 108]. Coincidently around stage 5, collagen IV fibers present at the basal surface of the epithelium appear to increase in density and acquire a fibril-like organization oriented perpendicular to the A-P axis [41, 47, 43] (Figure 1.5). Since both the actin cytoskeleton and the ECM display alignment across the entire tissue at the onset of elongation, the appearance of this form of planar polarity led to the formulation

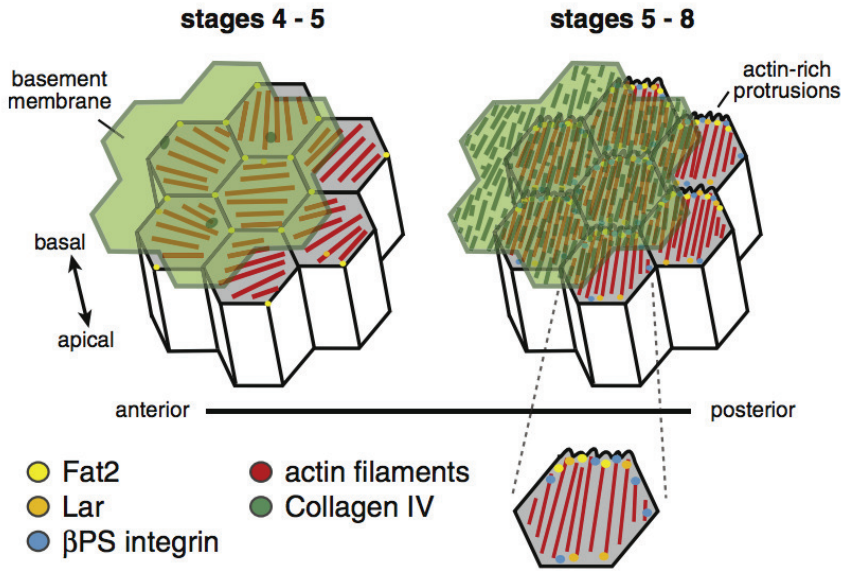

Figure 1.5: Schematic representation of planar polarity in the *Drosophila* egg chamber FC epithelium. During stage 4, the ECM lacks a fibril-like organization and basal actin organization is poorly coordinated across cells. After stage 5, collagen IV displays a tissue-scale fibril-like structuture perpendicular to the A-P axis. Basal actin filaments follow the same organization across the entire tissue. Figure adapted from [8].

of the "molecular corset" hypothesis [1, 40]. In this model, the circumferential arrangement of ECM fibrils and the cytoskeleton promotes preferential elongation along the A-P axis by mechanically constraining growth [43].

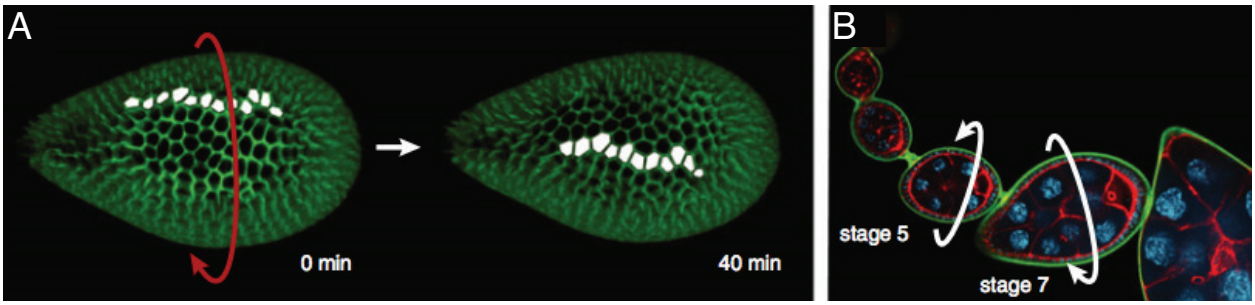

Figure 1.6: *Drosophila* egg chambers undego rotation as a result of migration of the FC epithelium. A) Live imaging of a rotating stage 7 egg chambers. Cells are pseudocolored in white to show advancement. B) Still image of an ovariole depicting rotation stages. Figure adapted from [8].

Importantly, between stages 5 and 8, the egg chamber also displays a form of migration. Follicle cells migrate in a circumferential trajectory, perpendicular to the A-P axis [41] (Figure 1.6). There is evidence that rotation of the egg chamber is driven at the cellular level by the classical mechanisms of cell migration [57], however this remains to be confirmed. In the absence of tissue-scale spatial patterning of actin and the ECM, rotation is blocked, however the causal relationship between cell migration and establishment of tissue-scale planar polarity remains unknown [57, 108, 41].

1.5 Thesis motivation

This work addresses the mechanisms that guide cell migration at different scales. First, the subcellular mechanisms for contact guidance were investigated. In order to carry out this study, a simplified experimental system was developed where ECM geometry is controlled at a micrometer scale. This system enabled the study of the effect of inter-fibrillar spacing on cell shape and migration. To characterize systematically contact guidance phenotypes, quantitative metrics that describe asymmetries in cell shape and migration direction were defined. Additionally, since leading edge protrusion determines migration direction, custom image analysis routines that enable the identification of leading edge protrusions were developed. This allowed the characterization of protrusion dynamics in cells migrating on ECM patterns with different inter-fibrillar spacing. Since the molecular mechanisms that control leading edge protrusion have been well described, this enabled us to disrupt the spatial regulation of leading edge protrusion. By studying the outcome of misregulation of protrusions on contact guidance, we were able to determine the role of lamellipodia regulation during this process. Using this quantitative approach, we arrived at an integrated understanding of contact guidance, where rather than focusing on the effects of a single perturbation to lamellipodial dynamics on shape elongation and directed migration, we established the physical parameters of protrusion that control contact guidance.

Secondly, the relationship between cell migration and tissue scale polarity are explored using *Drosophila* egg chambers as a model system. This work addressed the role of collective cell migration in the development of the cytoskeletal patterning observed in *Drosophila* egg chambers, as well as the cellular mechanisms of migration. While at the tissue scale, FC migration results in rotation of the egg chamber, the mechanisms underlying individual FC migration remained unexplored. Using the vast knowledge that exists on the molecular mechanisms of cell migration, immunofluorescence and live imaging experiments were carried out to determine the molecular machinery responsible for individual FC motility. Once the molecular mechanisms of FC migration were established, this allowed us to perform perturbations to cell motility to shed light into the relationship between migration and the establishment of the tissue level actin pattern. There is compelling evidence that rotation builds the polarized ECM. However, the relationship between rotation and the basal actin bundles remained unknown. By blocking rotation at discrete time points and employing a new quantitative method to characterize actin organization, we determined the requirement of migration for tissue-scale actin polarity at different egg chamber developmental stages.

1.6 Publications

1. The figures and contents of Chapters 2 and 3 were submitted for publication in Fall 2016.

2. The figures and contents of Chapter 4 were first published in Nature Communications [12].

CHAPTER 2

MICROPATTERNING AND QUANTITATIVE IMAGE ANALYSIS AS TOOLS TO STUDY CONTACT GUIDANCE

.

2.1 Preface

All the data presented in this chapter was collected by the author of this document. The experimental design was conceived by the author with critical input from Margaret Gardel and Patrick Oakes. The development and implementation of the quantitative metrics presented in this chapter was done by the author with critical input from Patrick Oakes.

2.2 Introduction

In classical tissue culture conditions all of the external cues provided by structure of the microenvironment are abolished. Novel bioengineering approaches have made possible to recreate *in vitro* certain characteristics of the *in vivo* microenvironment. Several culturing conditions such as cell-derived matrices and hydrogels are capable of recapitulating the micron scale fibrillar structure observed in *in vivo* ECMs [53, 10]. However, in most of these systems, the control of physical parameters such as density, stiffness and composition is not reliable. Therefore to conduct a systematic study of contact guidance, UV micropatterning was developed as a system to isolate the effect of variations in inter-fibrillar spacing on cell migration and elucidate the mechanisms of contact guidance. Using this technique it is possible to have control of both the stiffness and geometry of the microenvironment.

ECM patterns can be created with micrometer precision on PAA by direct exposure of the gel to deep UV (180 nm) through an optical quartz mask [100]. A drop of acrylamide solution

is placed directly on the chromium side of the optical mask and covered with an activated glass coverslip (For a protocol on coverslip activation see [4]). After PAA is polymerized, the sandwich is exposed to deep UV through the micropatterned transparent regions of the optical mask. Deep UVs generate ozone which activate the PAA. The coverslip along with the PAA gel is then removed from the mask and coated with crosslinker and fibronectin, which adsorbs only on the UV-exposed regions (Figure 2.1). The direct contact with the optical mask during PAA polymerization and UV-exposure allows for a faithful reproduction of the spatial features on the mask with subcellular spatial resolution (Figure 2.2).

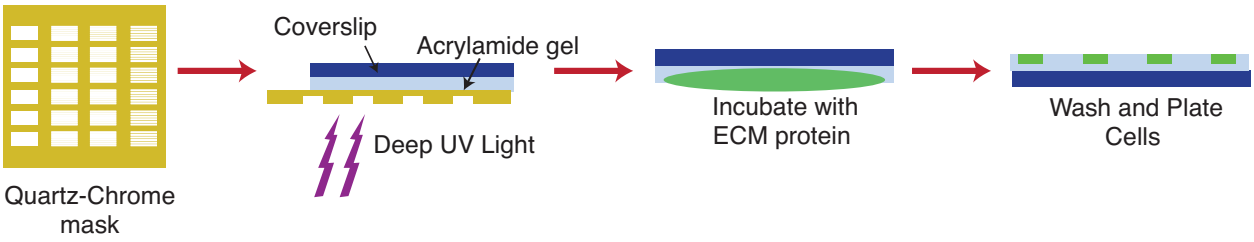

Figure 2.1: Schematic representation of UV micropatterning. PAA gels are polymerized between a coverslip and a Quartz-Chrome mask. After polymerization the sandwich is exposed to UV light, activating the transparent regions in the mask. After removal from the mask, the coverslip and gel are incubated with crosslinker and ECM protein, yielding subcellular resolution micropatterns.

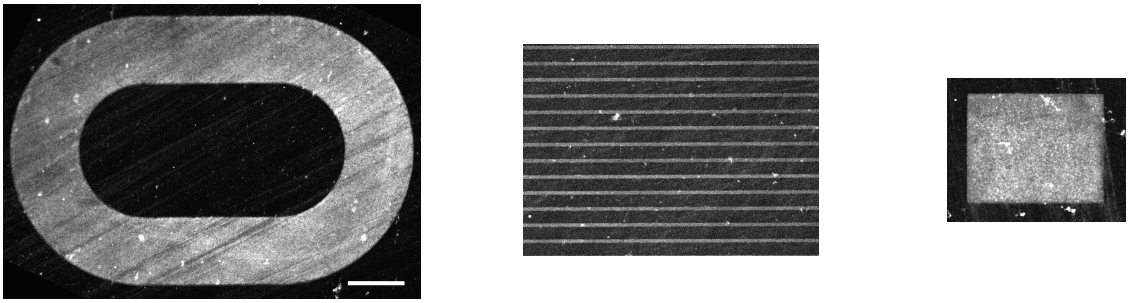

Figure 2.2: Collagen I patterns on PAA. Different shapes can be produced reliably with micrometer resolution. Scale bar= 50μm.

In addition to establishing an experimental system to study contact guidance, quantitative image analysis tools were developed to analyze migration dynamics. During contact guidance cells adjust their shape and migration direction in response to changes in matrix adhesive cues. Therefore, to study contact guidance it is necessary to define metrics that describe cell shape and migration directionality. This chapter describes the experimental system and the metrics developed to describe cell motility in the context of contact guidance, as well as image analysis tools used to track changes in cell protrusion.

2.3 Materials and methods

2.3.1 Cell culture

NIH 3T3 fibroblasts (American Type Culture Collection, Manassas, VA) were cultured in DMEM media (Mediatech, Herndon, VA) and supplemented with 10% FBS (HyClone; Thermo Fisher Scientific, Hampton, NH), 2 mM L-glutamine (Invitrogen, Carlsbad, CA), and penicillin-streptomycin (Invitrogen).

2.3.2 Immunofluorescence

Cells were rinsed in warm cytoskeleton buffer (10 mM MES, 3 mM MgCl2, 1.38 M KCl, and 20 mM EGTA) and then fixed and permeabilized in 4% PFA (Electron Microscopy Sciences, Hatfield, PA), 1.5% bovine serum albumin (Thermo Fisher Scientific), and 0.5% Triton X-100 in cytoskeleton buffer for 15 min at 37C. Coverslips were then rinsed three times in PBS and incubated with Alexa Fluor 488 phalloidin (1:800; Invitrogen), mouse anti-paxillin (1:400; Millipore) and rabbit anti-fibronectin (1:400; Sigma-Aldrich) overnight at 4C temperature. The coverslips were then rinsed 3 times in PBS and incubated for an hour with an AlexaFluor 647 donkey anti-mouse (1:800; Invitrogen) or Alexa Fluor 568 goat anti-rabbit (1:400; Invitrogen) secondary antibodies. Coverslips were mounted on glass slides using the SlowFade Antifade kit (Invitrogen).

2.3.3 UV micropatterning

Micropatterning via deep-ultraviolet illumination on polyacrylamide gels was done according to [74]. Briefly, a chrome-plated quartz photomask (Microtronics, Newtown, PA) was cleaned with water and wiped with 0.5 mL hexane (SigmaAldrich). A polyacrylamide gel mixture (7.5%/0.3% weight percentages of acrylamide/bis-acrylamide) was polymerized for 30 min between the photomask and an activated glass coverslip, yielding a gel with a shear elastic modulus of 8.6 kPa. Once the gel was polymerized, the photomask was placed in a UVO-Cleaner 342 (Jelight, Irvine, CA) and illuminated with a combination of 185- and 254-nm ultraviolet light for 120s. The coverslip and gel were then detached from the photomask by submerging the entire complex in water and gently lifting a corner of the coverslip with a tweezers. Gels were incubated in a solution containing 5 mg/mL EDC (Thermo Fisher Scientific) and 10 mg/mL NHS (Thermo Fisher Scientific) for 15 min. The EDC-NHS solution was then aspirated and replaced with a solution containing 10μg/mL fibronectin in a buffer of HEPES (pH 8.5) for 20 min. Gels were washed with phosphate buffered saline (PBS) and incubated overnight in DMEM before cells were plated.

2.3.4 Microscopy and live cell imaging

For live imaging of migration cells were mounted in a gupton chamber (Warner Instruments, Hamden, CT). Imaging media was supplemented with 10 mM HEPES and 30 mL/mL Oxyrase (Oxyrase Inc., Mansfield, OH). Imaging of migration and spreading was performed on a temperature-controlled inverted Nikon Ti-E microscope with a Lumen 200 Pro light source (Prior) and an HQ2 cooled CCD camera (Roper Scientific) controlled via Metamorph acquisition software (MDS Analytical Technologies). Images were acquired using a 20X or 10X 0.75 Plan Fluor air objective (Nikon).

Fixed samples and cells for protrusion analysis were imaged on an inverted microscope (Ti-E; Nikon, Melville, NY) with a confocal scanhead (CSU-X; Yokogawa Electric, Musashino,

Tokyo, Japan), laser merge module containing 491, 561, and 642 laser lines (Spectral Applied Research, Richmond Hill, Ontario, Canada), and an HQ2 chargecoupled device camera (Roper Scientific, Trenton, NJ). METAMORPH acquisition software (Molecular Devices, Eugene, OR) was used to control the microscope hardware. Images were acquired using a 60X 1.2 NA Plan Apo water-immersion objective or a 20X 0.75 NA Plan Fluor multi-immersion objective (Nikon) or a 20X Plan Fluor air objective.

2.4 Results

2.4.1 UV micropatterning can be used to study the effects of ECM geometry on cell migration

Deep UV micropatterning onto poly-acrylamide (PAA) gels provides an easy method to have combined geometrical and mechanical control of the cellular microenvironment [100, 99]. To study the mechanisms of contact guidance, patterns that reproduced a fibril-like environment were designed. To mimic fibrillar geometry and isolate the effects of variations in inter-fibrillar spacing, we micropatterned parallel lines of fibronectin of a constant width (2 μm). The spacing between lines varied from 0 to 10 μm (Figure 2.3). These dimensions were chosen such that NIH 3T3 fibroblasts were able to spread on multiple lines and the width of each line was large enough for typical focal adhesion formation [25, 56].

To test the designed patterns, fibronectin was patterned onto PAA gels and NIH 3T3 fibroblasts were plated onto these substrates. Immunofluorescence of fibronectin and paxillin confirmed that focal adhesions were excluded from unpatterned regions and formed on fibronectin stripes, allowing cells to attach to several pattern features (Figure 2.4).

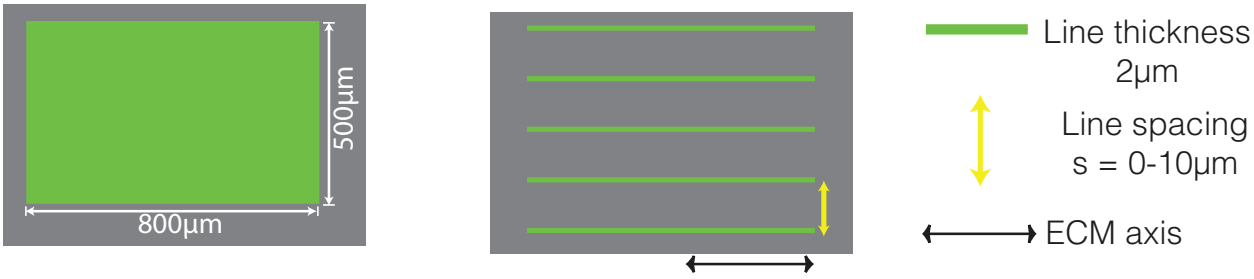

Figure 2.3: Schematic representation of patterns used to mimic fibrillar ECM. Large rectangular regions where patterned by uniformly coating with ECM or with parallel lines. Line thickness was maintained constant for all patterns (2 μm), while line spacing for different patterns was varied between 0 and 10 μm.

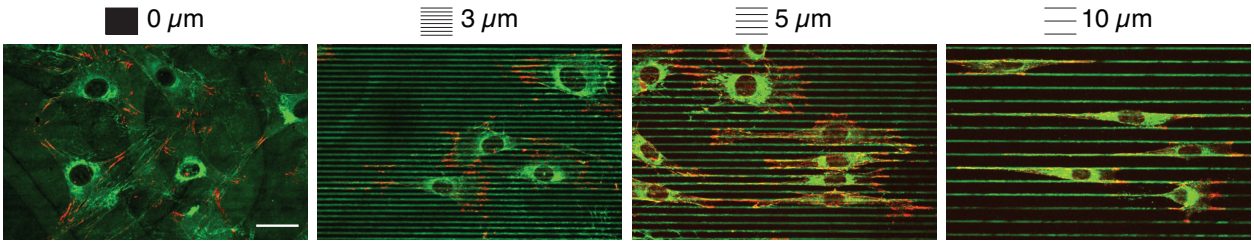

Figure 2.4: Cells plated on fibronectin micropatterns visualized by immunofluorescence. Green channel shows Fibronectin localization. Red channel shows the localization of paxillin. Legend on top shows the line spacing for each pattern. Scale bar=20 μm.

2.4.2 Characterization of cell shape

One of the characteristic phenotypes of contact guidance are changes in cell morphology [80]. To determine if the changes in ECM geometry imposed by the designed patterns had an impact on cell morphology, we stained cells plated on structured substrates with phalloidin. Fibroblasts plated on uniformly coated substrates (0μm spacing) acquired a characteristic polarized morphology with no preferred directional orientation [66] . By contrast, on all line patterns cells elongated and became preferentially aligned to the ECM (Figure 2.5).

Interestingly, cells appeared to elongate and orient parallel to the ECM as the spacing between lines in the patterns increased. To measure these differences in cellular phenotypes across patterns, we defined two metrics to describe changes in cell morphology. Fixed sam-

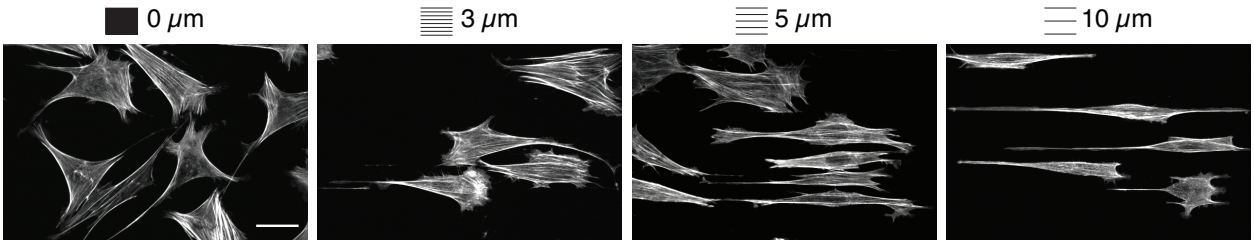

Figure 2.5: Actin cytoskeleton of cells plated on fibronectin micropatterns visualized by phalloidin staining. Legend on top shows the line spacing for each pattern. Scale bar=20 μm.

ples of cells on patterns with phalloidin labelled F-actin were thresholded in Matlab to obtain a mask representing the cell. The built in "regionprops" function was used to fit an ellipse to each cell mask and obtain its major (b) and minor (a) axes. Cell shape elongation was defined by the ratio b/a. Orientation was defined as $\langle cos^2(\theta) \rangle$, where θ is the angle between a line parallel to the ECM and the long axis, b, of the cell ellipse.

Characterization of cell shape using these two metrics showed that cell elongation increased linearly with line spacing (Figure 2.6 A), without significant changes to spread area (Figure 2.6 B). Orientation increased sharply from 0 to 2μm spacing, with a mean orientation with respect to the ECM lines of 0.62 out of a maximum possible value of 1. The orientation between 2 and 10μm then slowly increased until it reached a mean value of 0.9596, indicating almost complete alignment with the ECM (Figure 2.6 C) . Thus, fibril spacing controls cell shape and orientation.

2.4.3 Characterization of migration dynamics

During cell migration the axis of cell shape polarization corresponds the direction of migration [80, 55]. Since cells oriented their long axis parallel to the ECM, we next analyzed spontaneous cell migration. To this end, cells were plated on ECM patterns and were allowed to attach to the substrate for four hours. After this time, live cell imaging was performed at

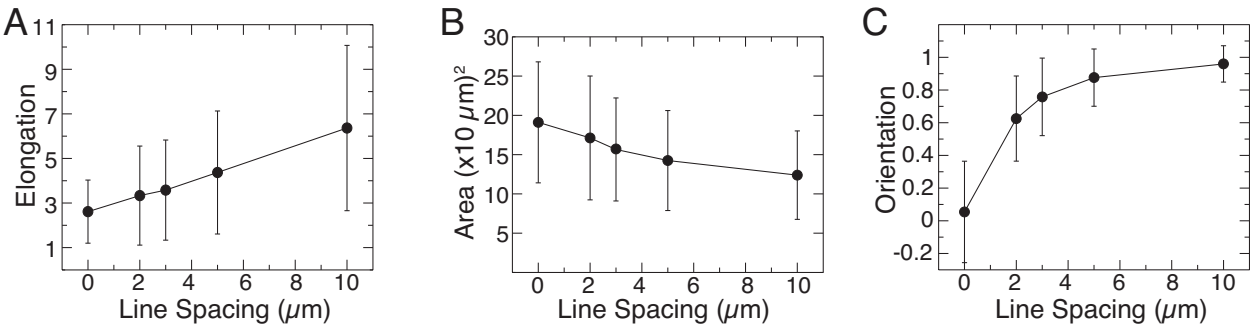

Figure 2.6: Quantification of cell shape elongation, area and orientation. A) Quantification of cell shape elongation as a function of ECM pattern line spacing. Elongation is measured by taking the ratio of the long over short cellular axes. Mean and s.d. are plotted. B) Quantification of cell area as a function of ECM pattern line spacing. Mean and s.d. are plotted. C) Quantification of cell shape orientation as a function of ECM pattern line spacing. Orientation is determined by measuring the angle θ between the long axis of the cell and a line parallel to the ECM and calculating $\langle cos^2(\theta)\rangle$. Mean and s.d. are plotted.

10 minute intervals to obtain 10 hour long movies of cell migration. Cells where manually tracked using the Manual tracking plugin in ImageJ. Figure 2.7 shows rose plots of the trajectories of ≈100 cells during a period of 10 hours.

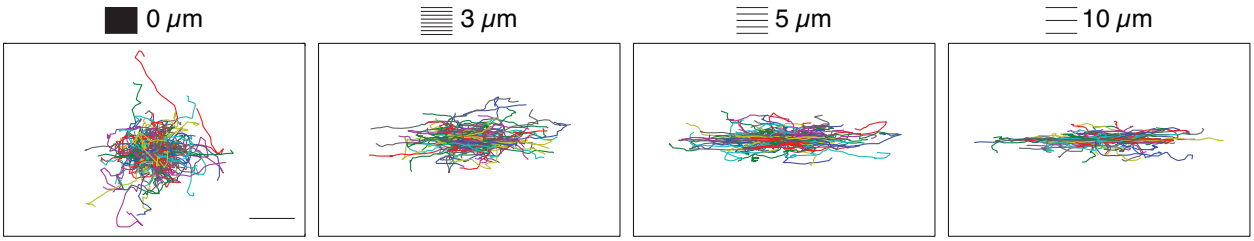

Figure 2.7: Migration trajectories of cells on uniform (0μm) and linear ECM patterns. Line spacing is indicated by legend on top. Scale bar=100 μm.

Migration dynamics of cells on patters were characterized by the mean speed of migration and a guidance parameter that was defined to score the directionality of migration relative to the ECM. The instantaneous speed was measured from cell displacements at 20 minute intervals. For each cell the mean of the instantaneous speed over a period of 10 hours was considered as the representative speed measure. To assess directionality of migration we

analyzed cell trajectories over a period of 10 hours. For each time step in a trajectory we calculated the angle θ , between the displacement vector of a cell and the ECM. We defined a guidance g parameter such that:

$$g(t) = \begin{cases} 0, & \text{if } \theta \geq 25 \\ 1, & \text{if } \theta \leq 25 \end{cases}$$

for every displacement in a cell's trajectory. Once guidance values were obtained we calculated the mean guidance as a function of lag time according to:

$$g(\tau) = \sum_{t-t_i}^{t_i+\tau} g(t)/\tau$$

Figure 2.8 shows the guidance values plotted as a function of lag time τ, for the trajectories of the cells shown in Figure 2.7. The guidance value increases as a function of lag time up to $\approx$ 160 minutes, becoming flat afterwards. The guidance value at τ=320 was considered a representative measure of the orientation of the trajectories relative to the ECM since around this value the curves for all line spacings are flat.

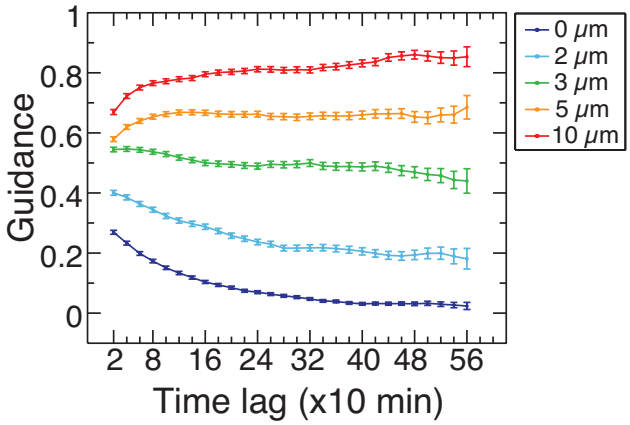

Figure 2.8: Guidance as a function of lag time for cells plated on patterns with different line spacings.

Using these metrics, the mean speed of migration and migration guidance were calculated for cells migrating on patterns with different line spacings. Strikingly, the instantaneous migration speed was unaffected over the range of line spacings measured (Figure 2.9 A). However, cell trajectories became oriented parallel to the ECM with increasing line spacing. The guidance parameter demonstrates that migration direction becomes increasingly parallel to the ECM as a function of line spacing, having its sharpest increase from 2 to 3μm (Figure 2.9 B). Taken together these results demonstrate that micrometer-scale variations in fibril-like spacing, from 2 to 3μm, can direction of cell migration parallel to the ECM, without affecting the speed of migration.

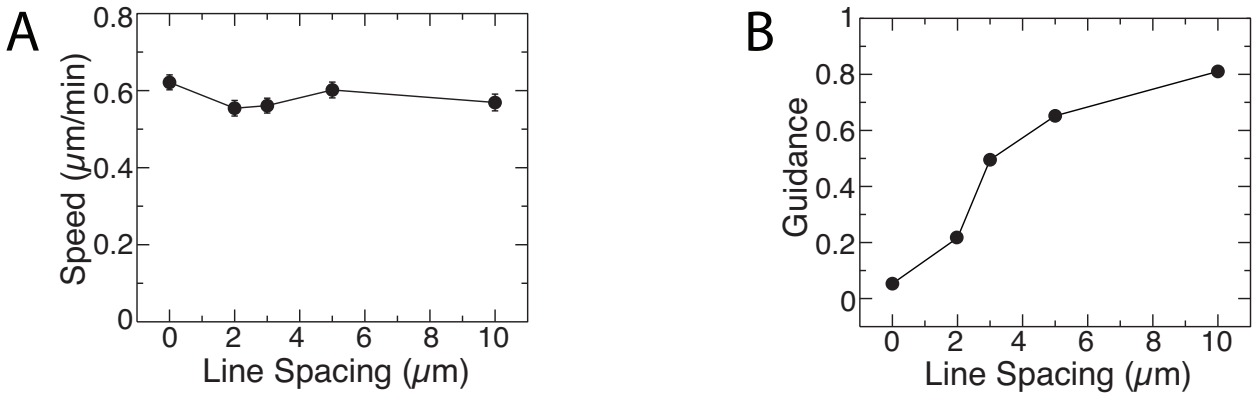

Figure 2.9: Quantification migration dynamics. A) Quantification of migration speed as a function of ECM pattern line spacing. Mean of the average cell speed for n>100 cells and s.e.m. are plotted. B) Quantification of migration directionality (guidance) as a function of ECM pattern line spacing. A guidance value of 1 indicates migration parallel to the ECM. Guidance for τ= 320 min is plotted.

2.5 Quantification of spatial organization of leading edge protrusion

In the previous sections, it was established that cells are sensitive to changes in ECM geometry at the micrometer scale (Figure 2.6, 2.9). In order to study the subcellular mechanisms underlying this behavior, it is also necessary to describe migration dynamics at this scale. Cell migration at the micrometer scale is controlled primarily by leading edge protrusion dynamics [35], therefore a method to describe the spatial organization of cell protrusion quantitatively was developed.

To investigate cell protrusion dynamics for cells migrating on patterns, we followed shape changes in cells with minute time resolution. To facilitate the identification of the cell edge, cells were transfected with the fluorescent membrane marker GFP-stargazin (Figure 2.10 A). From live cell imaging movies, contours of each cell were obtained by thresholding GFP-stargazin imaging (Figure 2.10 B). Contour plots showed an apparent change in the spatial localization of leading edge protrusions.

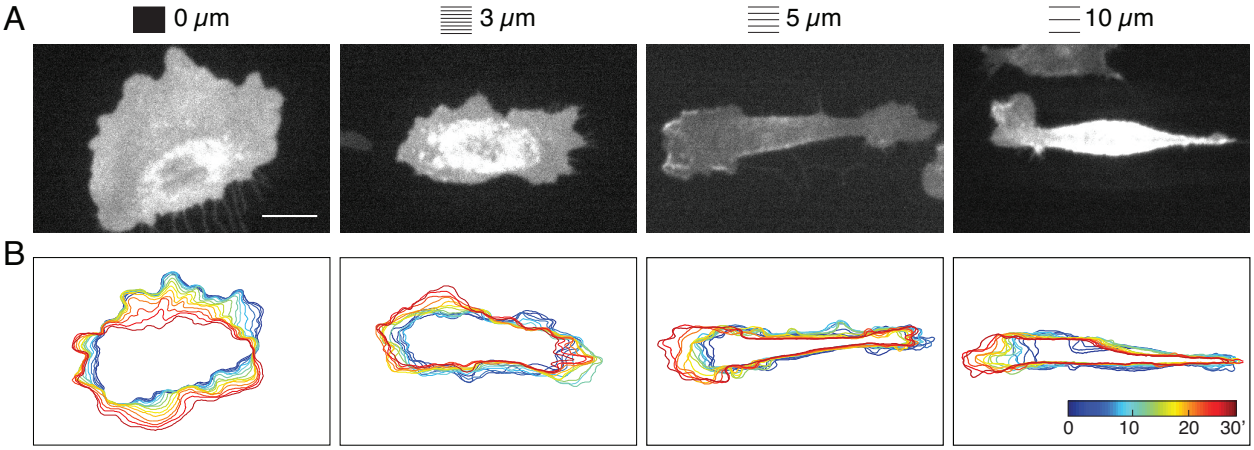

Figure 2.10: A) Fluorescence images of cells transfected with GFP-stargazin on linear ECM patterns. B) Contour plots showing cell shape changes during a 30 minute time interval of migration. Line spacing is indicated by legend on top. Scale bar= 20μm

To characterize protrusion dynamics quantitatively custom Matlab software was developed to identify the areas of leading edge growth. Protrusions were defined as regions where area increased between contours at times t and t+2 min (Figure 2.11 A, B). This time interval was chosen to avoid tracking leading edge fluctuations and following only stable, longer lived protrusions. Each protrusion was then described by two physical parameters: area and orientation relative to the ECM. Areas of protrusions were obtained using the built in "regionprops" function in Matlab. Orientation with respect to the ECM pattern was determined by calculating $S = \langle cos^2(\theta) \rangle$, where θ is the angle between a parallel to the ECM and the line defined by the centroid of the cell and the centroid of the protrusive region (Figure 2.11 C). The average was calculated over the angles of all protrusions that occur in a single cell during a 30-minute time interval. Since ECM patterns are symmetric with respect to the y-axis, angles greater than 90 were reflected across the y-axis such that $\theta \in [0, 90]$.

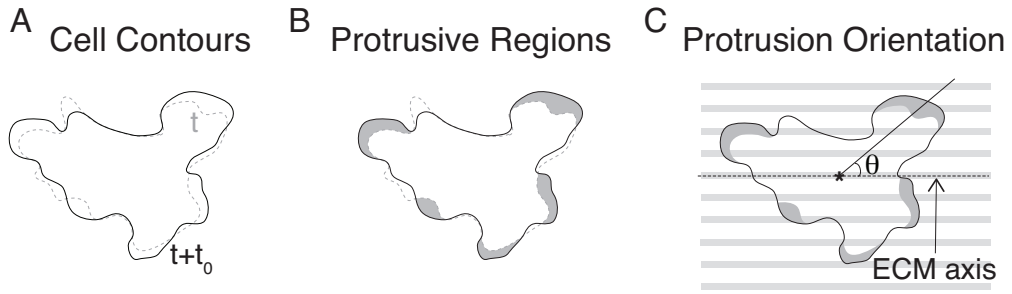

Figure 2.11: Schematic representation of leading edge protrusion analysis. A,B) From cell contours, at time t and $t + t_0$, areas of leading edge growth are identified as protrusions. C) Protrusion orientation is quantified by measuring the angle θ between a line connecting the protrusion center with the cell center and a parallel to the ECM. Final orientation values are obtained by calculating $S = \langle cos^2(\theta) \rangle$, where the average is taken over all cellular protrusions that occur during a period of 30 minutes.

Characterization of leading edge protrusion for cells migrating on line patterns revealed that their average area was unaffected by changes in line spacing (Figure 2.12 A). However, as the line spacing increased, protrusions became oriented with respect to the ECM lines (Figure 2.12 B). This result suggests that contact guidance is predominantly regulated by the

spatial control of protrusions, rather than its overall magnitude. This is particularly true at smaller line spacings, since these results don't rule out the possibility that at larger spacings protrusion size could limit migration perpendicular to the ECM.

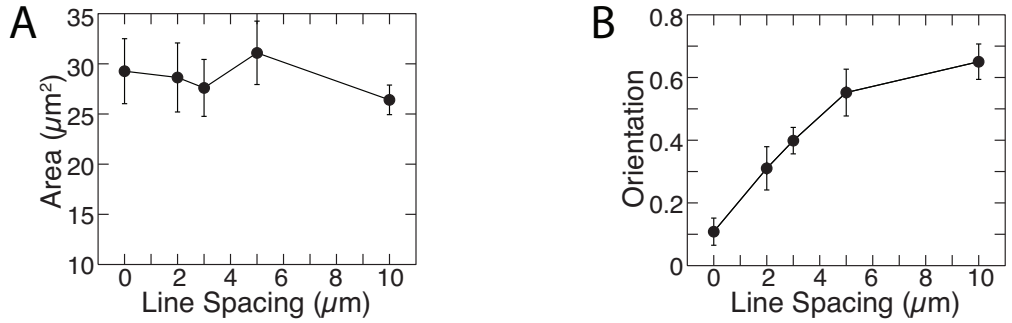

Figure 2.12: Quantification of leading edge protrusion. A) Area of individual cell protrusions as a function of ECM line spacing. Mean and s.e.m. are plotted for $n \geq 12$ cells. B) Orientation of individual cell protrusions as a function of ECM line spacing. Mean and s.e.m are plotted for $n \geq 12$ cells.

2.6 Discussion

The ability of cells to change shape and direct their migration in response to ECM geometric cues has been characterized for decades and remains an area of active research [116, 20, 96, 26, 69, 23]. Recent advances in micropatterning have allowed the subcellular control of ECM geometrical cues, however a systematic study that characterized the influence of a single geometrical parameter on cell shape and migration had been lacking. In this work, UV micropatterning was established as an experimental system to study systematically the impact of micrometer changes in inter-fibrillar spacing on cell shape and migration direction. Patterning parallel arrays of fibronectin lines showed that micrometer-scale variations in fibril-like spacing, from 2 to 3μm, can tune cell shape and bias the direction of cell migration parallel to the ECM. Central to these results was the development of quantita-

tive metrics to describe migration and cell shape orientation. Since the goal of this project was to elucidate the subcellular mechanisms of contact guidance, additional metrics were developed to describe migration dynamics at the micrometer scale. Measurements of leading edge protrusion area and orientation showed that protrusions aligned parallel to the ECM as line spacing was increased. Altogether these results point to spatial control of protrusions as the subcellular scale mechanism underlying contact guidance. To further investigate this hypothesis in the next chapter the effect of perturbations to the regulation of protrusive activity is explored. The metrics developed in this chapter are used to compare migration and protrusion phenotypes across different experimental conditions.

CHAPTER 3

UNDERSTANDING THE SUBCELLULAR MECHANISMS OF CONTACT GUIDANCE

3.1 Preface

All the data presented in this chapter was collected by the author of this document. The experimental design was conceived by the author with critical input from Margaret Gardel and Patrick Oakes. The development and implementation of the quantitative metrics presented in this chapter was done by the author with critical input from Patrick Oakes.

3.2 Introduction

During cell migration the spatial organization of cell protrusive activity is controlled by numerous intra- and extra- cellular cues [13, 85]. Most relevant to this work, are the well-established feedbacks between cell shape [48, 33, 28, 79] and cell-matrix adhesion to local protrusive activity [116, 71] (Figure 3.1).

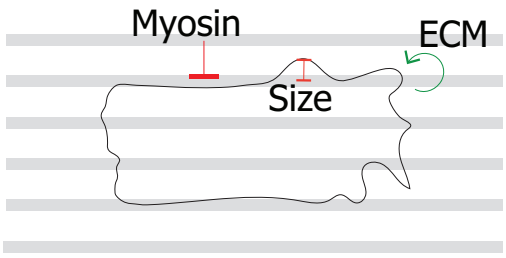

Figure 3.1: Subcellular feedbacks that regulate cell migration. Myosin II contractility inhibits protrusion at sites of low cellular curvature. Protrusion formation is stimulated at sites of ECM adhesion through focal adhesion signaling. The physical dimensions of the lamellipodia could limit protrusion stabilization perpendicular to the ECM.

The feedback between cell shape and protrusion regulation is mediated by myosin II contractility. Myosin II preferentially assembles onto cortical regions of minimal surface curvature

while also acting to minimize curvature. Perturbations of Rho/ROCK signalling or myosin II ATPase function disrupt curvature minimization and protrusion regulation [28]. Similarly on patterned substrates, treatment with blebbistatin, a myosin II inhibitor, has been linked to loss of polarity and disassembly of stress fibers [48].

Another major regulator of protrusion is the small GTPase Rac1. Rac activity controls the several aspects of leading edge protrusion including formation, growth and size [88, 78, 72]. Spatial regulation of Rac activity is crucial for cell migration, high levels of Rac have been previously shown to impede directed migration by promoting the formation of several lamellipodial fronts [78]. Activation of Rac can be achieved through several pathways, of particular interest to this work is Rac activation by adhesion signalling [15, 18]. Positive feedback between sites of new adhesion and protrusion formation is controlled by PAK-mediated changes in paxillin phosphorylation, which recruit the Rac GEF β-pix [71] to adhesion sites. Knockdown of β-pix has been linked to defects in leading edge protrusion dynamics, causing an increased number of lamellipodia protrusions and defects in directed migration [54, 77]. Downstream of Rac1 activation, lamellipodia construction depends on the activity of the the Arp2/3 complex [115, 93]. Depletion of Arp2/3 results in decreased lamellipodia protrusion [115].

Our previous results show that in fibril-like environments cells align leading edge protrusions parallel to the ECM (Figure 2.12). Since cells are sensitive to changes in the ECM geometry at the scale of the lamellipodia, the importance of this organelle in the regulation of contact guidance will be studied in this chapter. Figure 3.1 shows the relevant mechanisms responsible for spatial regulation of protrusion in this context. In this chapter, the importance of these feedbacks will be investigated by perturbing molecularly these distinct modules. The effects of these molecular perturbations on contact guidance will be characterized using the migration metrics described in the previous chapter. Furthermore, to

understand the origin of these migration phenotypes, leading edge protrusion dynamics will be analyzed quantitatively.

3.3 Materials and Methods

3.3.1 Cell culture and reagents

NIH 3T3 fibroblasts (American Type Culture Collection, Manassas, VA) were cultured in DMEM media (Mediatech, Herndon, VA) and supplemented with 10% FBS (HyClone; Thermo Fisher Scientific, Hampton, NH), 2 mM L-glutamine (Invitrogen, Carlsbad, CA), and penicillin-streptomycin (Invitrogen). The ARP2/3 inhibitor CK-666 and control compound CK-689 was purchased from Calbiochem. Y-27632 was purchased from Sigma-Aldrich. Cells were plated for 4 hours and then incubated for 3 hours in CK-666 or 45 minutes in Y-27632 before imaging or fixation at the concentration indicated for all experiments. Cells were transiently transfected with plasmid DNA constructs encoding GFP-Stargazin (a gift from A. Karginov, University of Illinois at Chicago, Chicago, IL) and RacQ61L (a gift from the G. Borisy Laboratory, Northwestern University). Transfections were performed using a Neon electroporation system (Invitrogen).

3.3.2 KD by sh-RNA

shRNA construct sets for mouse β-pix (GIPZ Arhgef7 shRNA set) were purchased from from Dharmacon, through Thermofisher. Transfection of constructs was performed using a Neon electroporation system (Invitrogen). Puromycin and fluorescence selection of expressing cells were performed per the manufacturers protocols. Knock down efficiency was determined by Western blotting, and a stable cell line was maintained for the V3LMM_521424 clone.

3.3.3 UV micropatterning

Micropatterning via deep-ultraviolet illumination on polyacrylamide gels was done according to [4]. Briefly, a chrome-plated quartz photomask (Microtronics, Newtown, PA) was cleaned with water and wiped with 0.5 mL hexane (SigmaAldrich). A polyacrylamide gel mixture (7.5%/0.3% weight percentages of acrylamide/bis-acrylamide) was polymerized for 30 min between the photomask and an activated glass coverslip, yielding a gel with a shear elastic modulus of 8.6 kPa. Once the gel was polymerized, the photomask was placed in a UVO-Cleaner 342 (Jelight, Irvine, CA) and illuminated with a combination of 185- and 254-nm ultraviolet light for 120s. The coverslip and gel were then detached from the photomask by submerging the entire complex in water and gently lifting a corner of the coverslip with a tweezers. Gels were incubated in a solution containing 5 mg/mL EDC (Thermo Fisher Scientific) and 10 mg/mL NHS (Thermo Fisher Scientific) for 15 min. The EDC-NHS solution was then aspirated and replaced with a solution containing 10g/mL fibronectin in a buffer of HEPES (pH 8.5) for 20 min. Gels were washed with phosphate buffered saline (PBS) and incubated overnight in DMEM before cells were plated.

3.3.4 Immunofluorescence

Cells were rinsed in warm cytoskeleton buffer (10 mM MES, 3 mM MgCl2, 1.38 M KCl, and 20 mM EGTA) and then fixed and permeabilized in 4% PFA (Electron Microscopy Sciences, Hatfield, PA), 1.5% bovine serum albumin (Thermo Fisher Scientific), and 0.5% Triton X-100 in cytoskeleton buffer for 15 min at 37C. Coverslips were then rinsed three times in PBS and incubated with Alexa Fluor 488 phalloidin (1:800; Invitrogen), mouse anti-paxillin (1:400; Millipore) and rabbit anti-fibronectin (1:400; Sigma-Aldrich) overnight at 4C temperature. The coverslips were then rinsed 3 times in PBS and incubated for an hour with an AlexaFluor 647 donkey anti-mouse (1:800; Invitrogen) or Alexa Fluor 568 goat anti-rabbit (1:400; Invitrogen) secondary antibodies. Coverslips were mounted on glass slides using the SlowFade Antifade kit (Invitrogen).

3.3.5 Microscopy and live cell imaging

For live imaging of migration cells were mounted in a gupton chamber (Warner Instruments, Hamden, CT). Imaging media was supplemented with 10 mM HEPES and 30 mg/mL Oxyrase (Oxyrase Inc., Mansfield, OH). Imaging of migration and spreading was performed on a temperature-controlled inverted Nikon Ti-E microscope with a Lumen 200 Pro light source (Prior) and an HQ2 cooled CCD camera (Roper Scientific) controlled via Metamorph acquisition software (MDS Analytical Technologies). Images were acquired using a 20X or 10X 0.75 Plan Fluor air objective (Nikon).

3.4 Results

3.4.1 Leading edge protrusions are oriented parallel to the ECM on line patterns via Myosin II contractility and ECM feedback

In the previous chapter, it was found that orientation of migration and protrusion parallel to the ECM, occurs concomitantly with changes in cell shape. Therefore, to determine the relative contributions of the feedbacks between cell shape and cell-matrix adhesion to local protrusive activity, the initial stages of cell spreading were analyzed.

During spreading, cells undergo rapid, Rac1-mediated isotropic spreading after initial attachment [83, 114]. Live imaging revealed that on uniformly coated substrates cells spread isotropically, by contrast, cells spread anisotropically on line patterns and quickly orient their long axis along linear patterned features (Figure 3.2).

The rapid orientation of cell shape upon ECM attachment suggests that positive feedback with the ECM may be sufficient to guide protrusion dynamics, even in the absence of myosin II-mediated regulation, that could contribute in elongated cells. To determine the role of myosin-II activity in the ability of cells to orient along ECM lines during initial spreading, we observed spreading dynamics in cells treated with 20 μM of the Rho kinase (ROCK)

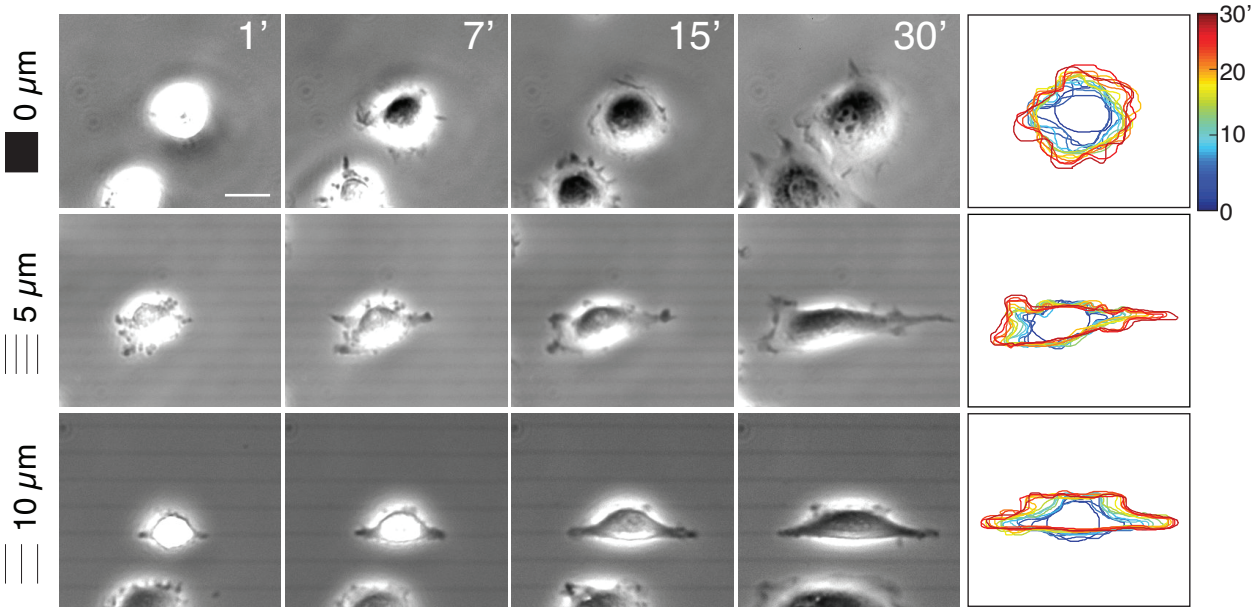

Figure 3.2: Representative images from time-lapse phase contrast microscopy of NIH 3T3 fibroblasts spreading on uniform (0μm) and ECM striped patterns spaced by 5 and 10μm respectively. Images correspond to 1, 5, 10, 15 and 30 minutes, contour plots show entire time lapse. Scale bar=20μm.

inhibitor Y-27632. ROCK inhibited cells failed to orient parallel to the ECM, spreading isotropically in line patterns. (Figure 3.3).

To compare quantitatively the spreading phenotypes of control and ROCK-inihibited cells, area, elongation of cell shape and orientation were measured. First, it was noted that spreading dynamics were not altered by ECM patterning since cell area increased at the same rate for all cells (Figure 3.4 A). Remarkably, control cells spread anisotropically on line patterns within four minutes after initial contact with the ECM (Figure 3.4 C). After initial orientation, cells elongated gradually, notably elongation continued to increase even after cells had reached their maximum spread area (Figure 3.4 A, B). The rapid orientation of cell shape upon ECM attachment suggested that positive feedback with the ECM may be sufficient to guide protrusion dynamics, even in the absence of myosin II-mediated regulation. However, ROCK inhibited cells failed to elongate during spreading on all line spacings (Figure 3.4 B). Furthermore, cells had severe defects orienting parallel to the ECM (Figure 3.4 C), achiev-

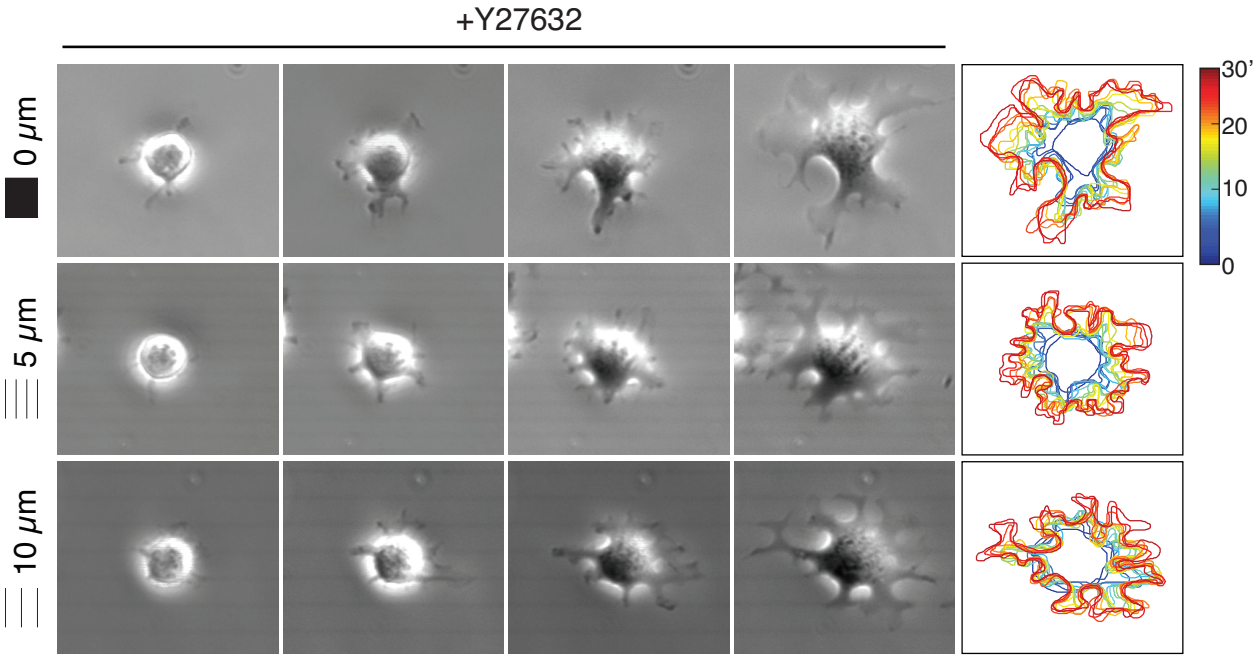

Figure 3.3: Representative images from time-lapse phase contrast microscopy of NIH 3T3 fibroblasts spreading on uniform (0 μm) and ECM striped patterns spaced by 5 and 10μm respectively. Cells were treated with 20 μM Y-27632 upon assembly of imaging chamber. Images correspond to 1, 5, 10, 15 and 30 minutes, contour plots show entire time lapse. Scale bar=20μm.

ing orientation only at 10μm spacing at later times during spreading, showing that ECM feedback is not sufficient to direct protrusions parallel to the ECM.

Altogether these results suggest that spatial regulation of protrusion on structured ECM is dependent on ROCK-mediated contractility. However, the data does not exclude the possibility that sites of new adhesion formation can localize the extension of new protrusions parallel to the ECM.

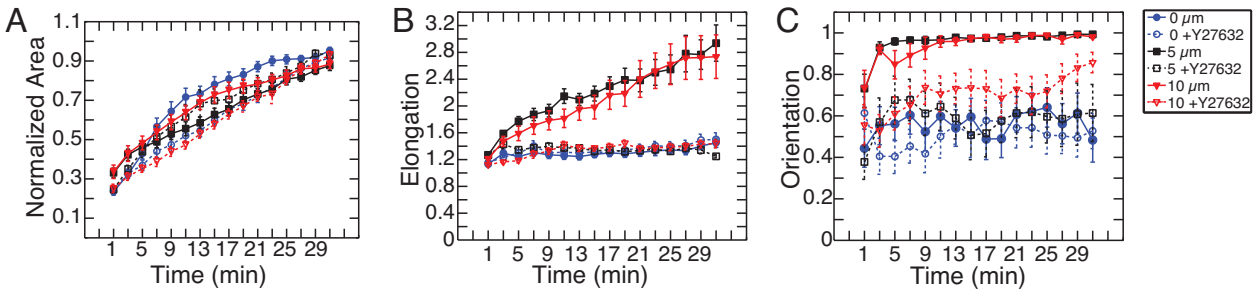

Figure 3.4: Quantification of cell spreading for control and Y-27632 treated cells for 0μm, 5μm and 10μm spacings. Mean and s.d. are plotted for n$\geq$15 cells. A) Cell area as a function of time during cell spreading for all ECM patterns. For each time point areas are normalized to the maximum cell area. B) Cell shape elongation during spreading. C) Cell shape orientation as a function of time.

3.4.2 Misregulation of protrusive activity due to inhibition of Myosin II contractility impairs contact guidance

Since ROCK-mediated contractility was required to polarize cells during spreading, we next explored its role in contact guidance. We first analyzed the shape of fully spread cells after treatment with ROCK inhibitor for 45 minutes. Consistent with the characteristic morphology of ROCK-inhibited cells, cells often had multiple protrusive fronts and a tail retraction defect (Figure 3.5 A) [76].

In contrast to WT cells, ROCK-inhibited cells did not elongate further when placed on line patterns (Figure 3.6 A) However, these ROCK-inhibited cells exhibited a similar tendency to orient along the ECM fibril axis as WT cells (Figures 3.5 A, 3.6 B). During cell migration the axis of cell shape polarization corresponds to the direction of migration. Despite this, migration directionality was severely affected in ROCK-inhibited cells (Figure 3.5 B). Similar to control cells, the trend in guidance was to increase as a function of line spacing. However, guidance values dropped by half their value relative to controls, being reduced from 0.8 to 0.4 at the largest line spacing (Figure 3.6 C).

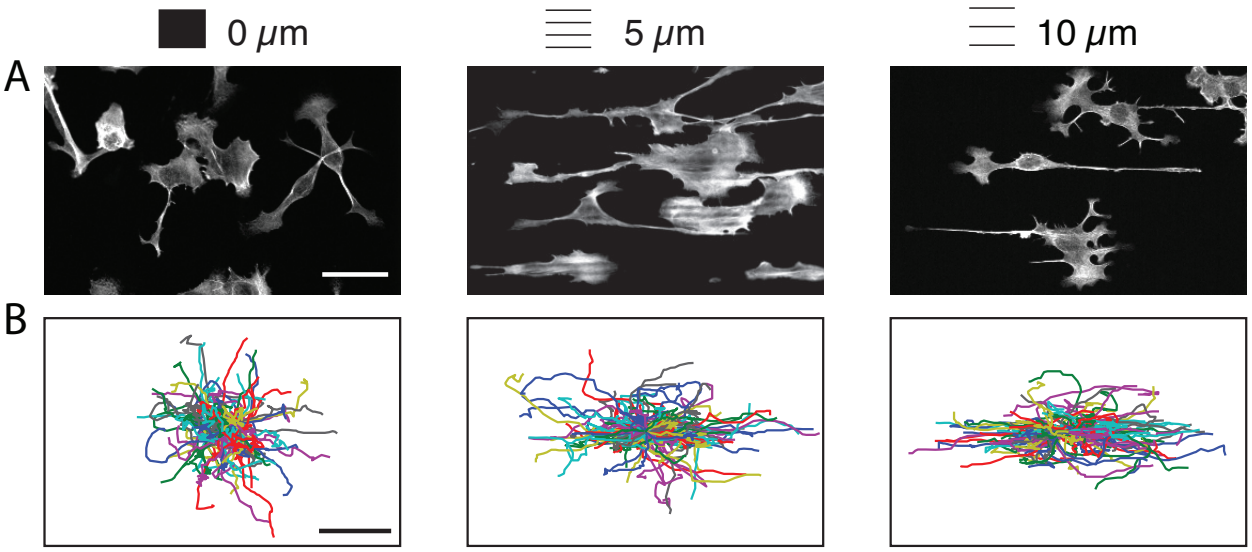

Figure 3.5: Effects of contractility inhibition on contact guidance. A) Representative images of F-actin visualized by fluorescent phalloidin for cells on linear ECM linear patterns. Cells shown were treated with 20μM Y-27632 . Top legend indicates spacing. Scale bar=20μm. B) Migration trajectories of cells on uniform (0μm) and linear ECM patterns. Cells were treated with 20μM Y-27632. Scale bar =100μm.

To determine the mechanisms causing the migration guidance defect in ROCK-inhibited cells, we analyzed protrusions using the method described in the previous chapter. Consistent with known effects of ROCK-inhibition, cells had disorganized protrusions and poorly defined leading edge fronts (Figure 3.7 A). Protrusion area doubled relative to controls for spacings smaller that 10μm (Figure 3.7 B). More strikingly, protrusions failed to organize parallel to the ECM as shown by a sharp decrease in orientation for line spacings smaller than 10μm (Figure 3.7 C). Compared to control cells, the orientation of protrusions diminished by 50% (Figure 3.7 C). Altogether these results show that ROCK-mediated contractility is necessary to organize protrusions spatially in response to structured ECM, promoting contact guidance. Previous work suggested that inhibition of Myosin II contractility reduced the response of cells to ECM surface micro- and nano- topography [90, 30]. Our results demonstrate that the mechanism is likely through the important role of ROCK-mediated contractility in spatial organization of protrusions [59]. To further establish spatial regulation of protrusion as the underlying mechanism for contact guidance, we next explored the impact of more direct

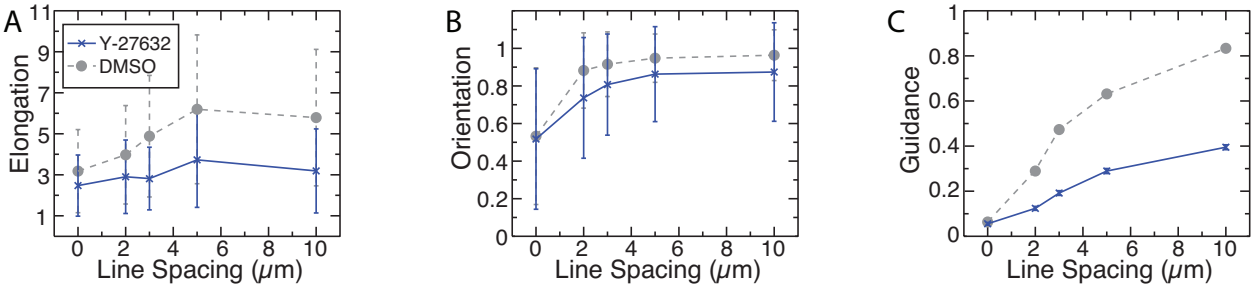

Figure 3.6: Quantification of the effects of contractility inhibition on contact guidance. A) Cell shape elongation as a function of line spacing for cells treated with 20μM Y-27632 (solid line). Dashed line shows elongation for control cells treated with DMSO. B) Cell shape orientation as a function of line spacing for cells treated with 20μM Y-27632 (solid line). Dashed line shows orientation for control cells treated with DMSO. C) Cell migration guidance as a function of ECM pattern line spacing for cells treated with 20μM Y-27632 (solid line). Dashed line shows guidance for control cells treated with DMSO.

perturbations on the regulation of leading edge protrusive activity.

3.4.3 Perturbations to protrusive activity via misregulation of Rac1 impair contact guidance

Spatial regulation of Rac activity controls the formation, growth and size of leading edge protrusions [88, 78, 72]. High levels of Rac activity have been previously shown to impede directed migration by promoting the formation of several lamellipodial fronts [78]. Therefore, to promote global activation of Rac and disrupt the spatial regulation of lamellipodia formation, we expressed the constitutively active form RacQ61L. RacQ61L cells were rounder (Figure 3.8 A), as shown as by the 50% decrease in elongation for all line spacings relative to WT cells (Figure 3.8 C). Elongation values in these cells were greater than one, allowing us to define a long axis to measure cell shape orientation (Figure 3.8 C). Intriguingly, orientation values in RacQ61L cells were comparable to wild type cells (Figure 3.8 D). In contrast, migration trajectories were no longer parallel to the ECM (Figure 3.8 A), except at 10μm line spacing where cells exhibited limited guidance (Figure3.8 E). The defect in guidance

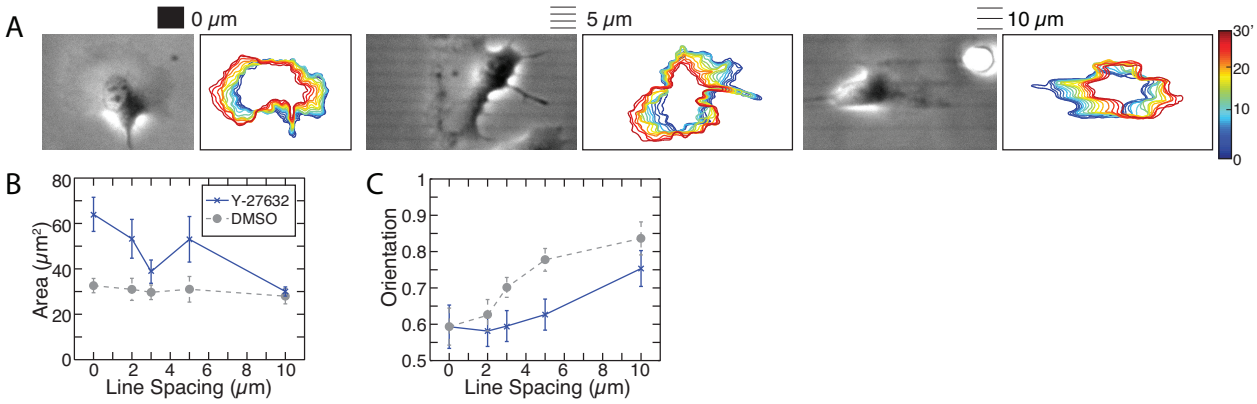

Figure 3.7: Quantification of leading edge protrusion area and direction in Y-27632 treated cells. A) Phase contrast images of cells on linear ECM patterns treated with 20μM Y-27632. Legend on top indicated line spacing. Scale bar=20μm. Contour plots show cell outlines for a 30 minute time interval during migration. Scale bar=20μm. B) Area of individual cell protrusions as a function of ECM line spacing for cells treated with 20M Y-27632 (solid line). Dashed line shows orientation for control cells treated with DMSO. Mean and s.e.m. are plotted for n$\geq$8 cells. C) Orientation of individual cell protrusions as a function of ECM line spacing for cells treated with 20μM Y-27632 (solid line). Dashed line shows orientation for control cells treated with DMSO. Mean and s.e.m are plotted for n$\geq$8 cells.

was more pronounced than for ROCK inhibited cells, since for all line spacings, guidance in RacQ61L cells was reduced by at least 50% (Figure 3.8 E).

To determine how protrusive activity was altered in cells expressing RacQ61L, we next measured area and orientation of leading edge protrusions. First, we noticed that cells exhibited protrusions around the entire cell body (Figure3.9 A). Measurements showed that protrusion areas in these cells were comparable or lower than wild type cells (Figures 3.9 B). By contrast, protrusions failed to orient parallel to the ECM as a function of line spacing (Figure 3.9 C), decreasing in orientation by 60% or greater relative to wild type cells (Figure 3.9 C). This trend of protrusion orientation mimics the trend observed for guidance (compare Figures 3.8 E and 3.9 C), demonstrating that the ability of cells to migrate parallel to the ECM relies heavily on biasing protrusive activity in the direction parallel to the lines.

Another major regulator of protrusive activity relevant to our context is the positive feed-

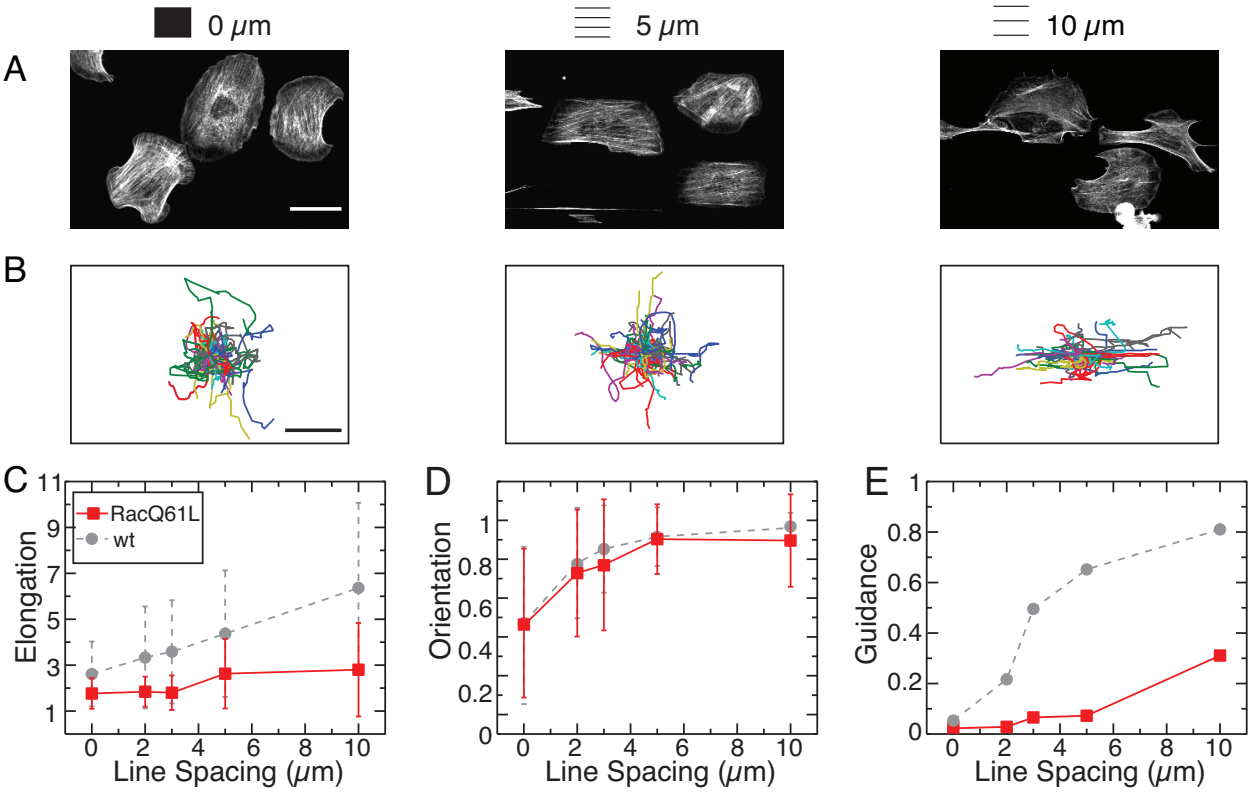

Figure 3.8: Effects of misregulation of Rac on contact guidance. A) Representative images of F-actin visualized by fluorescent phalloidin for cells on linear ECM patterns. Cells shown were transfected with RacQ61L (first row). Top legend indicated line spacing. Scale bar=20μm. B) Migration trajectories of RacQ61L cells on linear ECM patterns. Scale bar =100μm. C) Cell shape elongation as a function of line spacing for RacQ61L cells treated (solid line). Dashed line shows elongation for WT cells. D) Cell shape orientation as a function of line spacing for RacQ61L cells (solid line). Dashed line shows orientation for WT cells. E) Cell migration guidance as a function of ECM pattern line spacing for RacQ61L cells (solid line). Dashed line shows guidance for WT cells.

back between sites of new adhesion and protrusion formation, controlled by PAK-mediated changes in paxillin phosphorylation, which recruits the Rac GEF β-pix [71]. Knockdown of β-pix has been linked to increased lamellipodia protrusion and defects in directed migration [54, 77]. To explore how disruption to this feedback may affect contact guidance, we knocked down β-pix to 30% of its wt levels (Figure 3.10).

For cells on lines, β-pix KD led to a slight reduction in elongation for line spacings greater than 3μm (Figure 3.11 A), reaching only 70% of the non-targeting-control (NT) cell values

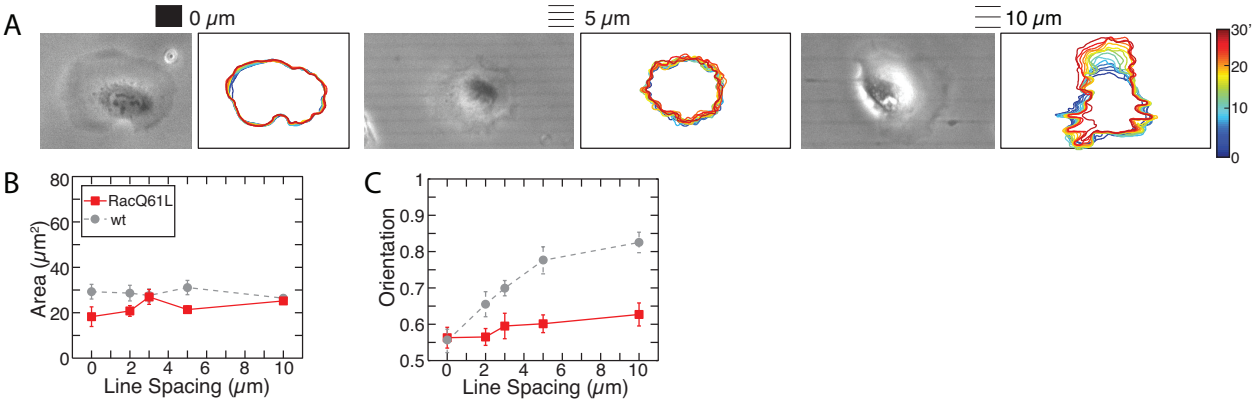

Figure 3.9: Quantification of leading edge protrusion area and direction in RacQ61L cells. A) Phase contrast images of RacQ61L cells on linear ECM patterns. Legend on top indicated line spacing. Scale bar=20μm. Contour plots show cell outlines for a 30 minute time interval during migration. Scale bar=20μm. B) Area of individual cell protrusions as a function of ECM line spacing for RacQ61L cells (solid line). Dashed line shows orientation for WT cells. Mean and s.e.m. are plotted for n$\geq$8 cells. C) Orientation of individual cell protrusions as a function of ECM line spacing for RacQ61L cells (solid line). Dashed line shows orientation for WT cells. Mean and s.e.m are plotted for n$\geq$8 cells.

(Figure 3.11 C). Similar to previously analyzed cells, β-pix KD had no defects in cell orientation parallel to the ECM (Figure 3.11 A, D). Strikingly, migration guidance was reduced in these cells by about 50% compared to the NT-control cells (Figure 3.11 B, E). Together these results show that feedback between adhesion and protrusion initiation is not essential for cell shape anisotropies during contact guidance, however it plays an important role to direct migration in the direction of the ECM. Since β-pix is required for the positive feedback between adhesion and protrusion, we expected -pix KD cells to mislocalize protrusions similar to RacQ61L cells. Surprisingly cell protrusions occurred mostly along the ECM axis (Figure 3.12 A). Quantification of protrusion orientation revealed that protrusions localized parallel to the ECM to levels comparable to non-targeting control cells (Figures 3.12 C). In contrast with RacQ61L cells, we observed that β-pix KD cells had large protrusions that fluctuated heavily in size, as evidenced by the two-fold increase we measured in protrusion area and the large fluctuations of this measurement (Figure 3.12 A).

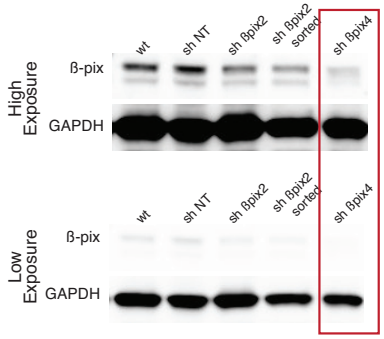

Figure 3.10: Western blot of β-pix and GAPDH showing knock-down of β-pix

.

Altogether these results show that spatial regulation of protrusive activity is required for contact guidance. Similar to our previous results with ROCK-inhibited cells, the axis of cell shape orientation does not correlate with migration direction upon disruption to Rac1 regulation. Our β-pix KD data shows that in addition to localization of protrusions, the size of protrusions can regulate the directed migration for cells on patterns. This supports our previous hypothesis, where the size of protrusions could limit the ability of cells to migrate perpendicular to the ECM (Figure 3.1). To further test this idea we decided to explore in detail whether changes to protrusion size could impact contact guidance.

3.4.4 Reduction of protrusion size increases contact guidance

The Arp2/3 complex is required for lamellipodia construction. Depletion of Arp2/3 results in decreased lamellipodia protrusion [115]. Thus, to modulate protrusion size in the reverse direction and establish the relevance of this physical parameter for contact guidance, we treated cells with 100μM of the Arp2/3 inhibitor CK-666. Upon first inspection Arp 2/3 inhibited cells appeared to be more elongated and polarized in the direction of the ECM (Figure 3.13 A). Quantification confirmed that these cells had increased elongation compared to cells treated with the control molecule CK-869, particularly at line spacings smaller than 5μm (Figure 3.13 C), while cell orientation was comparable to controls (Figures 3.13 D). More significantly, we observed higher values for guidance at all line spacings, with a

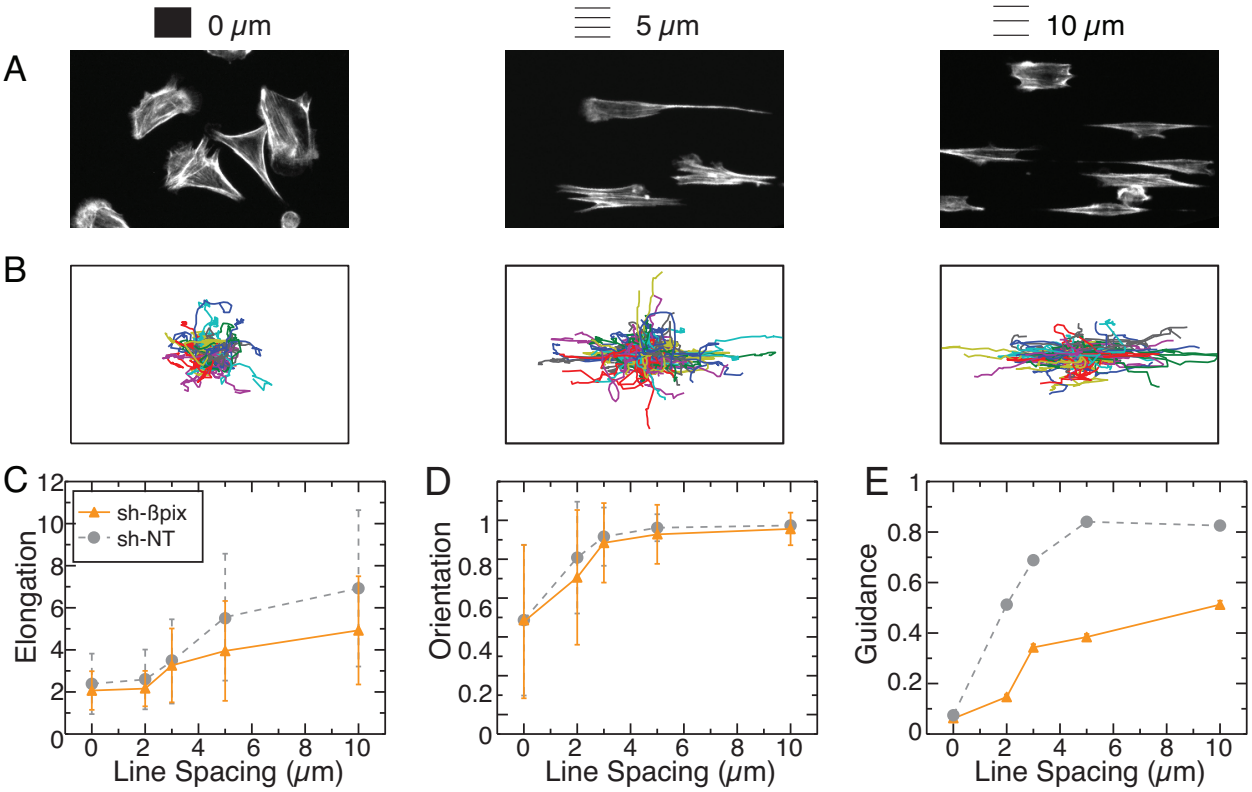

Figure 3.11: Effects of β-pix KD on contact guidance. A) Representative images of F-actin visualized by fluorescent phalloidin for cells on linear ECM patterns. Cells shown were KD for β-pix. Top legend indicated line spacing. Scale bar=20μm. B) Migration trajectories of β-pix KD cells on linear ECM patterns. Scale bar =100μm. C) Cell shape elongation as a function of line spacing for β-pix KD cells. Dashed line shows elongation for NT-control cells. D) Cell shape orientation as a function of line spacing for β-pix KD cells (solid line). Dashed line shows orientation for NT-control cells. E) Cell migration guidance as a function of ECM pattern line spacing for β-pix KD cells (solid line). Dashed line shows guidance for NT-control cells.

two-fold increase at spacings smaller than 5 μm compared to controls (Figures 3.13 E).

Our previous results show that contact guidance depends inversely on protrusion size and directly on localization of protrusions parallel to the ECM, therefore we expected Arp 2/3 inhibited cells to have reduced protrusion size and/or highly localized protrusions. Indeed, cell protrusions appeared to be smaller and directed almost exclusively in the direction of the ECM (Figure 3.14 A). Quantitative analysis confirmed that protrusions in Arp2/3 inhibited

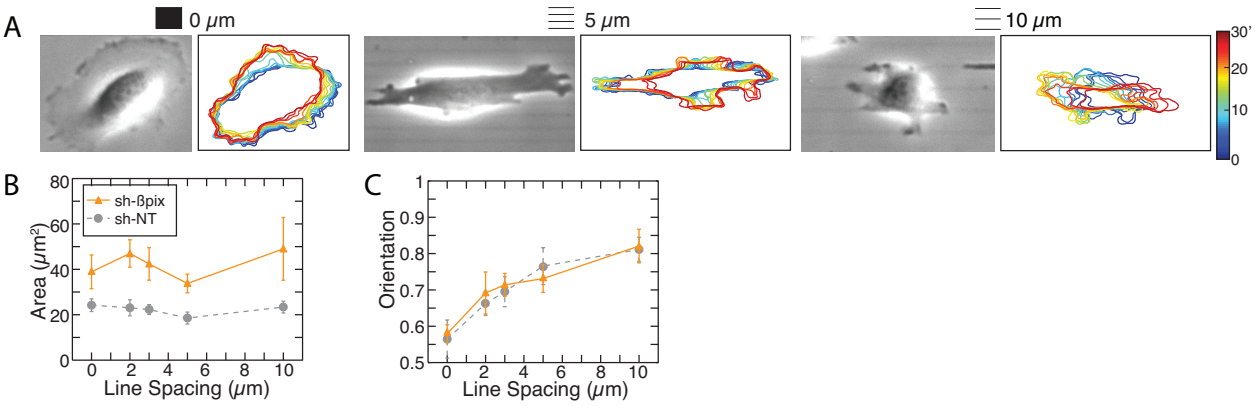

Figure 3.12: Quantification of leading edge protrusion area and direction in β-pix KD cells. A) Phase contrast images of β-pix KD cells on linear ECM patterns. Legend on top indicated line spacing. Scale bar=20μm. Contour plots show cell outlines for a 30 minute time interval during migration. B) Area of individual cell protrusions as a function of ECM line spacing for β-pix KD cells (solid line). Dashed line shows orientation for NT-control cells. Mean and s.e.m. are plotted for n$\geq$8 cells. C) Orientation of individual cell protrusions as a function of ECM line spacing for β-pix KD cells (solid line). Dashed line shows orientation for NT-control cells. Mean and s.e.m are plotted for n$\geq$8 cells.

cells decreased by 40% in area compared to cells treated with the control molecule (Figure 3.14 B). Remarkably, orientation of protrusions followed the same trend as migration guidance, increasing 2-fold for cells on line spacings smaller that 5μm (Figures 3.13, 3.14). Our results are surprising since Arp 2/3 depletion leads to defects in other ECM sensing processes such as haptotaxis [115, 52]. However, it is possible that during contact guidance, the spatial constrains of adhesive cues are sufficient to organize adhesion and direct protrusions.

Together with our β-pix KD measurements, these results further validate that contact guidance can be tuned by changes in protrusion size. Furthermore, this demonstrates how contact guidance can be improved by modulation of a subcellular organelle, namely the lamellipodia.

3.5 Discussion

The ability of cells to change shape and direct their migration in response to ECM geometric cues has been characterized for decades and remains an area of active research. However,

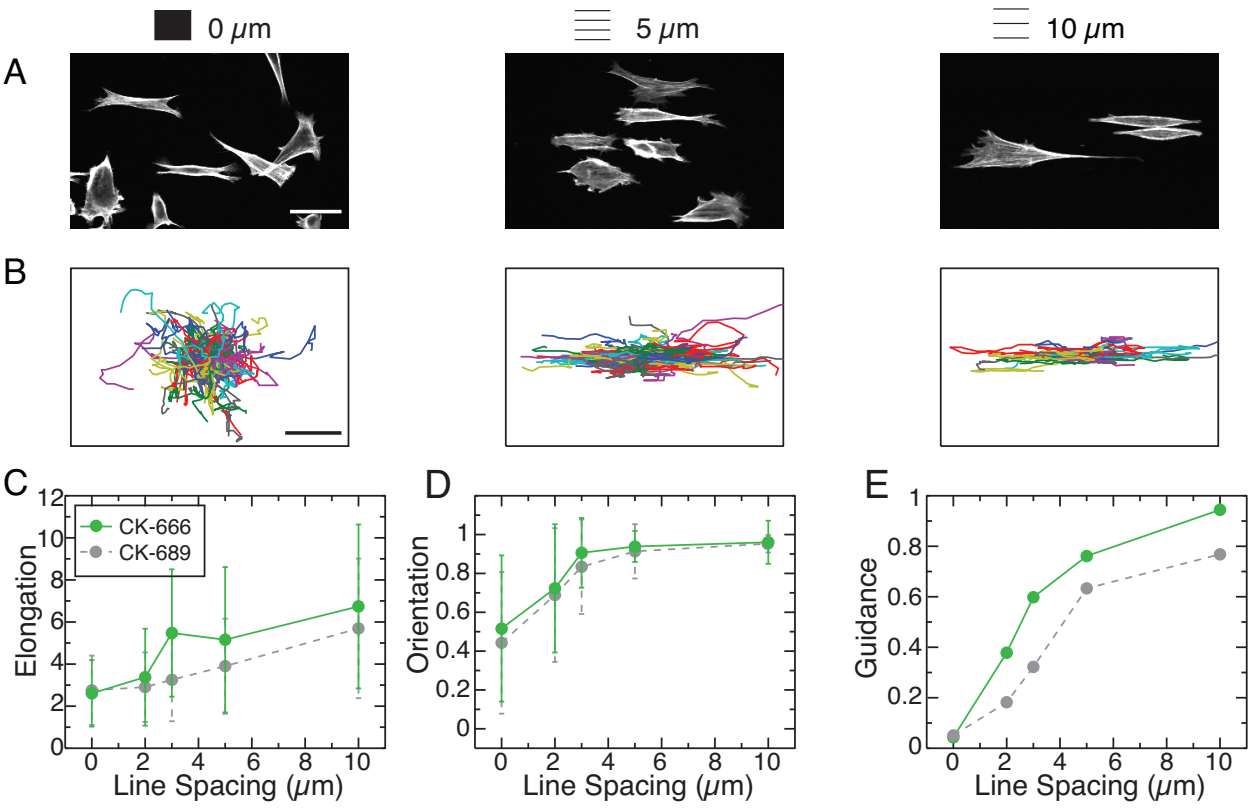

Figure 3.13: Effects of Arp 2/3 inhibition on contact guidance. A) Representative images of F-actin visualized by fluorescent phalloidin for cells on linear ECM patterns. Cells shown were treated with 100 μM CK-666. Top legend indicated line spacing. Scale bar=20μm. B) Migration trajectories cells treated with 100 μM CK-666 on linear ECM patterns. Scale bar =100μm. C) Cell shape elongation as a function of cells treated with 100μM CK-666. Dashed line shows elongation for cells treated with the control molecule CK-689. D) Cell shape orientation as a function of line spacing for cells treated with 100 μM CK-666 (solid line). Dashed line shows orientation for cells treated with the control molecule CK-689. E) Cell migration guidance as a function of ECM pattern line spacing for cells treated with CK-666. (solid line). Dashed line shows guidance for cells treated with the control molecule CK-689.

mechanistic understanding of how cells sense changes in ECM geometry and direct migration has been lacking. By manipulating the regulation of protrusive activity using different cellular mechanisms we show that contact guidance relies on spatial control of protrusive activity to direct migration. Specifically, we prove that area and orientation are two physical parameters of protrusion that determine the ability of cells to undergo contact guidance.

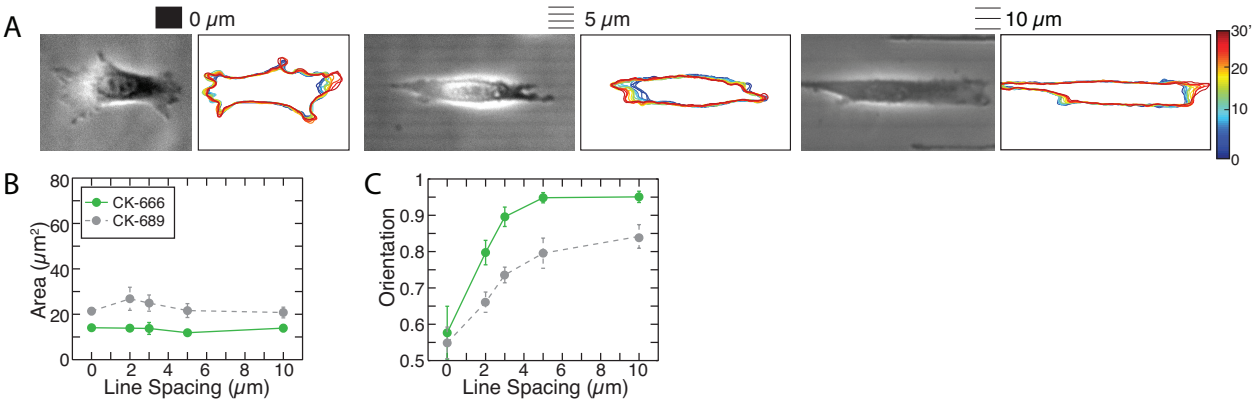

Figure 3.14: Quantification of leading edge protrusion area and direction in Arp 2/3 inhibited cells. A) Phase contrast images of cells treated with CK-666 on linear ECM patterns. Legend on top indicated line spacing. Scale bar=20μm. Contour plots show cell outlines for a 30 minute time interval during migration. B) Area of individual cell protrusions as a function of ECM line spacing for Arp 2/3 inhibited cells (solid line). Dashed line shows orientation for cells treated with the control molecule. Mean and s.e.m. are plotted for n$\geq$8 cells. C) Orientation of individual cell protrusions as a function of ECM line spacing for Arp 2/3 inhibited cells (solid line). Dashed line shows orientation for cells treated with the control molecule. Mean and s.e.m are plotted for n$\geq$8 cells.

Comparison across experimental conditions shows that perturbations that have defects in contact guidance fail to localize protrusions (Compare figures 3.15 B with 3.15 C) or have protrusions with increased area (Compare figures 3.15D with 3.15 C). While Arp 2/3 inhibition improves contact guidance by decreasing protrusion area (Compare figures 3.15D with 3.15 C). Collectively these results show that contact guidance relies on spatial control of leading edge protrusion. The defects we observe in migration guidance can be explained by changes in two distinct parameters of protrusion: orientation and size. Specifically, contact guidance is controlled independently by each one of these parameters since disruption of either one is sufficient to produce loss of contact guidance. Thus, we envision that contact guidance is a function of protrusion area and orientation, where these two parameters are independent of each other and can be regulated through different cellular pathways (3.16).

Additionally, from our analysis of cell shape orientation we can conclude that cells are able to orient their major axis parallel to the ECM independently of their state of lamellipodia spa-

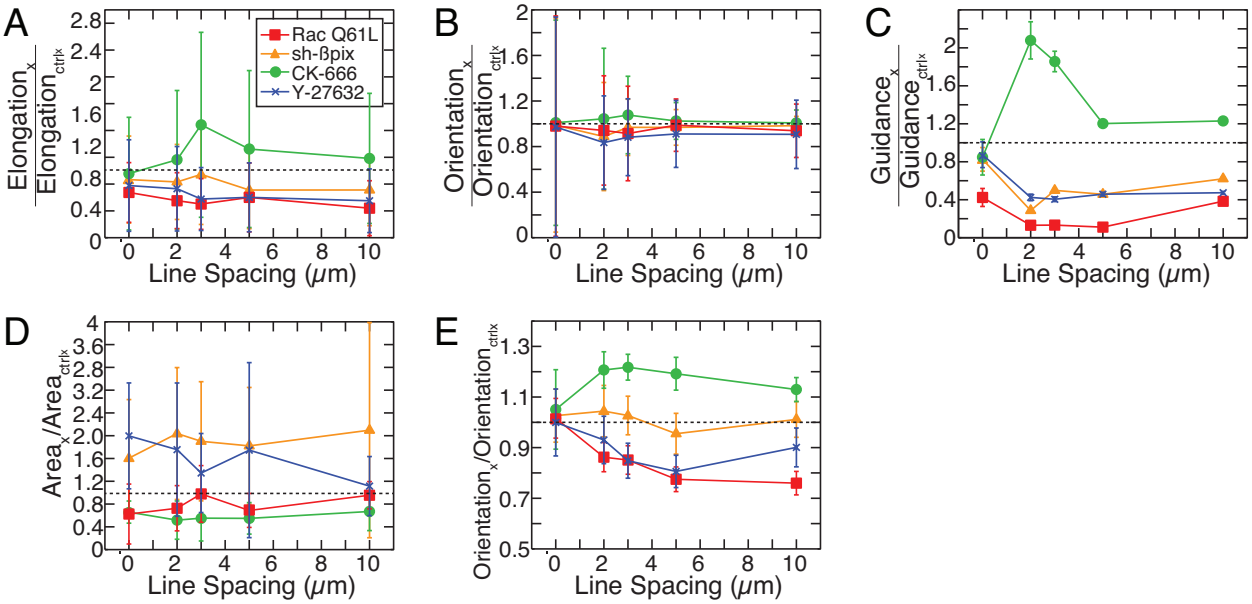

Figure 3.15: Comparison of contact guidance and protrusion phenotypes across experimental conditions. A) Fold change in elongation of cells transfected RacQ61L, an sh-RNA to β-pix, treated with 100M CK-666, or 20M Y-27632, relative to their respective controls: wt, sh-NT, CK-689 or DMSO. B) Fold change in orientation of cells transfected RacQ61L, an sh-RNA to β-pix, treated with 100M CK-666, or 20M Y-27632, relative to their respective controls: wt, sh-NT, CK-689 or DMSO. C) Fold change in guidance of cells transfected RacQ61L, an sh-RNA to -pix, treated with 100M CK-666, or 20M Y-27632, relative to their respective controls: wt, sh-NT, CK-689 or DMSO.

tial activity (Figures 3.15 B, E). Therefore, cell shape polarity is independent from migration direction in the context of contact guidance. Future work remains to be done to investigate other cellular pathways that may control localization and size of protrusive activity. Focal adhesion signaling is a possible candidate since perturbations to adhesion maturation result in reduced contact guidance.

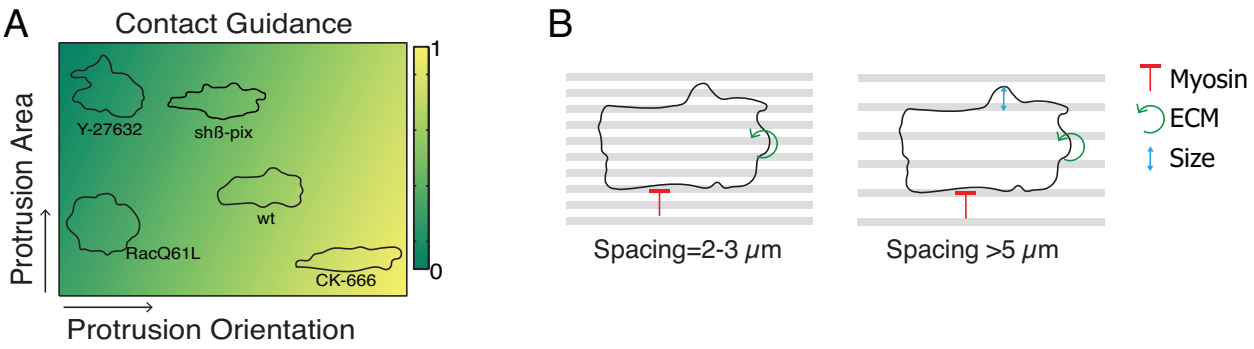

Figure 3.16: Cartoon representation of model for contact guidance. A) Phase space describing the ability of cells to undergo contact guidance. B) Cellular feedbacks involved in contact guidance.

CHAPTER 4

CELL MIGRATION AS A MECHANISM TO DIRECT TISSUE-SCALE PATTERNING IN *DROSOPHILA* EGG CHAMBERS

4.1 Preface

The experiments described in this chapter were designed and performed by the author (G.R.R.-S.J) and Maureen Cetera (M.C.). Data analysis was also performed by G.R.R.-S.J and M.C. Sally Horne-Badovinac supervised the project with critical input from Margaret Gardel. Patrick Oakes made important intellectual contributions and designed the quantitative method used to measure actin bundle alignment. Lindsay Lewellyn made important intellectual contributions. Michael J. Fairchild and Guy Tanentzapf provided key reagents for the experiments.

4.2 Introduction

As described with detail in the introduction, *Drosophila* egg chambers constitute a minimal system to study the mechanisms underlying changes in tissue polarity and organ shape. Egg chambers with disrupted cell-ECM and cell-cell interactions fail to undergo migration [7, 40, 17, 41, 32, 108]. In these mutant backgrounds along with migration, establishment of tissue level polarity is also disrupted. The discovery that egg chamber elongation coincides with migration of the FCs has led to two major challenges in understanding this system. The first is to determine the mechanisms underlying individual FC motility. The second is to determine the relationship between migration, tissue scale polarity and egg chamber elongation. There is compelling evidence that migration builds the polarized ECM membrane associated with the "molecular corset" [41]. However, the relationship between rotation and the basal actin bundles, remains unknown.

Tissue-level basal actin organization has been reported to fluctuate during the early stages of egg chamber development. The actin bundles first show a circumferential arrangement within the follicle cell precursors in the germarium [32]. However, this early tissue-level organization was reported to be lost on egg chamber formation, such that the basal actin bundles were still aligned within individual cells, but their global orientation was perturbed. The tissue-level alignment of the basal actin bundles was then thought to re-emerge at stage five, concurrent with the time that rotation and ECM polarization were reported to begin (Figures 4.1, 4.2) [32, 41]. Recent work has shown that when rotation ends at stage nine, the actin bundles undergo oscillating, Myosin II-mediated contractions to produce a circumferentially constrictive force around the egg chamber to further elongate the tissue [42].

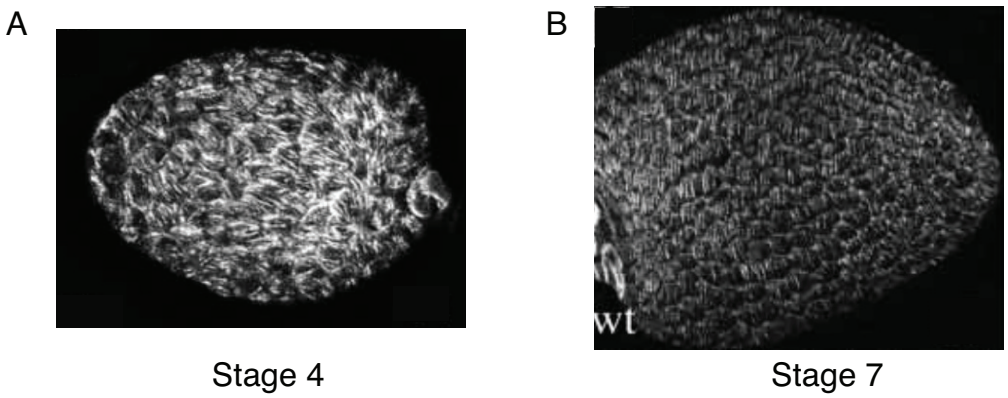

Figure 4.1: Actin organization in stage 4 and stage 7 egg chambers. A) Actin staining of a *wild-type* stage 4 egg chamber. B) Actin staining of a *wild-type* stage 7 egg chamber. The actin cytoskeleton exhibits a tissue-scale alignment perpendicular to the A-P axis. Figure adapted from [32].

In this chapter, the cellular mechanisms that drive FC migration are explored. Once the cellular basis for rotation is determined, the relationship between FC migration and the establishment of the basal actin tissue-scale patterning is investigated using genetic and pharmacological perturbations. To measure tissue scale polarity, at the cellular and tissue

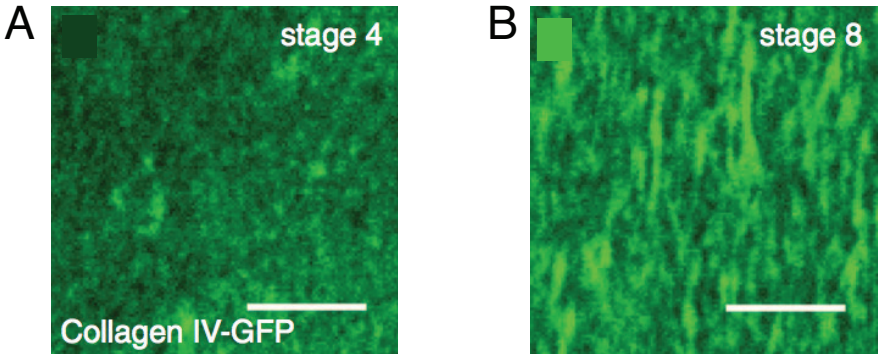

Figure 4.2: A) Collagen IV-GFP of a *wild-type* fixed stage 4 egg chamber. B) Collagen IV-GFP of a *wild-type* fixed stage 8 egg chamber. The ECM exhibits a tissue-scale alignment perpendicular to the A-P axis. Figure adapted from [41].

scales, a new quantitative method is developed. By blocking migration at distinct time points and measuring tissue-scale polarity, the dependance of global actin polarity on migration is determined. This work sheds light on the cellular mechanisms that drive egg chamber rotation and demonstrates how cell migration can be harnessed to build a tissue-level actin organization.

4.3 Materials and Methods

4.3.1 Drosophila genetics

For most experiments, crosses were raised at $25°C$ and experimental females were aged 1-3 days at the same temperature. Exceptions included His2AvRFP, which was kept and aged at room temperature, and $UAS - Abi - RNAi/+$ along with its corresponding control, which was aged at $29°C$. $SCAR^{\delta 37}$ mosaic egg chambers were produced using $FRT40A$ with $GR1 - Gal4$ driving FLP recombinase expression. For flipout clones, UAS lines were crossed to flies containing the FLP recombinase under a heat shock promoter as well as the act5c>> Gal4, UAS-GFP (or UAS-RFP) flipout cassette. The heat shock was induced by incubating third instar larvae and pupae at $37°C$ for 1h with a 1-h recovery period at

$25°C$ followed by another hour at $37°C$ for 3 over 2 days. Females that eclosed during the heat shock process or the following day were placed on yeast with males overnight and dissected the next day. Most stocks were obtained from the Bloomington Stock Center with the following exceptions. vkg-GFP (CC00791), indy-GFP (CC00377) and Nrg-GFP (G00305) are from the Carnegie Protein Trap Library [11]. tj-Gal4 (104055) and UAS-Abi-RNAi are from the Drosophila Genetic Resource Center in Kyoto. UAS-ena-RNAi is from the Vienna Drosophila Resource Center. UAS-UtrophinABD::GFP is from T. Lecuit [86] , Sqh-Sqh::mCherry is from E. Wieschaus [63] and UAS-Pax::GFP is from D. Montell [42]. GR1-Gal4, UAS-FLP was a generous gift from T. Schpbach. UAS-MoeABD::mCherry was a generous gift from B. McCartney.

4.3.2 Time-lapse image acquisition and microscopy

One- to three- day old females were aged on yeast with males for 13 days before dissection. Ovaries were dissected as described previously described in [2] [82] . As young egg chambers are more prone to damage during the dissection process and damaged egg chambers do not rotate, all egg chambers were inspected for damage before and after imaging. When possible, 6μM FM464 (Invitrogen) membrane dye was added to the live imaging media to highlight damaged tissue. ImageJ and Adobe Photoshop were used for image processing.

For imaging performed on an upright scanning confocal microscope, ovarioles were transferred in live imaging media to an agar pad (live imaging media with 0.4% NuSieve GTG low-melt agarose) that was formed on a gas permeable membrane slide (Greiner Bio-One, discontinued product). Live imaging media was removed from the pad and a coverslip was placed on top of the sample, stabilized with vacuum grease at each corner. The coverslip was then gently compressed onto the sample and halocarbon oil 27 (Sigma) was added around the coverslip to keep the media from evaporating. Egg chambers were imaged with 40/1.3 numerical aperture (NA) EC Plan-NeoFluor oil-immersion objective on a laser-scanning con-

focal microscope (Zeiss LSM510) controlled by the LSM acquisition software.

For near-total internal reflection fluorescence imaging, ovarioles were transferred in live imaging media to a coverslip that was fused with melted parafilm to an aluminum slide with a 12-mm circular cut out. Twenty-micrometre polystyrene beads (Bangs Laboratories Inc.) were added to the media and a 16-mm2 coverslip was placed on top of 45 ovarioles and 510 beads to compress the egg chambers against the bottom coverslip [2]. Egg chambers were imaged with a 100/1.49 NA CFI Apo oil-immersion total internal reflection fluorescence objective (Nikon) using an Andor iXon3 897 EM-CCD camera on an inverted microscope (Ti-E; Nikon) controlled by Metamorph software (Molecular Devices).

For imaging performed on an inverted spinning disk microscope, ovarioles were transferred into $37°C$ live imaging media with 0.8% NuSieve GTG low-melt agarose on the aluminum slide. Ovarioles either sank in the media or were gently moved to the bottom with an eyelash tool before the media solidified at room temperature. The gas permeable membrane was placed on top of the slide to prevent evaporation. Egg chambers were imaged on an inverted microscope (Ti-E; Nikon) with a spinning disk confocal unit (CSUX; Yokogawa Electric Corporation) and an HQ2 camera (Roper Scientific) or a Rolera em-c2 camera (Q imaging) using a 60/1.2 NA Plan Apo water immersion objective (Nikon) or a 20/0.75 NA Plan Fluor multi-immersion objective (Nikon) controlled by Metamorph software.

4.3.3 Immunohistochemistry

Ovaries were dissected in S2 media warmed to room temperature and fixed in PBS+0.1% Triton+4% EM-grade formaldehyde (Polysciences). For actin staining only, ovaries were washed 3 times in PBS+0.1% Triton (PBT), then egg chambers were removed from the muscle sheath by gentle pipetting. Staining was performed with rhodamine phalloidin (1:200, Sigma), AlexaFluor-488 Phalloidin (1:200, Invitrogen) or AlexaFluor-647 Phalloidin (1:75,

Invitrogen) for 15 min in PBT at room temperature while rocking. Egg chambers were then washed 3 times in PBT and mounted in SlowFade Antifade (Invitrogen). Egg chambers stained with primary antibodies were incubated overnight at $4°C$ with rocking in PBT+0.1% BSA+Phalloidin. Egg chambers were incubated in AlexaFluor-488- or 555-conjugated secondary antibodies (1:200, Invitrogen) in PBT+0.1% BSA+Phalloidin for 3h at room temperature with rocking. The following primary antibodies were used: anti-Ena (1:200 concentrate, DSHB), anti-SCAR (1:300)43 and anti-SCAR (1:200 concentrate, DSHB). For SCAR staining, primary and secondary incubations along with all washes following the primary incubation, PBT3 (PBS+0.3% Triton) was used instead of PBT. Fixed egg chambers were imaged with a laser-scanning confocal or a spinning disk confocal (described above). Image J and Adobe Photoshop were used for image processing.

4.3.4 Drug treatment

To show that egg chamber rotation can be acutely disrupted with a pharmacological treatment, ovaries were dissected as stated above in live imaging media with 2.5% dimethyl sulphoxide (DMSO). Ovarioles were transferred in the live imaging media to the aluminum slide and imaged on an inverted spinning disk microscope. After 20min, the imaged ovarioles were quickly washed 3 times in live imaging media with 2.5% DMSO and 250μM of the Arp2/3 inhibitor (CK-666, Millipore) or control molecule (CK-689, Millipore), and imaged in the third wash for an additional hour.

To visualize the actin cytoskeleton in drug-treated egg chambers live, UtrophinABD::GFP-expressing ovarioles were dissected in live imaging media with the inhibitor and imaged on the laser-scanning confocal microscope as described above. For fixed images, three females were dissected per experiment in live imaging media with 2.5% DMSO and 250μM of the inhibitor or control molecule. Approximately 20 ovarioles were incubated for 1h then fixed and stained with phalloidin as described above.

4.3.5 Quantification of egg chamber rotation rate

Rotation speed was measured from time-lapse images of egg chambers expressing His2AvRFP or a membrane-targeted green fluorescent protein (GFP). A line was drawn over a row of follicle cells in the direction of migration to generate kymographs. Migration rates were obtained from the slope of the lines in the kymograph. All analyses were performed using Metamorph software (Molecular Devices).

4.3.6 Quantification of cell-level actin bundle alignment

Actin bundle orientation was calculated using fixed samples where F-actin was labelled with phalloidin. A local director representing actin alignment was determined as follows. First, each image was broken down into a series of 2.6μm by 2.6μm overlapping windows. A symmetric Gaussian filter was applied to each window to minimize edge effects and the 2D FFT of the filtered window was calculated. Windows with oriented actin bundles resulted in asymmetrically skewed transforms, where the direction of skew is directly related to the orientation of the actin bundle. Windows with no predominant orientation yielded a uniform transform. The principle direction of the skewed transform was determined by calculating the angle of the axis for the least second moment of the transform. The average orientation of the actin in real space (that is, image window) is orthogonal to the principle direction of the skewed transform in frequency space (the 2D FFT). To determine the direction of alignment at the cellular scale, we averaged the directors within each cell. Only directors within 1 s.d. of the mean were included in this average, as outliers were often the product of edge effects in the analysis. All calculations were performed using custo written routines in MATLAB.

4.3.7 Quantification of tissue-level actin bundle alignment

To assess the tissue-level alignment of the basal actin bundles, we calculated an order parameter, S, for each egg chamber by considering the directors of all the cells visible in an image, as determined above. We defined an order parameter, $S = 2(\langle cos^2\theta_{ij}\rangle - 1/2)$. Where θ_{ij} is the angle between the directors of cells i and j. The average was performed over all unique cell pair combinations in an image. S ranges from zero (randomly oriented directors) to one (parallel directors). As cells visible in a fixed image corresponded only to a fraction of the entire epithelium, we tested whether measuring local order (a limited number of cells) was representative of global polarity patterns (the entire egg chamber). We first binned each egg chamber into regions that included an increasing number of adjacent/neighbouring cells. The size of the bin varied from two (adjacent cells only) up to n-connected cells, where n was the maximum distance (in cells) between two visible cells in an image. The order parameter S was calculated for each bin and averaged over regions of the same connectivity in egg chambers of the same developmental stage. We observed no dependence of the average order parameter on the size of the region analysed. Thus, our local measurements can be taken as representative of global actin bundle organization in the egg chamber.

4.3.8 Quantification of Collagen IV organization

Collagen IV orientation was calculated from fixed egg chambers expressing Vkg-GFP. Each image was broken down into windows (50x50 pixels per $20.06\mu m^2$) that overlapped by 2.23μm. A director was obtained for each window following the same procedure described for the actin bundles. The order parameter, S, of the director field obtained was then calculated to quantify the orientation of fibril-like structures in the basement membrane.

4.4 Results

4.4.1 Lamellipodia protrusions drive FC migration

Migrating cells typically have two types of actin-based protrusions at their leading edges that drive forward motility, filopodia and lamellipodia [35, 88]. To determine whether both of these structures are present at the basal follicle cell surfaces, egg chambers were stained for their characteristic markers. Enabled/VASP (Ena) is an actin-binding protein required for filopodia formation [65]. This protein localizes in a punctate pattern at the edge of the protrusions, consistent with localization to filopodial tips (Figure 4.3 A). The SCAR/Wave complex is an activator of the actin nucleator Arp2/3, which is required to produce the dynamic branched actin network of the lamellipodium [35, 88]. SCAR localizes broadly across the leading edge of each follicle cell, consistent with localization to lamellipodial structures (Figure 4.3 B). Thus, the protrusive edge of each follicle cell contains both lamellipodia and filopodia.

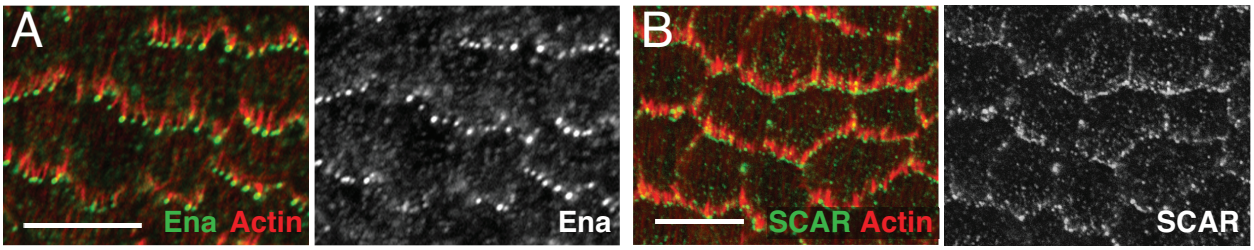

Figure 4.3: Immunofluoresce images showing localization of ENA and SCAR at the leading edge of FCs. A) Endogenous Ena localizes to the tips of filopodia. Stage 7 egg chamber. B) Endogenous SCAR localizes more broadly within the leading edge protrusions, revealing the lamellipodia. Stage 8 egg chamber. Scale bars=10μm.

To determine whether lamellipodia and filopodia were required for leading edge formation and migration, Ena and the SCAR complex component Abelson interacting protein (Abi) were depleted. Depletion of Ena changed protrusion morphology by eliminating the finger-like, filopodial actin structures (Figure 4.4 A). Depletion of the SCAR complex component

Abelson interacting protein (Abi) eliminates all actin-based protrusions in a cell-autonomous manner (Figure 4.4 B). Live imaging was used to determine the requirement of lamellipodia

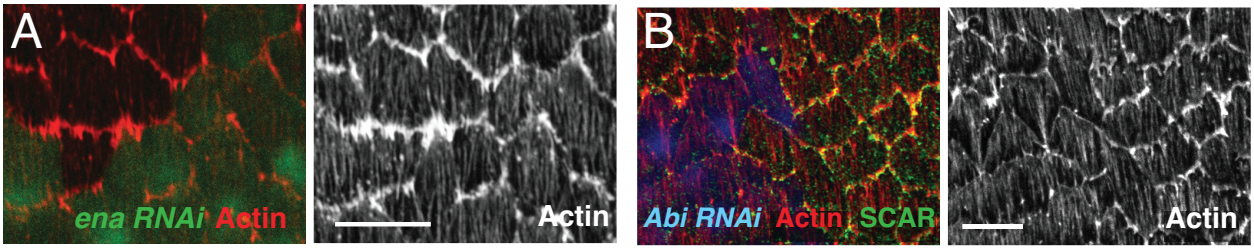

Figure 4.4: Immunofluoresce images showing the effects of depletion of ENA and SCAR at the leading edge of FCs. A) Clonal expression of ena RNAi (green) reduces filopodia compared to adjacent wild-type cells. B) Clonal expression of Abi RNAi (blue) eliminates SCAR enrichment (green) and protrusions at the leading edge. Stage 8 egg chambers. Scale bars=10μm.

(Abi) and filopodia (Ena) to FC migration. Ena and SCAR activities in FCs were manipulated using the traffic jam-Gal4 (tj-Gal4) driver, this driver is expressed in both the follicle cell precursors and follicle cells at all developmental stages [58]. Depletion of Ena throughout the epithelium by RNA interference (RNAi) did not disrupt FC migration or egg chamber elongation (Figure 4.5 A,B). In contrast, expressing Abi RNAi in all follicle cells throughout oogenesis blocked FC migration and decreased egg chamber elongation (Figure 4.5 A, B). These findings show that Abi is required for egg chamber rotation, presumably due to its role in stimulating lamellipodial activity at each FC's leading edge.

4.4.2 Follicle cell migration and tissue-scale actin polarity begin at stage 1

Follicle cell migration was reported to begin at stage five [41]. However, a polarized distribution of SCAR at the basal epithelial surface was observed on a stage 2 egg chamber (Figure 4.6 A). Given that FC migration depends on SCAR activity, this suggested that rotation could begin earlier than previously thought. Through long-term live imaging of entire ovarioles, it was determined that egg chamber rotation began at stage one and continued slowly through stage five before increasing in speed at stage six (Figure 4.6 B, C). These data show

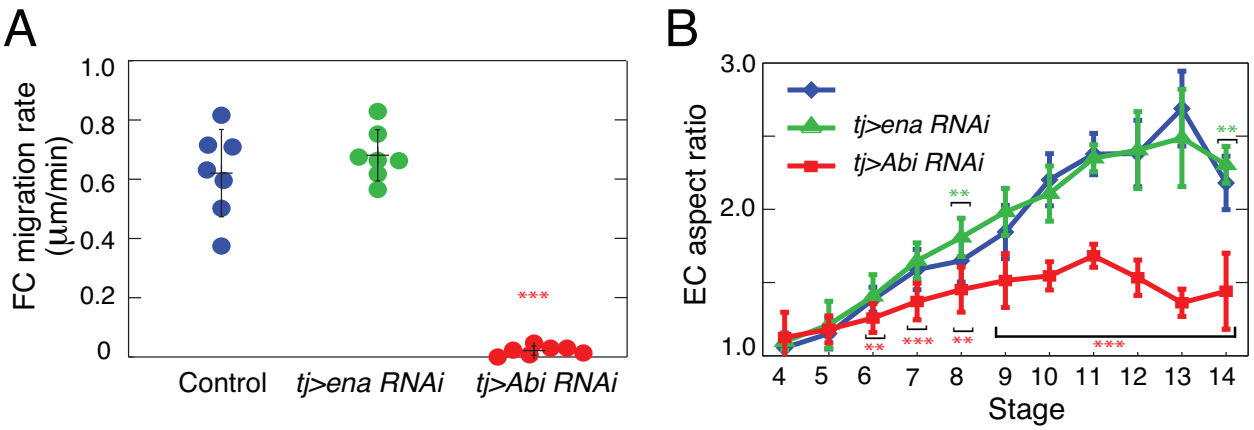

Figure 4.5: Quantification of the effects of ena and abi depletion on FC migration and egg chamber elongation. A) Follicle cell migration rate for control, ena RNAi and abi RNAi stage 7-8 egg chambers. B) Egg chamber aspect ratio for control, ena RNAi and abi RNAi egg chambers. The aspect ratio is the length of the egg chamber divided by its width. For stages 4-10 n≥6, stages 11-13 n≥3, stage 14 n≥25.

that rotation occurs in two phases: an early slower phase and a later faster phase. Previous work showed that global alignment of actin in the egg chamber arose at stage 5 and coincided with the onset of FC migration [32, 7, 41, 108]. However, if tissue-scale actin polarity truly emerges at stage 5, the finding that FC migration begins at stage 1 would imply that planar polarity in the egg chamber is temporally decoupled and thus independent of FC migration. To investigate this possibility it was necessary to develop a method to compare quantitatively tissue scale polarity across developmental stages and samples.

4.4.3 Quantitative image analysis can be used to measure tissue-scale polarity in Drosophila *egg chambers*

To investigate whether tissue-scale actin polarity occurred after the onset of FC migration, we developed a quantitative method to assess tissue polarity from fixed egg chamber images where F-actin was labelled with phalloidin (Figure 4.7 A). In the FC epithelium, alignment of actin filaments can occur within individual cells and globally across all cells in the ep-

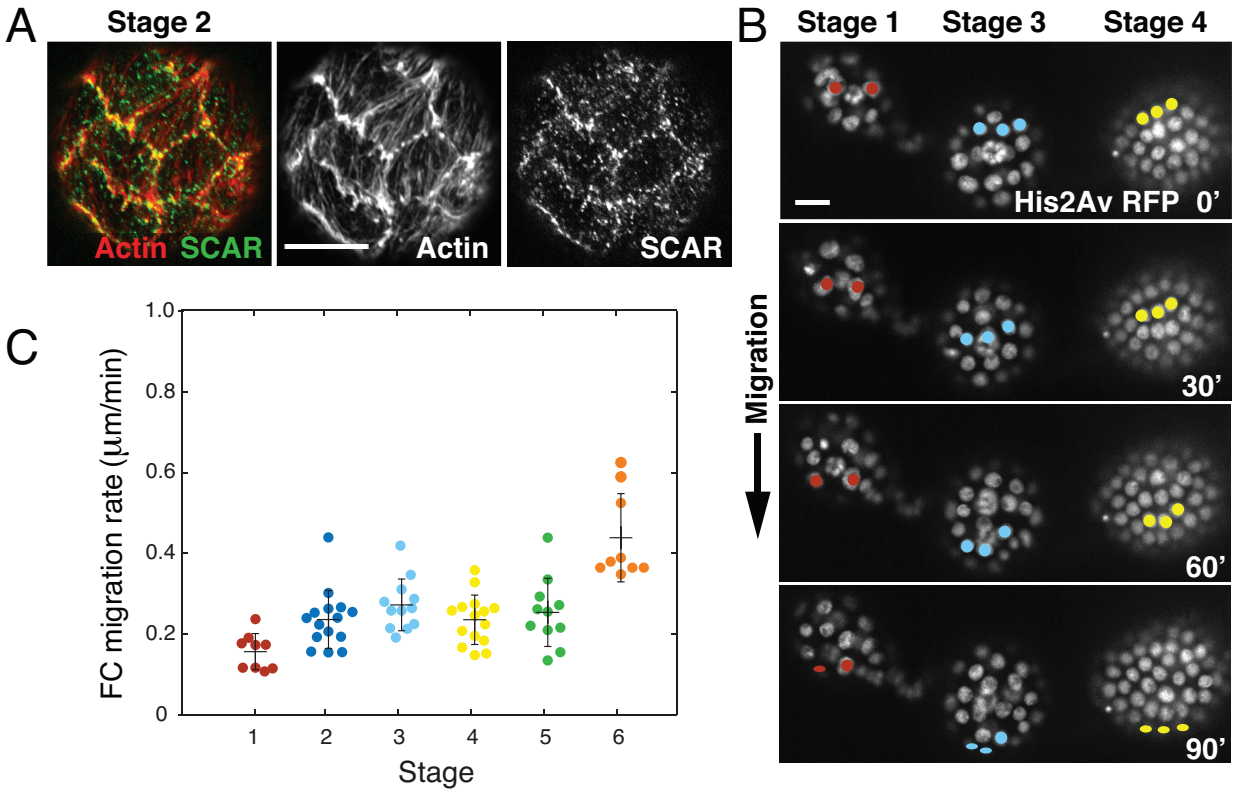

Figure 4.6: Follicle cell migration begins at stage 1. A) Immunofluorescence of a actin and scar showing the basal epithelial surface of a stage two egg chamber. B) Representative images from a time series of His2Av RFP-expressing egg chambers that show rotation occurring at stages 1, 3 and 4. The coloured dots mark the same set of nuclei through each 30-min interval. C) Quantification of FC migration rate. Each data point represents and individual egg chamber with mean±s.d. Scale bars=10μm.

ithelium. Therefore to describe planar polarity in the epithelium two measurements were needed: alignment of actin filaments within individual FCs and global tissue alignment.

To describe actin filament alignment at the cellular scale, the epithelium was segmented into individual cells using cell membranes and cortical actin as markers (Figure 4.7 B). Each cell was then broken down into a series of 2.6 μm by 2.6 μm windows (Figure 4.7 C).

The local alignment of actin filaments within each window was determined as follows. First, a symmetric Gaussian filter was applied to each window to minimize edge effects and the 2D FFT of the filtered window was calculated. Windows with oriented actin bundles (Figure

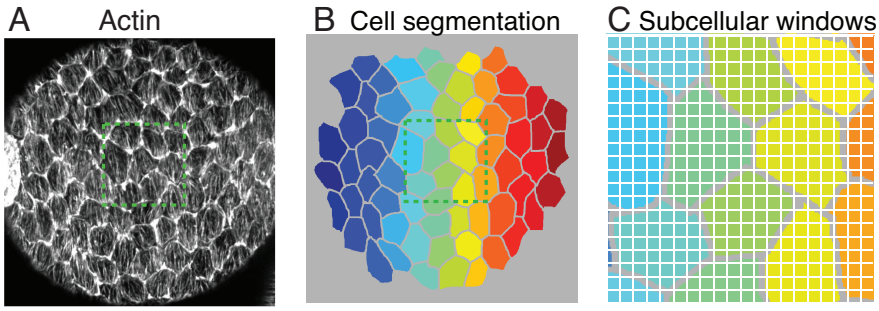

Figure 4.7: Egg chamber segmentation used to quantify actin alignment within individual FCs. A) Representative image of a stage five egg chamber where the actin is labelled with phalloidin. B) Pattern obtained by segmenting the epithelium into individual cells. C)To analyze actin bundle alignment, individual cells are broken into subcellular windows of $6.74\mu m^2$ (windows are not shown to scale).

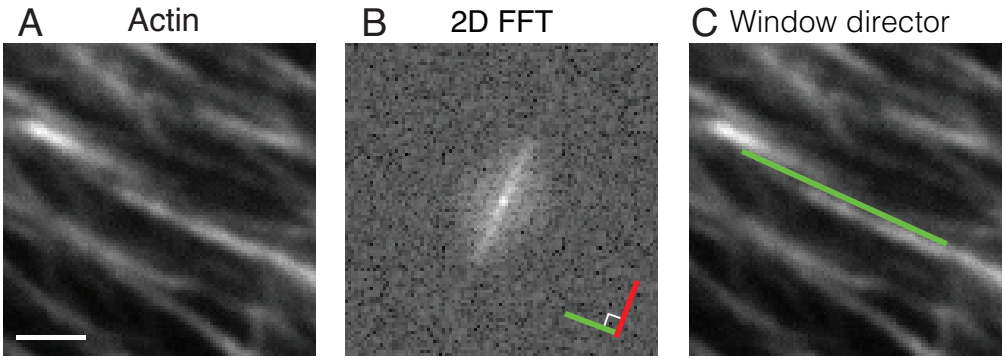

Figure 4.8: Measurement of actin alignment within subcellular windows. A) Representative image of the basal actin bundles in a subcellular window as defined in figure 4.7. Scale bar=2μm B) 2D FFT of the actin image shown in (A). The red line indicates the principal direction of the FFT, orthogonal to the orientation of the actin bundles (green line). C) Director indicating the local alignment of the actin image.

4.8 A) resulted in asymmetrically skewed transforms (Figure 4.8 B), where the direction of skew is directly related to the orientation of the actin bundle. The principle direction of the skewed transform was determined by calculating the angle of the axis for the least second moment of the transform. The average orientation of the actin in real space is orthogonal to the principle direction of the skewed transform in frequency space. Alignment for each window was then described by a director orthogonal to the principle direction of the skewed 2D FFT (Figure 4.8 C). Iteratively performing this calculation yields a director field that

represents a local measure of actin bundle orientation at a subcellular length scale (Figure 4.9 A). To determine the direction of alignment at the cellular scale, we averaged the directors within each cell. Only directors within one s.d. of the mean were included in this average (Figure 4.9, green lines), as outliers were often the product of edge effects in the analysis (Figure 4.9, magenta lines). As a measure of actin orientation within individual FCs, the angle between the directors inside a cell was calculated. Smaller angles indicated that actin bundles were parallel to one another within the cell. Figure 4.9 shows the results of performing this calculation in control egg chambers at different stages of development. The mean angle between the directors inside a single FC is less than 10 degrees at all developmental stages, indicating parallel alignment of bundles.

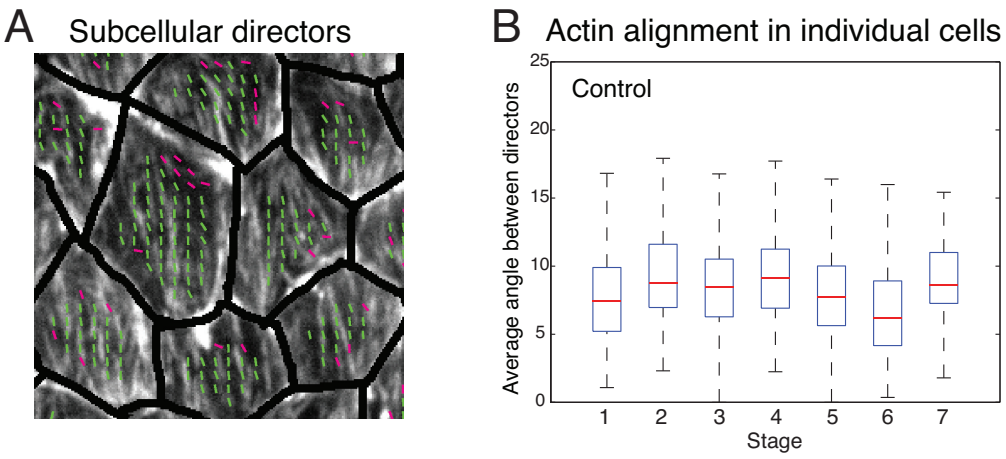

Figure 4.9: Measurement of actin alignment within individual FCs. A) Magnification of the epithelial region within the green rectangle in figure 4.7. Directors (green and magenta lines) indicate the local alignment of actin bundles within each cell. Directors deviating from the mean by more than one s.d. (magenta lines) were discarded. B)Actin bundle alignment within individual follicle cells throughout development in control egg chambers. Box plot shows the mean and the standard deviation of the angles between directors in an individual follicle cell.

To calculate tissue-scale polarity it was necessary to compare actin alignment across several cells in the tissue, to this end a mean orientation of the actin bundles was assigned to every cell, by averaging the local directors contained within it (Figure 4.10 A, yellow lines). Fi-

nally, to determine the tissue-level polarity of the actin bundles, we defined a nematic order parameter (S) (Figure 4.10 B), which compares the relative orientation of cellular-level directors of all the cells within a given image (Figure 4.10 B, yellow lines). The order parameter can vary from zero (random distribution of directors) to one (parallel directors). Since fixed samples of FC epithelia varied in the number of cells they contained at different stages of development, it was next tested whether the order parameter calculated to measure global actin polarity was indeed representative of polarity in the entire egg chamber. Figure 4.11 shows that the value of the order parameter is independent of the number of cells included in the image analyzed confirming that it is a representative measure of tissue-scale polarity.

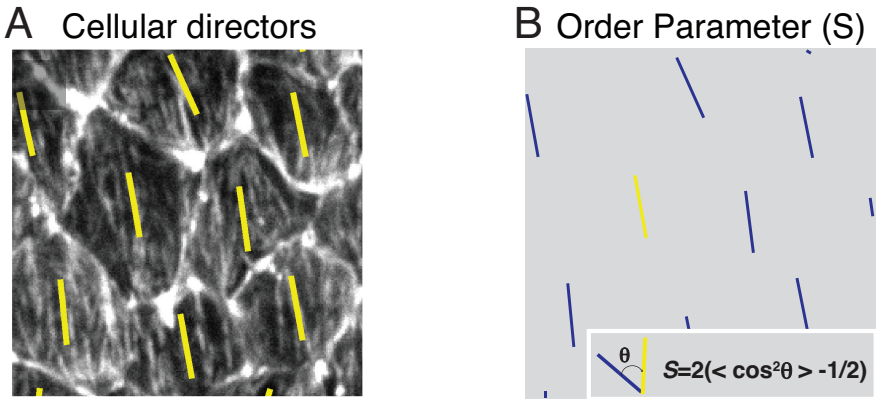

Figure 4.10: Measurement of global actin alignment within an egg chamber. A) Director field showing the mean orientation (yellow lines) of the green directors within each cell shown in figure 4.9 A. B) Order parameter (S) describing global tissue alignment is calculated by comparing the relative angle between all directors in an epithelium.

4.4.4 Tissue scale actin alignment is present from stage 1 and depends on FC migration

Using the method developed in the previous section, the timing of the establishment of global actin polarity was first investigated. To this end, egg chambers of stages 1 to 8 were fixed and stained for actin.

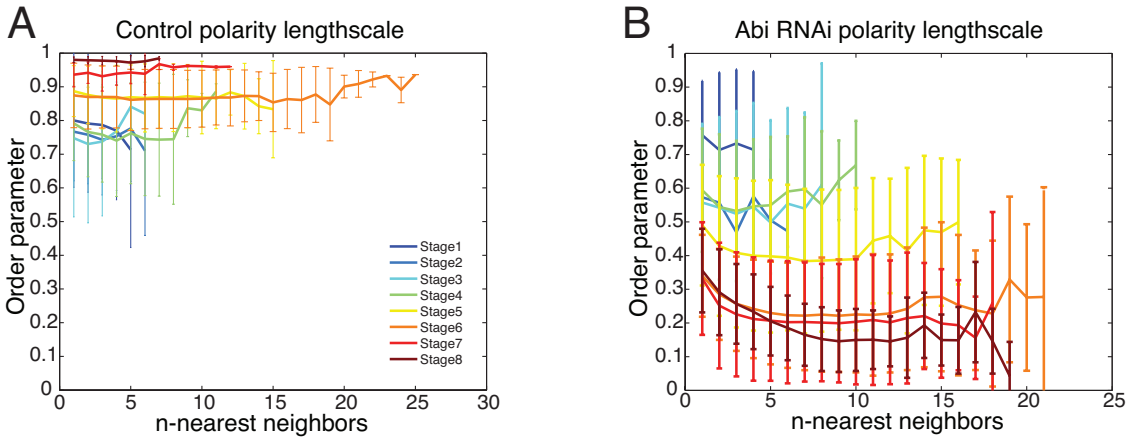

Figure 4.11: Order parameter as a function of the size of the region analyzed in stage 1-8 egg chambers. A) Average order parameter measured for control (A) and Abi RNAi (B) egg chambers as a function of the size of the epithelial region analyzed. The size of each region is varied from adjacent neighbors to n-connected regions.

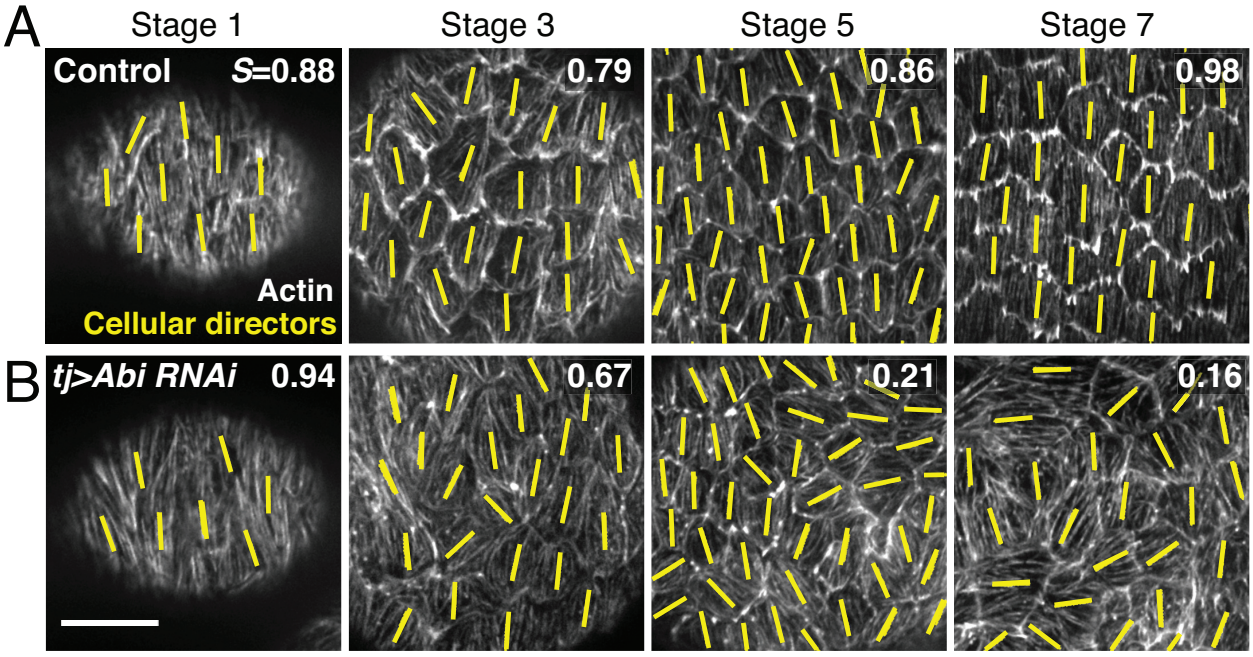

Figure 4.12: Tissue scale actin alignment is present at all developmental stages and requires cell migration. Representative images of basal actin bundle alignment in control (A) and Abi RNAi (B) epithelia at different stages. Yellow lines represent the mean orientation of the basal actin bundles in each cell. The value of the order parameter (S) is shown on the top right corner.

Upon visual inspection, actin appeared to be globally aligned at all developmental stages. In egg chambers of different stages, cellular directors showing actin alignment of individual FCs appeared to be perpendicular to the A-P axis (Figure 4.12 A). Measurement of the order parameter confirmed that actin alignment was present from stage 1 through stage 8 (Figure 4.13 B, blue line). On average, $S > 0.75$ for stages 1 though 5, then increased to a mean value > 0.9 for stages 5 through 8. This increase in orientation at stage 5 correlated with the increase observed in FC migration speed, suggesting that FC migration could play an active role in the maintenance of global tissue polarity. To explore this possibility, FC migration was perturbed and the impact on global actin alignment was analyzed.

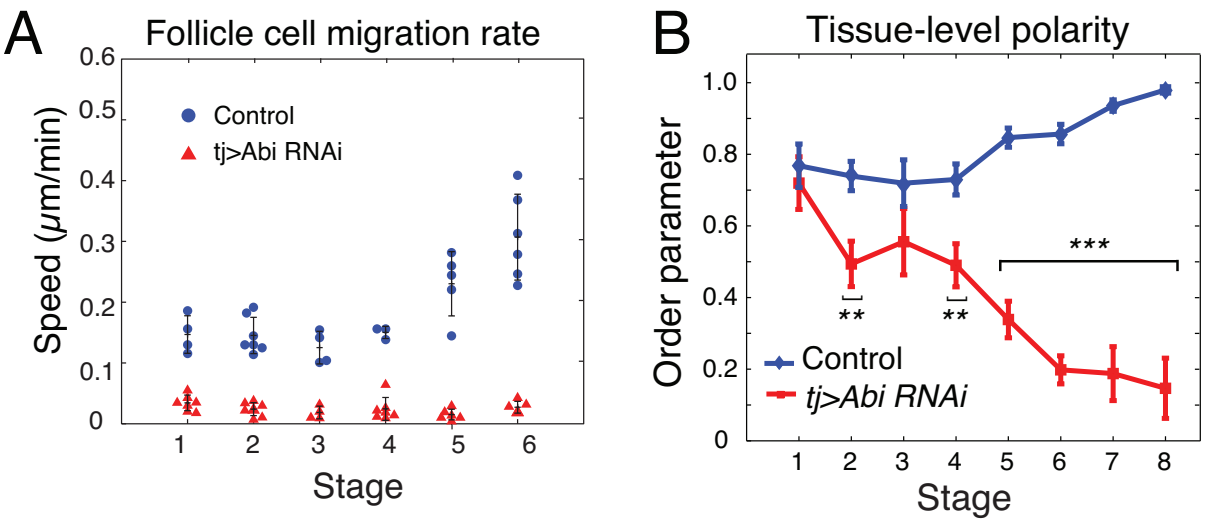

Figure 4.13: Abi RNAi blocks FC migration and disrupts global actin polarity. A) FC migration speed in control and Abi RNAi egg chambers through development. B) Average order parameters for control (blue line) and Abi RNAi (red line) epithelia at stages one through eight. For stages 16 n≥8, stage 7 n≥5 and stage 8 n≥4 . Data points represent mean±s.e.m.

FC motility relies on lamellipodia protrusion, particularly, Abi RNAi is required for FC migration at stages 7 and 8 (Figure 4.5). Therefore Abi RNAi was used to stop FC migration and determine the effects of this perturbation on global tissue actin polarity. First, it was

confirmed that Abi RNAi blocked FC migration at early developmental stages (Figure 4.13 A). Then, Abi RNAi egg chambers were fixed and global actin alignment was measured (Figures 4.12 B). In this case, the order parameter for stage 1 egg chambers was comparable to controls, however it decreased continuously throughout development, reaching a minimum value of 0.1 at stage 8 (Figure 4.13 B). This result indicated that migration is required to maintain global actin alignment beginning at stage 2. However since migration is blocked from stage 1 in Abi RNAi egg chambers, it was not possible to determine from these data if migration was actively required at later developmental stages to maintain the global actin pattern or if the defect observed was carried on from previous stages. To distinguish between these possibilities, migration was blocked selectively at later developmental stages using a genetic driver. The mirror-Gal4 driver (mirr-Gal4) [68] expresses weakly in the follicle cells at stages six and seven, and expresses highly at stage eight.

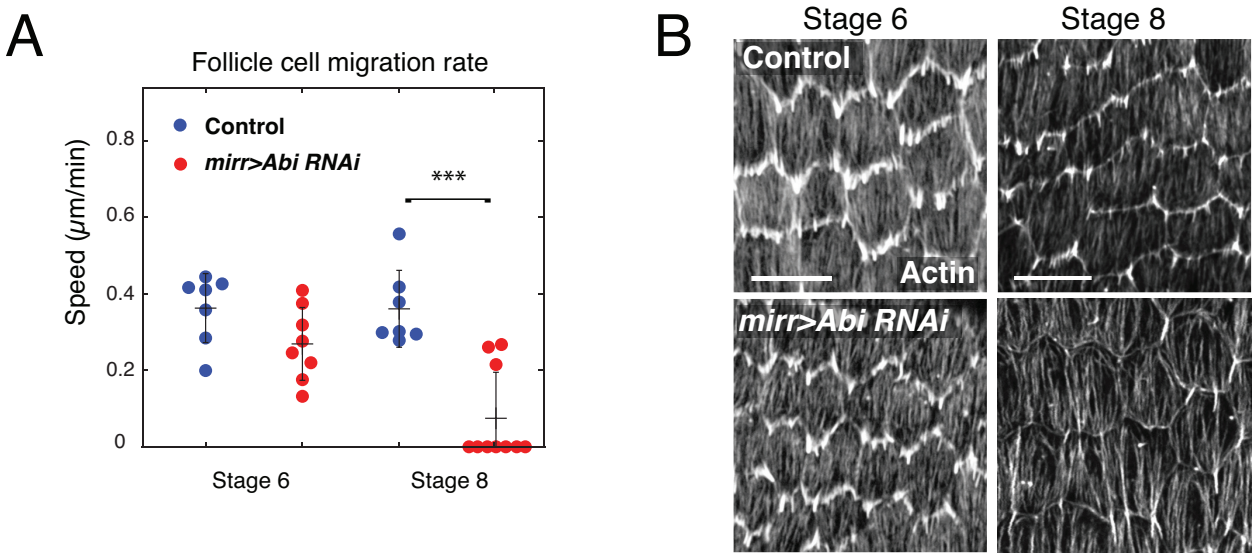

Figure 4.14: Effects of selective block of FC migration at stage 8. A) Migration speed of stage 6 and 8 egg chambers where mirror-Gal4 was used to express Abi RNAi. B) Basal actin pattern of stage six and eight egg chambers expressing control or Abi RNA using mirror-Gal4. One copy of SCAR was also removed in this genetic background.

When Abi RNAi is expressed using mirr-Gal4, FCs migrate and show proper basal actin

bundle alignment at stage six (Figure 4.14 B). However, by stage eight, leading edge protrusions disappear (Figure 4.14 B) and 70% of the egg chambers stop rotating (Figure 4.14 A). Significantly, the tissue-level alignment of the basal actin bundles is unaffected even though rotation has stopped prematurely. These data provide evidence that rotation becomes dispensable for maintaining the global actin pattern in stage-eight egg chambers.

To determine precisely when rotation contributes to tissue-level actin alignment, FC migration was acutely blocked using the Arp2/3 inhibitor CK-666 [73]. Egg chambers treated with the inhibitor stop rotating within an hour, whereas egg chambers treated with the control molecule CK-689 continue to rotate normally (Figure 4.15). Thus, ovarioles were treated with 100μM of the arp 2/3 inhibitor and immediately fixed for analysis.

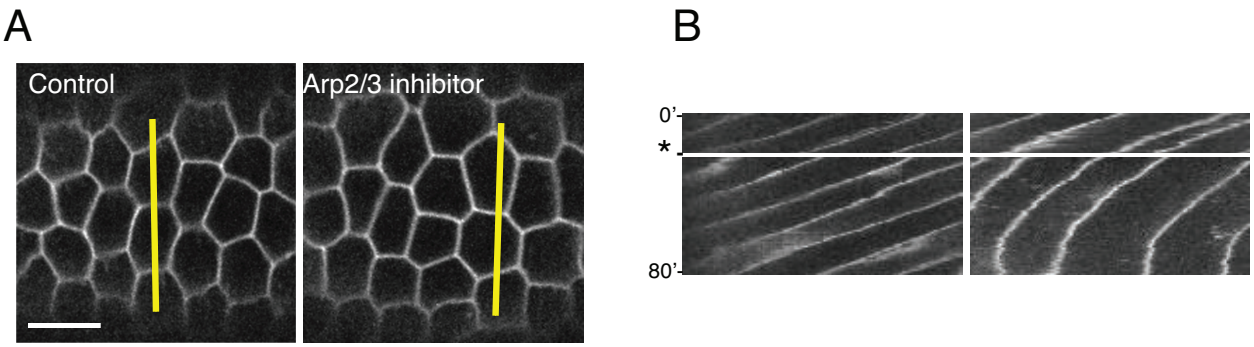

Figure 4.15: Arp2/3 inhibition blocks FC migration. A) Migrating epithelia treated with Arp2/3 inhibitor CK-666 or the control molecule CK-689. Egg chambers are expressing Indy GFP to mark FC membranes. B)Kymographs of rotating egg chambers treated with either with the Arp2/3 inhibitor CK-666 or the control molecule CK-689 (asterisk). The inhibitor stops FC migration within 1h. n=5 for each condition.

Blocking rotation with the inhibitor causes the tissue-level actin alignment to drop below control levels for stages two through five. However, during stages six through eight the tissue-level actin pattern persists in the absence of migration (Figure 4.16). These data show that the early rotation phase is essential to maintain the tissue-level actin bundle alignment, but at later stages the pattern is preserved by an alternate mechanism.

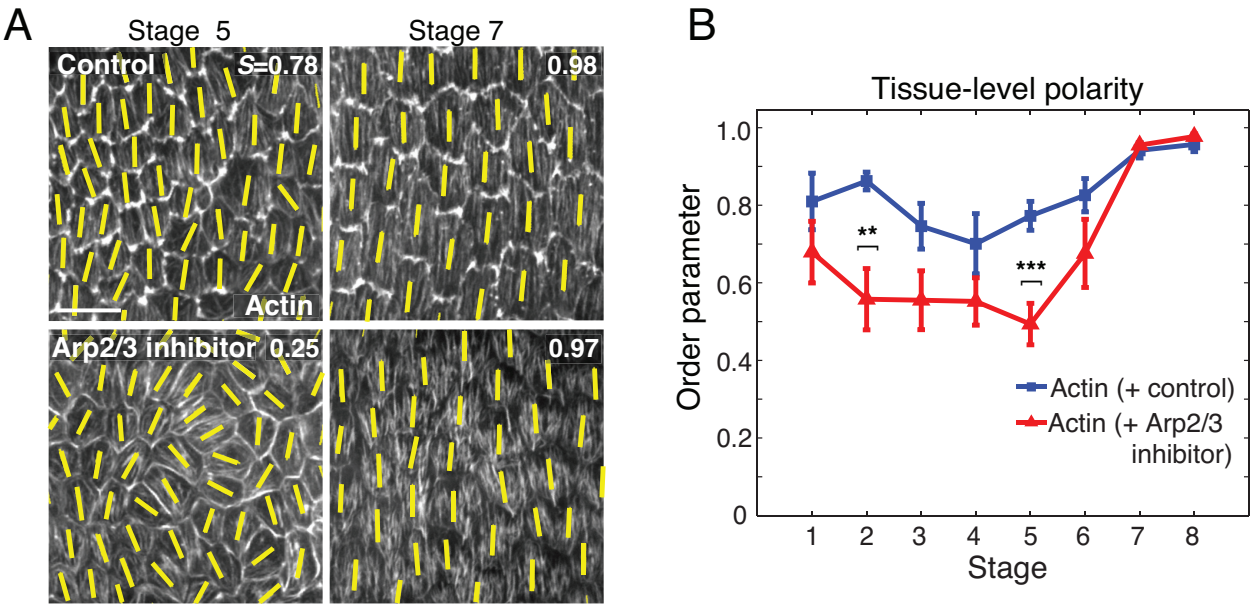

Figure 4.16: FC migration is required for global actin alignment from stages 2-5. A) Representative images of the basal actin bundle alignment after one hour of CK-666 treatment during each of the given stages with the corresponding order parameter value (S). B) Quantification of global actin alignment for egg chambers treated with the arp 2/3 inhibitor or control molecule.

Previous work has shown that ECM polarization in the FC epithelium begins at stage 6. This suggested that ECM polarization could provide an alternate mechanism to preserve global actin alignment in the absence of FC migration. To investigate this possibility, the dynamics of ECM polarization establishment were analyzed by measuring ECM alignment at different developmental stages, adapting the method used to measure global actin alignment (Figure 4.17 A). In agreement with previously published data, it was found that ECM polarization increases through time, reaching its maximum value at stages seven and eight (Figure 4.17 A, B). Importantly, there is a strong correlation between the period of maximal ECM polarization and the period when Fc migration becomes dispensable for maintaining the global actin bundle pattern (Figure 4.17 B). These data suggest that an interaction between the basal actin bundles and polarized ECM may maintain the tissue-level alignment of these structures at later developmental stages.

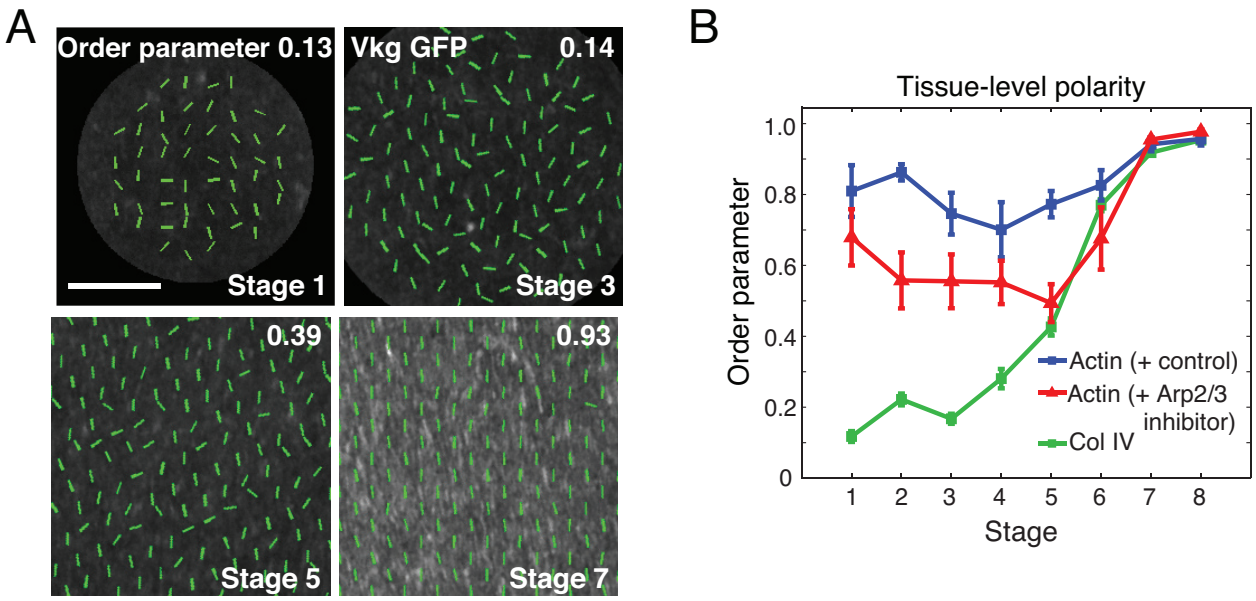

Figure 4.17: A) Representative images of Collagen IV alignment in stage 1-7 egg chambers. Quantification of collagen IV and actin global alignment though development. Actin alignment is shown for egg chambers treated with the arp 2/3 inhibitor or control molecule. Scale bar=10μm.

4.5 Discussion

In this chapter it was shown that FC migration begins shortly after egg chambers emerge from the germarium and that this motion is driven by SCAR-dependent lamellipodia at each follicle cells leading edge. Thus, the well-studied mechanisms that underlie individual cell motility also promote the collective migration of the follicle cells that causes the egg chamber to rotate. There is growing evidence that coherent rotational motion may be an intrinsic property of epithelial tissues that adopt circular or spherical geometries. This work highlights how epithelial rotation can be harnessed to organize a tissue for morphogenesis. It has been previously established that egg chamber rotation creates a system of polarized fibril-like structures in the follicular ECM required for egg chamber elongation [41]. This

data now show that rotation also promotes the tissue-level alignment of the basal actin bundles.

Based on these findings a three-step model for global alignment of basal actin filaments is proposed (Figure 4.18). First, the basal actin bundles become globally aligned within the follicle cell precursors in the germarium. Second, this tissue-level actin pattern is inherited by a stage one egg chamber and is then maintained by the newly discovered early FC migration phase. Third, FC migration creates the fibrillar pattern in the ECM, which then reinforces and stabilizes global actin bundle alignment through local cellmatrix interactions starting at stage six. In this way, epithelial rotation could provide a single mechanism to actively maintain, and then fix global actin alignment.

Going forward, the subcellular mechanisms that allow FC migration to maintain global tissue alignment remain to be uncovered. Furthermore, the functional significance of global actin alignment for egg chamber morphogenesis remains to be established. One possibility is that early FC migration transmits polarity information across the plane of the growing epithelium. From stages one to six, the number of follicle cells increases approximately tenfold. As these cells migrate as a sheet, newly formed daughter cells could quickly establish a frontrear axis through positional cues from their neighbors. An individual FC may then preferentially orient the polymerizing ends of its basal actin filaments towards the leading edge and the depolymerizing ends towards the trailing edge; however, the dynamics of the individual actin bundles remain to be investigated. Future work will also be required to determine how the actin bundles become organized into parallel arrays within each cell, as this phenomenon is not FC migration dependent.

Notably, it is not the lamellipodial actin networks themselves that orient the contractile actin bundles. When an egg chamber contains a small clone of Abi RNAi follicle cells, rota-

tion continues and the mutant cells are carried along. Under these conditions, the depleted cells lack leading edge protrusions but their basal actin bundles still show proper tissue-level alignment. In classic planar cell polarity systems, the presence of a small mutant clone can produce a phenotype in which planar polarity is perturbed in and around the clone, but is normal elsewhere in the tissue. In contrast, the tissue-level orientation of the basal actin bundles is an all-or-nothing process [39]. This phenomenon was first noted for fat2 mosaic egg chambers [108]. When fat2 mutant cells make up <60% of the epithelium, tissue-level actin bundle alignment is normal; when mutant cells exceed 60%, actin bundle orientation is globally perturbed. This all-or-nothing relationship also holds true for epithelia that are mosaic for Abi function (this work) or Misshapen function [57]. The model that emerges is that the deciding factor between global actin bundle alignment and global perturbation is whether there are enough wild-type cells in the epithelium to allow bulk tissue movement to proceed.

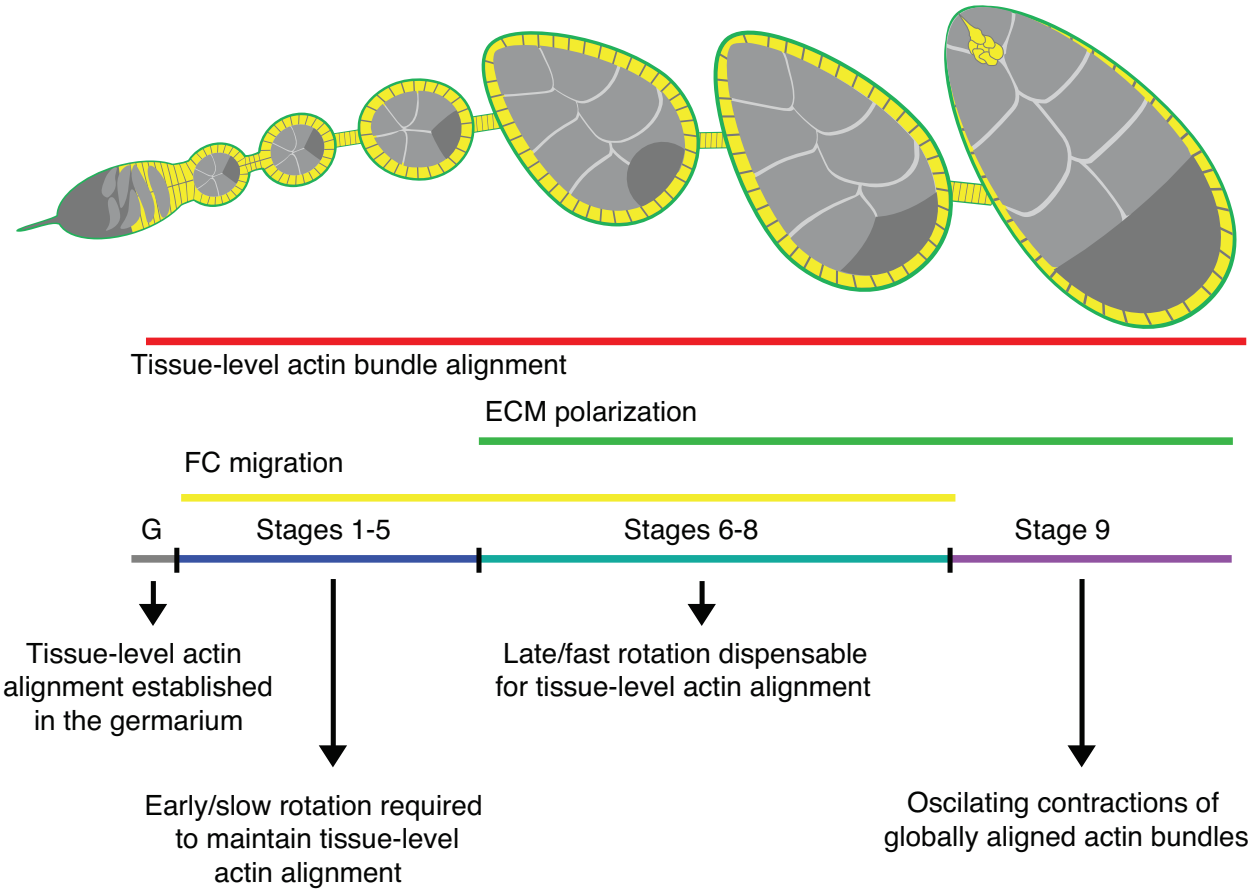

Figure 4.18: Tissue-level alignment of the basal actin bundles is established in the germarium. Slow rotation occurs between stages one and five. This phase of rotation is required to maintain tissue-level actin bundle alignment. Fast rotation occurs between stages six and eight but is dispensable for the maintenance of the global actin pattern. This phase correlates with the polarization of the basement membrane, which may function to stabilize the actin pattern. Tissue-level polarization of the actin bundles and the basement membrane is maintained after migration stops at stage nine and the oscillating actin bundle contractions begin.

CHAPTER 5

CONCLUSION

In this thesis work cell migration was studied at two different scales. First, the sub cellular mechanisms for contact guidance were investigated using UV micropatterning and establishing metrics to characterize cellular phenotypes. The contribution to contact guidance of the cellular feedbacks involved in the regulation of cell migration, including Rac spatial regulation, Myosin II activity and focal adhesion signaling, was established.

The ability of cells to change shape and direct their migration in response to ECM geometric cues has been characterized for decades and remains an area of active research [26, 69, 70, 23, 20, 96, 116]. Previous studies have characterized extensively the ability of a variety of cells to respond to changes in ECM geometry at scales ranging from nanometers [97, 60, 49] to hundreds of micrometers [104, 105]. Despite numerous studies that point that the ability of cells to sense their underlying matrix is ubiquitous across cell types and occurs at different scales, there have been very little studies that address the mechanisms of contact guidance. Efforts have focused on understanding the mechanisms of contact guidance in the extreme where cells are confined to a single line of ECM. In this case, cells move 1.5 times faster than in a classic 2D environment due to changes in lamellipodial dynamics and increased mechanical coupling between adhesions and the protrusive machinery [25, 24]. While the effects of different degrees of confinement on cell migration can be studied by varying the width of the ECM line, migration direction is trivially parallel to the ECM. Therefore, to understand the mechanisms by which cells adjust their direction of migration in response to changes in ECM geometry, we patterned microenvironments where the ECM line width was constant. By patterning ECM architectures with parallel lines of a fixed width that impose no limitations on adhesion formation, we show that in the absence of confinement cells are capable of directing migration parallel to the ECM.

Studies done on cell derived matrices and ECM protein hydrogels have shown that cells orient their motility and shape in response to anisotropies in the ECM in the absence of confinement [84, 54]. These experimental systems resemble more closely the *in vivo* microenvironment, however they have the disadvantage that it is challenging to control the degree in anisotropy of the ECM with subcellular resolution. In these cases, only binary comparisons can be made (aligned ECM vs not aligned ECM), making it impossible to discern whether cells are sensitive to a range of anisotropies in the ECM or if guidance is just a binary phenomenon. By varying the spacing between lines we are able to control the degree of anisotropy in the ECM. Thus, our study addresses a gap in the literature showing that variations in anisotropy of the ECM at the micrometer scale can influence migration in a continuous way. At the same time, we show that by changing the fibril-like spacing alone cells can tune their guidance behavior, in contrast with previous studies where surface topography and fibril-like spacing are changed simultaneously [20, 96, 84, 29, 102, 110, 109, 64].

Our work provides the foundation towards a mechanistic understanding of contact guidance at the micrometer scale. Previous work in structured ECM showed that Rac was activated at sites of adhesion formation, consequently stimulating protrusion formation at those sites [116]. While myosin II activity was shown to be important for the cell shape changes that occur in response to structured ECM [30, 90]. However, by manipulating the main feedbacks that regulate cell migration we show that defects in contact guidance stem from defects in the spatial control of protrusive activity. Our quantitative analysis enabled the characterization of contact guidance, allowing comparison of cellular phenotypes across different perturbations. Comparison across experimental conditions shows that perturbations where cells lose their ability to migrate parallel to the ECM fail to localize protrusions or have protrusions with increased area. By contrast, Arp 2/3 inhibition improves contact guidance by a decreasing in protrusion area and improved localization of protrusions along the lines. Collectively these results show that contact guidance relies on spatial control of leading edge

protrusion. The defects we observe in migration guidance can be explained by changes in two distinct parameters of protrusion: orientation and size. Specifically, contact guidance is controlled by each one of these parameters since disruption of either one is sufficient to produce loss of contact guidance. These two parameters are tuned subcellularly by a positive feedback between adhesion formation and protrusion initiation and a negative feedback between myosin II dependent elongated shapes and formation of protrusions perpendicular to the ECM. For spacings $\leq 5\mu m$ these two feedbacks are required to enforce elongated cell shapes and migration to the ECM. As spacing is increased, the physical size of protrusions limits the ability of protrusions to be stabilized perpendicular to the ECM, further enhancing contact guidance. The spacing at which this transition occurs is most likely cell type dependent since variations in lamellipodia size that are cell type dependent will influence this. Thus, we envision that contact guidance is a function of protrusion area and orientation, where these two parameters can be regulated through different cellular pathways. Future work remains to be done to investigate other cellular pathways that regulate the efficiency of contact guidance that may arise from focal adhesion signaling and protrusion dynamics. In addition, the connection between contact guidance at the micrometer scale and the nanometer scale remains to be explored. While there is little mechanistic understanding of contact guidance at the nanometer scale, there is evidence that focal adhesion and protrusion orientation correlate with the ability of cells to align parallel to the underlying matrix [96, 97, 49]. At this scale, other molecular feedbacks might become important for ECM sensing such as local curvature of cell shape and adhesion signaling driven by focal adhesion kinase [44, 98].

In the second part of this thesis, the role of egg chamber rotation for tissue-scale patterning was investigated, along with the cellular mechanisms that drive collective migration. There was evidence that rotation of the egg chamber was driven at the cellular level by the classical mechanisms of cell migration [57], however this remained to be confirmed. Our work revealed that components required to build lamellipodia and fillopodia localized at individual follicle

cell leading edges, including scar, abi and ena. Depletion of these components showed that follicle cells rely on lamellipodia but not fillopodia protrusions to move forward. Interestingly, lamellipodia are required for motility non-cell autonomously since clones where abi is depleted can move with the rest of the epithelium if most of the cells in the epithelium are *wild type*. This result is consistent with the phenotype observed in other migration defective egg chamber mutants where entirely mutant epithelia do not migrate collectively, but mutant clones can be carried along with their *wild type* neighbors [107, 41, 57, 91]. Together these observations suggest that collective cell migration in the FC epithelium is a robust "all or nothing" process, where long range interactions dominate over local defects.

Since the discovery of egg chamber rotation, the relationship between rotation and the establishment of the tissue-scale actin and ECM patterns became of interest. While the ECM was reported to acquire its oriented structure at stages 5-6 [41], the timing of the emergence of the actin pattern was poorly explored. Furthermore, the functional relationship between FC migration and the emerge of the tissue-scale actin pattern was not clear. Therefore to determine the relationship between collective migration and the tissue scale alignment of actin filaments, the dynamics of establishment of the pattern were analyzed in detail. Using a newly developed metric to measure tissue scale actin alignment, we determined that the global actin pattern is present from the onset of egg chamber formation at stage one, and persists through development. Since FC migration was reported to begin at stage 5 [41], this result would imply that tissue-scale actin alignment occurred earlier than collective cell migration, decoupling this events temporally. However, closer investigation of the dynamics of migration revealed that egg chamber rotation initiated at stage 1, not 5 as it was previously reported. Therefore collective migration and tissue scale actin patterning coincided temporally, but initiated earlier in development, at stage 1. Establishment of the mechanisms for FC migration provided us with the tools necessary to explore this relationship. By blocking migration using RNAi in the entire epithelium, it was shown that FC motility is

required for the maintenance of tissue-scale actin alignment, since under this condition egg chambers lost the global actin pattern increasingly as development progressed. Similar to the actin pattern, the ECM failed to organize in a fibril-like structure perpendicular to the A-P axis at a tissue scale in egg chambers expressing Abi RNAi. Since it was not possible to decouple the influences of motility and the ECM pattern in Abi RNAi egg chambers, drug treatment was used as a mean to acutely disrupt migration, without preventing ECM alignment. Treatment with the arp 2/3 inhibitor blocked migration but not ECM alignment in egg chambers of all developmental stages, establishing it as a tool to decouple the influence of migration and ECM alignment in the establishment tissue-scale actin alignment. Egg chambers where migration was blocked using the arp 2/3 inhibitor at stages 1 through 5 lost tissue scale actin alignment, in contrast with stage 6-8 egg chambers where actin alignment was preserved even in the absence of migration. Altogether these results suggest that collective migration of the FC epithelium maintains the tissue scale actin alignment inherited from the germarium at stages 1 through 5, however, at later stages where the ECM is aligned, migration is dispensable for the maintenance of the global actin pattern. Whether it is the fibrillar matrix or some other polarized feature of the epithelium that preserves the actin bundle alignment remains to be uncovered.

Our work established the requirement for migration to preserve the tissue scale actin pattern, however the mechanisms by which this occurs remained unclear. Recent evidence has called into question our results providing an example of a mutation where tissue-scale actin alignment is preserved in the absence of migration. It was shown that expression of a truncated form of the atypical cadherin Fat2 missing the intracellular domain (Fat2Δ IC), could rescue the loss of tissue-scale actin organization in a fat2 mutant epithelium. Intriguingly, Fat2Δ IC egg chambers are unable to migrate [5]. A different study showed that fat-2 interacts with the wave regulatory complex (WRC), providing a link between planar cell polarity and actin polimerization [91]. Similarly, the WRC interacts functionally with the ECM receptor

Lar, possibly relaying information to the ECM to direct motion as a result of directed actin polymerization [91]. Disruption of the interactions between Lar, fat2 and WRC results in loss of tissue scale actin alignment and defects in egg chamber elongation, however, these interactions are required non-cell autonomously since mosaic epithelia exhibit actin polarization. These results strongly suggest that fat2 is critical for the establishment of tissue scale actin alignment. If migration is indeed correlated with tissue scale actin alignment, as our results show, the fact that Fat2Δ IC egg chambers are unable to migrate is extremely puzzling. Unpublished data from the Horne-Badovinac lab is able to reconcile this apparent contradiction [6]. Contrary to the model that proposes that both Fat2 and Lar interact with WRC stimulating the formation of leading edge protrusions cell autonomously, these new data show that Fat2 plays a noncell-autonomous role stabilizing Lar, thus stimulating protrusion, in the leading edge of the cell directly behind. In order for fat2 to stimulate protrusion in neighboring cells, its intracellular domain is largely dispensable. Additionally, these new data show another mechanism by which fat2 might help coordinate FC migration. Fat2 null cells have elongated basal surface, a phenotype that reflects defects in tail retraction [57]. This opens up the possibility that lack of migration seen is Fat2Δ IC egg chambers stems from a defect in tail retraction. In this case, since fat2's intracellular domain is dispensable for the stimulation of leading edge protrusion these cells are primed for migration, however are unable to move due to defects in tail retraction; suggesting that the intracellular domain of fat2 is important for this function. In light of this evidence the conclusion that collective cell migration is required for tissue-scale actin polarization needs to be reformulated. A more precise description would be to say that tissue-scale actin polarization can be maintained as long as the epithelium is strained in the direction perpendicular to the A-P axis. In the case of Fat2Δ IC egg chambers, FCs might be strained due to their polarized protrusions and inability to retract their tails. In the case of migrating epithelia, motility itself imposes a strain in the tissue, orienting the actin filaments. This expanded conclusion highlights the importance of physical forces in the coordination of FC migration.

Altogether, the work presented in this thesis shows the importance of meaningful quantitative measurements in cell biology research. By identifying the control parameters of a cellular or tissue behavior it is possible to describe and compare the phenotypes observed, yielding insights into a process. Without identification of the parameters relevant in each case and development of metrics to describe them quantitatively, insights into the processes of contact guidance and establishment of tissue-scale actin polarity would not have been possible.

APPENDIX A

EXPERIMENTAL PROTOCOLS

A.1 Coverslip Activation

To coat with a polyacrylamide gel, coverslips need to be activated. The first part of the activation process requires 'squeaky cleaning' of the coverslips.

A.1.1 Squeaky cleaning

Eliminate as many bubbles as possible in every step.

1. Place new coverslips into a beaker of tap water, sonicate for 30 minutes.
2. Exchange solution to dilute versa-clean in DI water, sonicate for 30 minutes.
3. Exchange solution to DI water, sonicate for 30 minutes.
4. Exchange solution for 30% ethanol, sonicate 30 minutes.
5. Exchange solution for 70% ethanol, sonicate 30 minutes.
6. Exchange solution for 100% ethanol, sonicate 30 minutes.
7. Exchange solution with fresh 100% ethanol, sonicate 30 minutes.
8. Pour out 100% ethanol and place coverslips in a jar with 100% ethanol for storage.

A.1.2 Activating coverslip surface

1. Place squeaky clean coverslips in stainless steel rack. Flame coverslips individually to get rid of the ethanol.

2. Soak in 2% 3-aminopropyltrimethyoxysilane diluted in isopropanol for 10 minutes. Use a glass pasteur pipette to dispense aminosilane. Pipette bulb $\approx 1.5ml$, square dish $\approx 350ml$, so about 6 squirts in a dish.

3. Dispose of the waste in a chemical waste container. Rinse converslips in DI water 3-4 times.

4. Wash in DI water for 10 minutes. Rinse in DI water 3-4 times.

5. Dry coverslips at low temperature in incubator.

6. Immerse in 1% gluteraldehyde solution in H_2O for 30 minutes. Dispose of waste in chemical waste container.

7. Wash in DI water for 10 minutes, exchange solution and repeat 2 times.

8. Dry in incubator.

9. Cover in aluminum foil to keep dust away. Store at room temperature.

A.2 UV micropatterning

This technique uses a quartz-chrome photomask to create ECM patterns with micrometer resolution. The mask layout can be designed in AutoCAD (or similar software) and it can be sent to `http://www.micro-tronics.com/` for manufacturing. Figure A.1 shows a typical layout for a 5X5 inch photomask. Using this layout each white rectangular region fits a 22x40 mm coverslip. Each of these rectangular regions will contain the patterns designed in AutoCAD. It is recommended to include several repeats of each desired shape per coverslip. A reasonable rule for distributing shapes within a coverslip is to space each shape by its size. Additionally it is useful to include two replicates for each coverslip design, since coverslips can be lost during the patterning protocol.

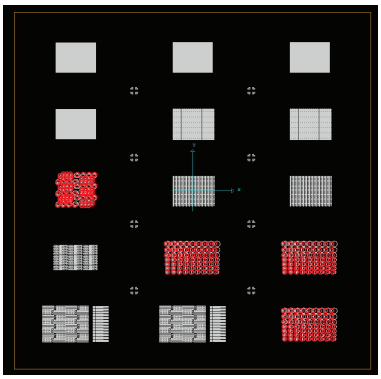

Figure A.1: Recommended layout for a 5x5mm Quartz-Chrome Photomask. Each white rectangular region should include several pattern repeats and fits a 22x40mm coverslip.

Once the mask design is complete, the following protocol can be used to obtain ECM patterns on PAA gels:

1. Clean the Quartz-Chrome mask

   Rinse with isopropanol $\approx 600\mu l$ and wipe off with a kimwipe.

   Under the hood: Use an insulin syringe to take $\approx 400\mu l$ of hexane and clean the surface again, wipe off excess with kimwipe.

   Finally rinse with $\approx 600\mu l$ of DI water and wipe off with a kimwipe.

2. Make gels

   Prepare polyacrylamide (PAA) gel of desired stiffness following the standard recipe on the Gardel lab PAA gel worksheet.

   Add $11 - 20\mu l$ of PAA mixture on top of the mask region that contains the desired patterns. This PAA volume is appropriate for 22mm round, 25mm round and 22x40mm rectangular coverslips.

   Drop an activated coverslip on each PAA drop.

   Let gel polymerize for 30 min protected from light.

3. Bake mask: Put mask upside down (glass side up) in UV oven (UVO-Cleaner 342, Jelight, Irvine, CA) and illuminate with a combination of 185- and 254-nm ultraviolet light for 2 minutes and let sit for 3 min (to get rid of the ozone).

4. While baking the mask weight 10mg of EDC and 17mg of NHS. Dissolve each one separately in 1ml of ddH_2O and vortex to dissolve. Combine both solutions to get 2ml.

5. Pipette 200μl of solution onto parafilm for every coverslip that is being patterned. Set aside.

6. Fill with DI water ($\approx$ half full) a rectangular PIREX dish and set aside.

7. Submerge the mask in water and scrape off coverslips with a razor blade and tweezers. Use caution when removing the coverslips since any scratches on the mask can take off the quartz layer distorting the patterned features.

8. Wick away the extra moisture of the coverslips by touching a kimwipe with the edge of the coverslip.

9. Invert coverslips onto EDC-NHS drops (Gel side should be touching the liquid). Incubate 10-15 minutes. It is recommended to wait 10 minutes and check for the formation on bubbles, if bubbles don't appear under the coverslip wait an extra 5 minutes.

10. A few minutes before coverslip incubation is done, prepare ECM protein

    For Collagen (Rat tail collagen I, Gibco, Cat: A1048301): Bring up to 0.5 mg/ml in 10mM PIPES (pH 7).

    For Fibronectin(Human plasma fibronectin, Millipore, Cat: FC010): Bring up to 0.08 mg/ml in 10mM HEPES (pH 8.5).

11. Pipette 50μl of protein solution per coverslip onto parafilm.

12. Invert coverslips onto ECM protein drops, incubate for 30 minutes at room temperature.

13. Rinse 3 times 5 minutes each with sterile PBS under the hood.

14. Cells can be added to patterns immediately or patterns can be stored in the incubator immersed in media for use the next day.

Troubleshooting:

- Coverslips can't be removed from mask after PAA polymerization.

  Use freshly activated coverslips, to make pattens, coverslips should not be more than 3 weeks old.

  Clean with hexane 2-3 times before polymerizing gel. Make sure that the mask is hydrophobic.

- Cells adhere to PAA gel outside of the regions patterned.

  Make sure to rinse thoroughly coverslips with sterile PBS before cells are added.

  Coverslips with cells can be rinsed with cell culture media using a 1ml pipette. This creates a faster flow than using a 5ml pipette and sometimes helps remove poorly attached cells outside of patterned regions.

- Cells do not attach at all to polyacrylamide gels.

  After several weeks of use, the mask can get dirty reducing the efficiency of patterning. In this case it is recommended to clean photomask in the UV oven by baking it for 15 minutes on each side. This will remove all dirt and also the hydrophobic coating, therefore it is recommended to wash with hexane 3-5 times in the next use.

A.3 Fix and Stain of cells

Reagents needed: Paraformaldehyde, 16% solution (Electron microscopy sciences). BSA, Fraction V heat shock isolation, 98% pure (EMD chemicals).
Solutions needed:

- Cytoskeletal buffer (500ml 10X stock, pH to 6.8): 0.1M MES, 0.03M $MgCl_2$, 1.38 M KCl, 0.02M EGTA.
- Fix solution: 4% Paraformaldehyde, 1.5% BSA, 0.5% Triton X in CB.
- Antibody solution: 1.5% BSA, 0.5% Triton X in CB.

Protocol:

1. Wash cells with 1ml warm cytoskeletal buffer (CB).
2. Aspirate CB and simultaneously wash in 1ml of warm fix solution.
3. Wash 3 times 5 minutes each with PBS.
4. Prepare primary antibodies by dissolving them in antibody solution (AB) to the right concentration. Use 100μl of solution for each coverslip.
5. Pipette 100 μl drops of primary antibody solution onto parafilm and invert coverslips. Incubate overnight at 4C.
6. Rinse coverslips 3 times 5 minutes each with PBS.
7. Prepare secondary antibodies by dissolving them in antibody solution (AB) to the right concentration.Use 100μl of solution for each coverslip.
8. Pipette 100 μl drops of secondary antibody solution onto parafilm and invert coverslips. Incubate at room temperature for an hour.
9. Rinse 3 times 5 minutes each.

10. Mount on glass slides using $10\mu l$ of prolong gold or antifade solution.

11. Seal with nail polish.

A.4 Antibody stain of Drosophila egg chambers

5-10 females should be fed yeast 1-3 days prior to dissection in the presence of males.

Solutions needed:

- Fix solution: 300 μl of S2 medium, 100 μl of 16% EM grade fomaldehyde.
- PBT: 1X PBS, 0.1% Triton X.

1. Dissect ovaries in S2 medium, carefully tease ovaries apart with forceps. To preserve actin structures, this step can be done in live imaging media.

2. Transfer ovaries to fix solution and incubate for 15 minutes while rocking.

3. Wash 3 times 5 minutes each with 600 μl of PBT while rocking.

4. Remove final wash and add 300 μl of PBT.

5. Disrupt ovaries by gently pipetting and let them settle for 10 minutes.

6. Wash 2 times 10 minutes each in 600 μl of PBT without rocking.

7. Incubate in primary antibody diluted in 100-200μl of PBT overnight at 4C.

8. Wash 4 times 10 minutes each without rocking.

9. Incubate in secondary antobody 1:200 in 200 μl of PBT for 3 hours at room temperature.

10. Wash 4 times 10 minutes each with PBT without rocking.

11. Remove final wash and add two drops of antifade solution.

12. Mount egg chambers on glass slide and seal the coverslip with nail polish.

A.5 Drosophila egg chamber live imaging protocol

Reagents needed for this protocol:

- FM464: Optional dye to detect egg chamber damage.
- Penstrep: Penicilin G-sodium 10,000 U/ml, streptomycin sulfte 10,000 μg/ml in 0.85% saline.
- Acidified water: 1 μl of HCl in 1ml of H_2O.
- S2 cocktail: S2, 15% FBS and 0.6X penstrep.
- Insulin solution: 1mg of insulin in 100μl of acidified H_2O.
- Low melt agarose (LMA): 2.5% dissolved in water.
- Live imaging media (L): 1.47 ml of S2 cocktail, 30 μl of insulin solution, 15 μl of FM464 (optional).
- Live imaging media + agarose (L+): 500 μl of S2 cocktail, 20 μl of insulin solution, 150 μl of LMA, 15 μl of FM464.

1. Prepare L and L+ media warming them up to 37C.
2. Clean and dry a 22x30 glass coverslip with glass washing solution and lens paper (a squeaky cleaned coverslip can also be used).
3. Glue coverslip to metal live imaging slide using parafilm.
4. Dissect 2 females in 500 μl of L solution.
5. Put a large drop $\approx$ 250 μl of L+ solution on the prepared live imaging slide. Take slide to dissection microscope.
6. Gather good ovarioles with a glass pipette and pipette onto live imaging slide.

7. Reposition ovarioles for optimum imaging with an eyelash tool.

8. Pipette off excess liquid and seal with a breathable slide.

9. Halocarbon oil can be added to the sides of the slide to prevent evaporation.

REFERENCES

[1] Microtubules and control of insect egg shape. *The Journal of Cell Biology*, 71(1):207–217, 10 1976.

[2] *Drosophila: Methods and Protocols, Methods in Molecular Biology.*, volume 1478. Springer, 2016.

[3] Yvonne Aratyn-Schaus and Margaret L Gardel. Transient frictional slip between integrin and the ecm in focal adhesions under myosin ii tension. *Curr Biol*, 20(13):1145–1153, Jul 2010.

[4] Yvonne Aratyn-Schaus, Patrick W. Oakes, Jonathan Stricker, Stephen P. Winter, and Margaret L. Gardel. Preparation of complaint matrices for quantifying cellular contraction. (46):e2173, 2010.

[5] Franziska Aurich and Christian Dahmann. A mutation in fat2 uncouples tissue elongation from global tissue rotation. *Cell Rep*, 14(11):2503–2510, Mar 2016.

[6] Kari Barlan, Maureen Cetera, and Sally Horne-Badovinac. Fat2 and lar define a basally localized planar signalling system. unpublished data.

[7] Jack Bateman, R.Srekantha Reddy, Haruo Saito, and David Van Vactor. The receptor tyrosine phosphatase dlar and integrins organize actin filaments in the drosophila follicular epithelium. *Current Biology*, 11(17):1317 – 1327, 2001.

[8] David Bilder and Saori L. Haigo. Expanding the morphogenetic repertoire: Perspectives from the drosophila egg. *Developmental Cell*, 22(1):12–23, 2012.

[9] Douglas G Brownfield, Gautham Venugopalan, Alvin Lo, Hidetoshi Mori, Kandice Tanner, Daniel A Fletcher, and Mina J Bissell. Patterned collagen fibers orient branching mammary epithelium through distinct signaling modules. *Current biology*, 23(8):703–709, 04 2013.

[10] Brian Burkel, Brett A. Morris, Suzanne M. Ponik, Kristin M. Riching, Kevin W. Eliceiri, and Patricia J. Keely. Preparation of 3d collagen gels and microchannels for the study of 3d interactions in vivo. *J. Vis. Exp.*, (111):e53989, 2016.

[11] Michael Buszczak, Shelley Paterno, Daniel Lighthouse, Julia Bachman, Jamie Planck, Stephenie Owen, Andrew D. Skora, Todd G. Nystul, Benjamin Ohlstein, Anna Allen, James E. Wilhelm, Terence D. Murphy, Robert W. Levis, Erika Matunis, Nahathai Srivali, Roger A. Hoskins, and Allan C. Spradling. The carnegie protein trap library: A versatile tool for drosophila developmental studies. *Genetics*, 175(3):1505–1531, 2007.

[12] Maureen Cetera, Guillermina R Ramirez-San Juan, Patrick W Oakes, Lindsay Lewellyn, Michael J Fairchild, Guy Tanentzapf, Margaret L Gardel, and Sally Horne-Badovinac. Epithelial rotation promotes the global alignment of contractile actin bundles during drosophila egg chamber elongation. *Nature communications*, 5:5511–5511, 2014.

[13] Guillaume Charras and Erik Sahai. Physical influences of the extracellular environment on cell migration. *Nat Rev Mol Cell Biol*, 15(12):813–824, 12 2014.

[14] Colin K Choi, Miguel Vicente-Manzanares, Jessica Zareno, Leanna A Whitmore, Alex Mogilner, and Alan Rick Horwitz. Actin and alpha-actinin orchestrate the assembly and maturation of nascent adhesions in a myosin ii motor-independent manner. *Nat Cell Biol*, 10(9):1039–1050, Sep 2008.

[15] Edwin A. Clark, Warren G. King, Joan S. Brugge, Marc Symons, and Richard O. Hynes. Integrin-mediated signals regulated by members of the rho family of gtpases. *The Journal of Cell Biology*, 142(2):573–586, 1998.

[16] John Condeelis and Jeffrey E. Segall. Intravital imaging of cell movement in tumours. *Nat Rev Cancer*, 3(12):921–930, 12 2003.

[17] Ryan Conder, Hong Yu, Baharak Zahedi, and Nicholas Harden. The serine/threonine kinase dpak is required for polarized assembly of f-actin bundles and apical–basal polarity in the drosophila follicular epithelium. *Developmental Biology*, 305(2):470 – 482, 2007.

[18] Miguel A del Pozo, Leo S Price, Nazilla B Alderson, Xiang-Dong Ren, and Martin Alexander Schwartz. Adhesion to the extracellular matrix regulates the coupling of the small gtpase rac to its effector pak. *The EMBO Journal*, 19(9):2008–2014, 2000.

[19] Isabelle Delon and Nicholas H. Brown. The integrin adhesion complex changes its composition and function during morphogenesis of an epithelium. *Development*, 136(24):e1–e1, 2009.

[20] E.T. den Braber, J.E. de Ruijter, L.A. Ginsel, A.F. von Recum, and J.A. Jansen. Quantitative analysis of fibroblast morphology on microgrooved surfaces with various groove and ridge dimensions. *Biomaterials*, 17(21):2037 – 2044, 1996.

[21] Wu-Min Deng, Cassandra Althauser, and Hannele Ruohola-Baker. Notch-delta signaling induces a transition from mitotic cell cycle to endocycle in drosophila follicle cells. *Development*, 128(23):4737–4746, 2001.

[22] Peter Devreotes and Alan Rick Horwitz. Signaling networks that regulate cell migration. *Cold Spring Harbor Perspectives in Biology*, 7(8), 2015.

[23] Richard B. Dickinson, Stefano Guido, and Robert T. Tranquillo. Biased cell migration of fibroblasts exhibiting contact guidance in oriented collagen gels. *Annals of Biomedical Engineering*, 22(4):342–356, 1994.

[24] Andrew D Doyle, Matthew L Kutys, Mary Anne Conti, Kazue Matsumoto, Robert S Adelstein, and Kenneth M Yamada. Micro-environmental control of cell migration–myosin iia is required for efficient migration in fibrillar environments through control of cell adhesion dynamics. *J Cell Sci*, 125(Pt 9):2244–2256, May 2012.

[25] Andrew D Doyle, Francis W Wang, Kazue Matsumoto, and Kenneth M Yamada. One-dimensional topography underlies three-dimensional fibrillar cell migration. *The Journal of Cell Biology*, 184(4):481–490, 02 2009.

[26] G. A. Dunn and T. Ebendal. Contact guidance on oriented collagen gels. *Experimental Cell Research*, 111(2):475–479, 1978.

[27] G.A. Dunn and J.P. Heath. A new hypothesis of contact guidance in tissue cells. *Experimental Cell Research*, 101(1):1 – 14, 1976.

[28] Hunter Elliott, Robert S. Fischer, Kenneth A. Myers, Ravi A. Desai, Lin Gao, Christopher S. Chen, Robert S. Adelstein, Clare M. Waterman, and Gaudenz Danuser. Myosin ii controls cellular branching morphogenesis and migration in three dimensions by minimizing cell-surface curvature. *Nat Cell Biol*, 17(2):137–147, 02 2015.

[29] R G Flemming, C J Murphy, G A Abrams, S L Goodman, and P F Nealey. Effects of synthetic micro- and nano-structured surfaces on cell behavior. *Biomaterials*, 20(6):573–588, Mar 1999.

[30] Margo T. Frey, Irene Y. Tsai, Thomas P. Russell, Steven K. Hanks, and Yu-li Wang. Cellular responses to substrate topography: Role of myosin ii and focal adhesion kinase. *Biophysical Journal*, 90(10):3774–3782, 2016/10/20 2006.

[31] Peter Friedl and Darren Gilmour. Collective cell migration in morphogenesis, regeneration and cancer. *Nat Rev Mol Cell Biol*, 10(7):445–457, 07 2009.

[32] Horacio M. Frydman and Allan C. Spradling. The receptor-like tyrosine phosphatase lar is required for epithelial planar polarity and for axis determination with drosophila ovarian follicles. *Development*, 128(16):3209–3220, 2001.

[33] Chiara Gabella, Elena Bertseva, Céline Bottier, Niccolò Piacentini, Alicia Bornert, Sylvia Jeney, László Forró, Ivo F. Sbalzarini, Jean-Jacques Meister, and Alexander B. Verkhovsky. Contact angle at the leading edge controls cell protrusion rate. *Current Biology*, 24(10):1126 – 1132, 2014.

[34] Beatrice Garber. Quantitative studies on the dependence of cell morphology and motility upon the fine structure of the medium in tissue culture. *Experimental Cell Research*, 5(1):132 – 146, 1953.

[35] Margaret L. Gardel, Ian C. Schneider, Yvonne Aratyn-Schaus, and Clare M. Waterman. Mechanical integration of actin and adhesion dynamics in cell migration. *Annual Review of Cell and Developmental Biology*, 26(1):315–333, 2010. PMID: 19575647.

[36] Julie Gates. Drosophila egg chamber elongation. *Fly*, 6(4):213–227, 2012. PMID: 22940759.

[37] Reinhard Gillitzer and Matthias Goebeler. Chemokines in cutaneous wound healing. *Journal of Leukocyte Biology*, 69(4):513–521, 2001.

[38] Alexandra M. Goldyn, Borja Aragüés Rioja, Joachim P. Spatz, Christoph Ballestrem, and Ralf Kemkemer. Force-induced cell polarisation is linked to rhoa-driven microtubule-independent focal-adhesion sliding. *Journal of Cell Science*, 122(20):3644–3651, 2009.

[39] Lisa V. Goodrich and David Strutt. Principles of planar polarity in animal development. *Development*, 138(10):1877–1892, 2011.

[40] H.O. Gutzeit, W. Eberhardt, and E. Gratwohl. Laminin and basement membrane-associated microfilaments in wild-type and mutant drosophila ovarian follicles. *Journal of Cell Science*, 100(4):781–788, 1991.

[41] Saori Haigo and David Bilder. Global tissue revolutions in a morphogenetic movement controlling elongation. *Science*, 331(1071):891–921, 2011.

[42] Li He, Xiaobo Wang, Ho Lam Tang, and Denise J Montell. Tissue elongation requires oscillating contractions of a basal actomyosin network. *Nature cell biology*, 12(12):1133–1142, 12 2010.

[43] Sally Horne-Badovinac. The drosophila egg chamber—a new spin on how tissues elongate. *Integrative and Comparative Biology*, 54(4):667–676, 2014.

[44] Andrew R. Houk, Alexandra Jilkine, Cecile O. Mejean, Rostislav Boltyanskiy, Eric R. Dufresne, Sigurd B. Angenent, Steven J. Altschuler, Lani F. Wu, and Orion D. Weiner. Membrane tension maintains cell polarity by confining signals to the leading edge during neutrophil migration. *Cell*, 148(1–2):175 – 188, 2012.

[45] Anna Huttenlocher and Alan Rick Horwitz. Integrins in cell migration. *Cold Spring Harbor Perspectives in Biology*, 3(9), 2011.

[46] Richard O. Hynes and Alexandra Naba. Overview of the matrisome—an inventory of extracellular matrix constituents and functions. *Cold Spring Harbor Perspectives in Biology*, 09 2011.

[47] Adam J Isabella and Sally Horne-Badovinac. Dynamic regulation of basement membrane protein levels promotes egg chamber elongation in drosophila. *Developmental biology*, 406(2):212–221, 10 2015.

[48] Jane James, Edgar D. Goluch, Huan Hu, Chang Liu, and Milan Mrksich. Subcellular curvature at the perimeter of micropatterned cells influences lamellipodial distribution and cell polarity. *Cell Motility and the Cytoskeleton*, 65(11):841–852, 2008.

[49] Kyung-Jin Jang, Min Sung Kim, Daniel Feltrin, Noo Li Jeon, Kahp-Yang Suh, and Olivier Pertz. Two distinct filopodia populations at the growth cone allow to sense nanotopographical extracellular matrix cues to guide neurite outgrowth. *PLoS ONE*, 5(12):e15966, 2010.

[50] Ray Keller. Cell migration during gastrulation. *Current Opinion in Cell Biology*, 17(5):533 – 541, 2005.

[51] Deok-Ho Kim, Karam Han, Kshitiz Gupta, Keon W. Kwon, Kahp-Yang Suh, and Andre Levchenko. Mechanosensitivity of fibroblast cell shape and movement to anisotropic substratum topography gradients. *Biomaterials*, 30(29):5433 – 5444, 2009.

[52] Samantha J. King, Sreeja B. Asokan, Elizabeth M. Haynes, Seth P. Zimmerman, Jeremy D. Rotty, James G. Alb, Alicia Tagliatela, Devon R. Blake, Irina P. Lebedeva, Daniel Marston, Heath E. Johnson, Maddy Parsons, Norman E. Sharpless, Brian Kuhlman, Jason M. Haugh, and James E. Bear. Lamellipodia are crucial for haptotactic sensing and response. *Journal of Cell Science*, 129(12):2329–2342, 2016.

[53] Matthew L. Kutys, Andrew D. Doyle, and Kenneth M. Yamada. Regulation of cell adhesion and migration by cell-derived matrices. *Experimental Cell Research*, 319(16):2434 – 2439, 2013. Special Issue: Cell Motility and Mechanics.

[54] Matthew L. Kutys and Kenneth M. Yamada. An extracellular-matrix-specific gef–gap interaction regulates rho gtpase crosstalk for 3d collagen migration. *Nat Cell Biol*, 16(9):909–917, 09 2014.

[55] Douglas A Lauffenburger and Alan F. Horwitz. Cell migration: A physically integrated molecular process. *Cell*, 84(3):359–369, 1996.

[56] Dirk Lehnert, Bernhard Wehrle-Haller, Christian David, Ulrich Weiland, Christoph Ballestrem, Beat A. Imhof, and Martin Bastmeyer. Cell behavior on micropatterned substrate: limits of extracellular matrix geometry for spreading and adhesion. *Journal of Cell Science*, 117:41–52, 2004.

[57] Lindsay Lewellyn, Maureen Cetera, and Sally Horne-Badovinac. Misshapen decreases integrin levels to promote epithelial motility and planar polarity in drosophila. *The Journal of Cell Biology*, 200(6):721–729, 2013.

[58] Michelle A. Li, Jeffrey D. Alls, Rita M. Avancini, Karen Koo, and Dorothea Godt. The large maf factor traffic jam controls gonad morphogenesis in drosophila. *Nat Cell Biol*, 5(11):994–1000, 11 2003.

[59] Chun-Min Lo, Denis B. Buxton, Gregory C.H. Chua, Micah Dembo, Robert S. Adelstein, and Yu-Li Wang. Nonmuscle myosin iib is involved in the guidance of fibroblast migration. *Molecular Biology of the Cell*, 15(3):982–989, 2004.

[60] W A Loesberg, J te Riet, F C M J M van Delft, P Schon, C G Figdor, S Speller, J J W A van Loon, X F Walboomers, and J A Jansen. The threshold at which substrate nanogroove dimensions may influence fibroblast alignment and adhesion. *Biomaterials*, 28(27):3944–3951, Sep 2007.

[61] Andrew D Luster, Ronen Alon, and Ulrich H von Andrian. Immune cell migration in inflammation: present and future therapeutic targets. *Nat Immunol*, 6(12):1182–1190, 12 2005.

[62] Shalina Mahajan-Miklos and Lynn Cooley. Intercellular cytoplasm transport during drosophila oogenesis. *Developmental Biology*, 165(2):336 – 351, 1994.

[63] Adam C. Martin, Matthias Kaschube, and Eric F. Wieschaus. Pulsed contractions of an actin-myosin network drive apical constriction. *Nature*, 457(7228):495–499, 01 2009.

[64] K Matsuzaka, F Walboomers, A de Ruijter, and J A Jansen. Effect of microgrooved poly-l-lactic (pla) surfaces on proliferation, cytoskeletal organization, and mineralized matrix formation of rat bone marrow cells. *Clin Oral Implants Res*, 11(4):325–333, Aug 2000.

[65] Pieta K. Mattila and Pekka Lappalainen. Filopodia: molecular architecture and cellular functions. *Nat Rev Mol Cell Biol*, 9(6):446–454, 06 2008.

[66] Alex Mogilner and Kinneret Keren. The shape of motile cells. *Current Biology*, 19(17):762–71, 2009.

[67] P. Monaghan, M. J. Warburton, N. Perusinghe, and P. S. Rudland. Topographical arrangement of basement membrane proteins in lactating rat mammary gland: Comparison of the distribution of type iv collagen, laminin, fibronectin, and thy-1 at the ultrastructural level. *Proc Natl Acad Sci USA*, 80, 1983.

[68] Clayton M. Morrison and Georg Halder. Characterization of a dorsal-eye gal4 line in drosophila. *genesis*, 48(1):spcone–spcone, 2010.

[69] N. Nakatsuji, A.C. Gould, and K.E. Johnson. Movement and guidance of migrating mesodermal cells in ambystoma maculatum gastrulae. *Journal of Cell Science*, 56(1):207–222, 1982.

[70] Norio Nakatsuji and Kurt E Johnson. Cell locomotion in vitro by xenopus laevis gastrula mesodermal cells. *Cell motility*, 2(2):149–161, 1982.

[71] Anjana Nayal, Donna J Webb, Claire M Brown, Erik M Schaefer, Miguel Vicente-Manzanares, and Alan Rick Horwitz. Paxillin phosphorylation at ser273 localizes a git1–pix–pak complex and regulates adhesion and protrusion dynamics. *The Journal of Cell Biology*, 173(4):587–589, 05 2006.

[72] Catherine D. Nobes and Alan Hall. Rho gtpases control polarity, protrusion, and adhesion during cell movement. *J. Cell*, pages 144–1235, 1999.

[73] B. J. Nolen, N. Tomasevic, A. Russell, D. W. Pierce, Z. Jia, C. D. McCormick, J. Hartman, R. Sakowicz, and T. D. Pollard. Characterization of two classes of small molecule inhibitors of arp2/3 complex. *Nature*, 460(7258):1031–1034, 08 2009.

[74] Patrick W. Oakes, Shiladitya Banerjee, M. Cristina Marchetti, and Margaret L. Gardel. Geometry regulates traction stresses in adherent cells. *Biophysical Journal*, 107(4):825 – 833, 2014.

[75] Patrick W Oakes, Yvonne Beckham, Jonathan Stricker, and Margaret L Gardel. Tension is required but not sufficient for focal adhesion maturation without a stress fiber template. *J Cell Biol*, 196(3):363–374, Feb 2012.

[76] T. Omelchenko, J. M. Vasiliev, I. M. Gelfand, H. H. Feder, and E. M. Bonder. Mechanisms of polarization of the shape of fibroblasts and epitheliocytes: Separation of the roles of microtubules and rho-dependent actin–myosin contractility. *Proceedings of the National Academy of Sciences*, 99(16):10452–10457, 2002.

[77] Tatiana Omelchenko, M. Angeles Rabadan, Rocío Hernández-Martínez, Joaquim Grego-Bessa, Kathryn V. Anderson, and Alan Hall. -pix directs collective migration of anterior visceral endoderm cells in the early mouse embryo. *Genes and Development*, 28(24):2764–2777, 2014.

[78] Roumen Pankov, Yukinori Endo, Sharona Even-Ram, Masaru Araki, Katherine Clark, Edna Cukierman, Kazue Matsumoto, and Kenneth M." Yamada. A rac switch regulates random versus directionally persistent cell migration. *The Journal of Cell Biology*, 170(5):793–802, 2005.

[79] Kevin Kit Parker, Amy Lepre Brock, Cliff Brangwyne, Robert J. Mannix, Ning Wang, Emanuele Ostuni, Nicholas A. Geisse, Josephine C. Adams, George M. Whitesides, and Donald E. Ingber. Directional control of lamellipodia extension by constraining cell shape and orienting cell tractional forces. *The FASEB Journal*, 16(10):1195–1204, 2002.

[80] Ryan J. Petrie, Andrew D. Doyle, and Kenneth M. Yamada. Random versus directionally persistent cell migration. *Nat Rev Mol Cell Biol*, 10(8):538–549, 08 2009.

[81] A. Ponti, M. Machacek, S. L. Gupton, C. M. Waterman-Storer, and G. Danuser. Two distinct actin networks drive the protrusion of migrating cells. *Science*, 305(5691):1782–1786, 2004.

[82] Mohit Prasad, Anna C-C Jang, Michelle Starz-Gaiano, Mariana Melani, and Denise J Montell. A protocol for culturing drosophila melanogaster stage 9 egg chambers for live imaging. *Nat. Protocols*, 2(10):2467–2473, 10 2007.

[83] Leo S. Price, Jie Leng, Martin Alexander Schwartz, and Gary M. Bokoch. Activation of rac and cdc42 by integrins mediates cell spreading. *Molecular Biology of the Cell*, 9(7):1863–1871, 1998.

[84] Paolo P Provenzano, Kevin W Eliceiri, Jay M Campbell, David R Inman, John G White, and Patricia J Keely. Collagen reorganization at the tumor-stromal interface facilitates local invasion. *BMC Medicine*, 4:38–38, 2006.

[85] Myrto Raftopoulou and Alan Hall. Cell migration: Rho gtpases lead the way. *Developmental Biology*, 265(1):23 – 32, 2004.

[86] Matteo Rauzi, Pierre-Francois Lenne, and Thomas Lecuit. Planar polarized actomyosin contractile flows control epithelial junction remodelling. *Nature*, 468(7327):1110–1114, 12 2010.

[87] Germán Reig, Eduardo Pulgar, and Miguel L. Concha. Cell migration: from tissue culture to embryos. *Development*, 141(10):1999–2013, 2014.

[88] Anne J. Ridley, Martin A. Schwartz, Keith Burridge, Richard A. Firtel, Mark H. Ginsberg, Gary Borisy, J. Thomas Parsons, and Alan Rick Horwitz. Cell migration: Integrating signals from front to back. *Science*, 302(5651):1704–1709, 2003.

[89] Tania Rozario and Douglas W. DeSimone. The extracellular matrix in development and morphogenesis: A dynamic view. *Developmental Biology*, 341(1):126–140, 5 2010.

[90] Elise Spedden, Matthew R. Wiens, Melik C. Demirel, and Cristian Staii. Effects of surface asymmetry on neuronal growth. *PLoS ONE*, 9(9):1–11, 09 2014.

[91] Anna Julia Squarr, Klaus Brinkmann, Baoyu Chen, Tim Steinbacher, Klaus Ebnet, Michael K. Rosen, and Sven Bogdan. Fat2 acts through the wave regulatory complex to drive collective cell migration during tissue rotation. *The Journal of Cell Biology*, 212(5):591–603, 2016.

[92] Xiaoyu Sun, Meghan K. Driscoll, Can Guven, Satarupa Das, Carole A. Parent, John T. Fourkas, and Wolfgang Losert. Asymmetric nanotopography biases cytoskeletal dynamics and promotes unidirectional cell guidance. *Proceedings of the National Academy of Sciences*, 112(41):12557–12562, 2015.

[93] Praveen Suraneni, Boris Rubinstein, Jay R. Unruh, Michael Durnin, Dorit Hanein, and Rong Li. The arp2/3 complex is required for lamellipodia extension and directional fibroblast cell migration. *The Journal of Cell Biology*, 197(2):239–251, 2012.

[94] András Szabó, Manuela Melchionda, Giancarlo Nastasi, Mae L. Woods, Salvatore Campo, Roberto Perris, and Roberto Mayor. In vivo confinement promotes collective migration of neural crest cells. *The Journal of Cell Biology*, 213(5):543, 06 2016.

[95] John L. Tan, Joe Tien, Dana M. Pirone, Darren S. Gray, Kiran Bhadriraju, and Christopher S. Chen. Cells lying on a bed of microneedles: An approach to isolate mechanical force. *Proceedings of the National Academy of Sciences*, 100(4):1484–1489, 2003.

[96] Ana I. Teixeira, George A. Abrams, Paul J. Bertics, Christopher J. Murphy, and Paul F. Nealey. Epithelial contact guidance on well-defined micro- and nanostructured substrates. *Journal of Cell Science*, 116(10):1881–1892, 2003.

[97] Ana I. Teixeira, Paul F. Nealey, and Christopher J. Murphy. Responses of human keratocytes to micro- and nanostructured substrates. *Journal of Biomedical Materials Research Part A*, 71A(3):369–376, 2004.

[98] Benjamin Kim Kiat Teo, Sum Thai Wong, Choon Kiat Lim, Terrence Y S Kung, Chong Hao Yap, Yamini Ramagopal, Lewis H Romer, and Evelyn K F Yim. Nanotopography modulates mechanotransduction of stem cells and induces differentiation through focal adhesion kinase. *ACS Nano*, 7(6):4785–4798, Jun 2013.

[99] Manuel Théry. Micropatterning as a tool to decipher cell morphogenesis and functions. *Journal of Cell Science*, 123(24):4201, 12 2010.

[100] Qingzong Tseng, Irene Wang, Eve Duchemin-Pelletier, Ammar Azioune, Nicolas Carpi, Jie Gao, Odile Filhol, Matthieu Piel, Manuel Thery, and Martial Balland. A new micropatterning method of soft substrates reveals that different tumorigenic signals can promote or reduce cell contraction levels. *Lab Chip*, 11:2231–2240, 2011.

[101] Vicki M Tysseling-Mattiace, Vibhu Sahni, Krista L Niece, Derin Birch, Catherine Czeisler, Michael G Fehlings, Samuel I Stupp, and John A Kessler. Self-assembling nanofibers inhibit glial scar formation and promote axon elongation after spinal cord injury. *The Journal of neuroscience : the official journal of the Society for Neuroscience*, 28(14):3814–3823, 04 2008.

[102] T G van Kooten and A F von Recum. Cell adhesion to textured silicone surfaces: the influence of time of adhesion and texture on focal contact and fibronectin fibril formation. *Tissue Eng*, 5(3):223–240, Jun 1999.

[103] Aleksandr Vasilyev, Yan Liu, Sudha Mudumana, Steve Mangos, Pui-Ying Lam, Arindam Majumdar, Jinhua Zhao, Kar-Lai Poon, Igor Kondrychyn, Vladimir Korzh, and Iain A Drummond. Collective cell migration drives morphogenesis of the kidney nephron. *PLoS Biol*, 7(1):1–14, 01 2009.

[104] Sri Ram Krishna Vedula, Hiroaki Hirata, Mui Hoon Nai, Agusti Brugues, Yusuke Toyama, Xavier Trepat, Chwee Teck Lim, and Benoit Ladoux. Epithelial bridges maintain tissue integrity during collective cell migration. *Nat Mater*, 13(1):87–96, Jan 2014.

[105] Sri Ram Krishna Vedula, Man Chun Leong, Tan Lei Lai, Pascal Hersen, Alexandre J. Kabla, Chwee Teck Lim, and Benoît Ladoux. Emerging modes of collective cell migration induced by geometrical constraints. *Proceedings of the National Academy of Sciences*, 109(32):12974–12979, 08 2012.

[106] Miguel Vicente-Manzanares, Jessica Zareno, Leanna Whitmore, Colin K. Choi, and Alan F." Horwitz. Regulation of protrusion, adhesion dynamics, and polarity by myosins iia and iib in migrating cells. *The Journal of Cell Biology*, 176(5):573–580, 2007.

[107] Ivana Viktorinová and Christian Dahmann. Microtubule polarity predicts direction of egg chamber rotation in drosophila. *Current Biology*, 23(15):1472–1477, 8 2013.

[108] Ivana Viktorinová, Tina König, Karin Schlichting, and Christian Dahmann. The cadherin fat2 is required for planar cell polarity in the drosophila ovary. *Development*, 136(24):4123–4132, 2009.

[109] X F Walboomers, H J Croes, L A Ginsel, and J A Jansen. Contact guidance of rat fibroblasts on various implant materials. *J Biomed Mater Res*, 47(2):204–212, Nov 1999.

[110] X F Walboomers, W Monaghan, A S Curtis, and J A Jansen. Attachment of fibroblasts on smooth and microgrooved polystyrene. *J Biomed Mater Res*, 46(2):212–220, Aug 1999.

[111] Hong-Rui Wang, Yue Zhang, Barish Ozdamar, Abiodun A. Ogunjimi, Evguenia Alexandrova, Gerald H. Thomsen, and Jeffrey L." Wrana. Regulation of cell polarity and protrusion formation by targeting rhoa for degradation. *Science*, 302(5651):1775–1779, 2003.

[112] Bernhard Wehrle-Haller and Beat A Imhof. Actin, microtubules and focal adhesion dynamics during cell migration. *The International Journal of Biochemistry and Cell Biology*, 35(1):39 – 50, 2003.

[113] Paul Weiss and Beatrice Garber. Shape and movement of mesenchyme cells as functions of the physical structure of the medium: Contributions to a quantitative morphology. *Proceedings of the National Academy of Sciences of the United States of America*, 38(3):264–280, 03 1952.

[114] Haguy Wolfenson, Thomas Iskratsch, and Michael P. Sheetz. Early events in cell spreading as a model for quantitative analysis of biomechanical events. *Biophysical Journal*, 107(11):2508–2514, 2016/10/24.

[115] Congying Wu, Sreeja B. Asokan, Matthew E. Berginski, Elizabeth M. Haynes, Norman E. Sharpless, Jack D. Griffith, Shawn M. Gomez, and James E. Bear. Arp2/3 is critical for lamellipodia and response to extracellular matrix cues but is dispensable for chemotaxis. *Cell*, 148(5):973–987, 2016/10/24.

[116] Nan Xia, Charles K. Thodeti, Tom P. Hunt, Qiaobing Xu, Madelyn Ho, George M. Whitesides, Robert Westervelt, and Donald E. Ingber. Directional control of cell motility through focal adhesion positioning and spatial control of rac activation. *The FASEB Journal*, 22(6):1649–1659, 2008.

[117] Sang-Hee Yoon, Young Kyun Kim, Eui Don Han, Young-Ho Seo, Byeong Hee Kim, and Mohammad R. K. Mofrad. Passive control of cell locomotion using micropatterns: the effect of micropattern geometry on the migratory behavior of adherent cells. *Lab Chip*, 12:2391–2402, 2012.

[118] Peter D Yurchenco. Basement membranes: cell scaffoldings and signaling platforms. *Cold Spring Harb Perspect Biol*, 3(2), Feb 2011.